UNIVERSITAT DE VALÈNCIA
FACULTAT DE CIÈNCIES BIOLÒGIQUES
Doctorado en Biotecnología

MORPHOMETRIC AND HISTOPATHOLOGICAL ANALYSIS OF ARTICULAR CARTILAGE REGENERATION ON TISSUE ENGINEERED SCAFFOLDS

DOCTORAL THESIS

BIOTECHNOLOGY PhD

Presented by:
Celso Pedraza Concha

Directors:
Dra. María Sancho-Tello Valls
Dra. Amparo Ruiz Saurí
Dra. Carmen Carda Batalla

Valencia, 2014

DOCTORAL THESIS

MORPHOMETRIC AND HISTOPATHOLOGICAL ANALYSIS OF ARTICULAR CARTILAGE REGENERATION ON TISSUE ENGINEERED SCAFFOLDS

Universidad de Valencia
Biotechnology PhD
2014

DOCTORAL THESIS

MORPHOMETRIC AND HISTOPATHOLOGICAL ANALYSIS OF ARTICULAR CARTILAGE REGENERATION ON TISSUE ENGINEERED SCAFFOLDS

Author: Celso Pedraza Concha

Thesis Supervisors: María Sancho-Tello Valls
Amparo Ruiz Saurí
Carmen Carda Batalla

Universidad de Valencia
Biotechnology PhD
2014

The investigation titled “Morphometric and histopathological analysis of articular cartilage regeneration on tissue engineered scaffolds” that is presented in this manuscript has been completed personally by Celso Fernando Pedraza Concha under our direction and supervision, to opt for the degree of Doctor of Philosophy in Biotechnology. This research complies with the stipulations required for its submission and presentation as a doctoral thesis. For the record in any purpose, we make this statement in Valencia, on January 10th 2014

El trabajo titulado “Morphometric and histopathological analysis of articular cartilage regeneration on tissue engineered scaffolds” que se presenta en esta memoria ha sido realizado por Celso Fernando Pedraza Concha personalmente, bajo nuestra dirección y supervisión, para optar al grado de Doctor en Biotecnología. Dicho trabajo reúne los requisitos necesarios para su presentación y defensa como tesis doctoral. Para que conste a los efectos oportunos, realizamos esta declaración en Valencia a 10 de Enero 2014.

Carmen Carda Amparo Ruiz María Sancho-Tello

Acknowledgements

Upon completion of this thesis, I would like to express my gratefulness to those people who have helped me in any way to make this project become a reality.

Initially and most certainly, to my thesis supervisors, Doctor María Sancho-Tello, Doctor Amparo Ruiz and Doctor Carmen Carda, who with patience have sympathetically set me in the correct direction every step of the process.

Naturally, I would like to thank the pathology department at Universidad de Valencia, for their assistance. Mr. José Benavent in particular, has been an enormous support with his logistic input in laboratory proceedings and software management.

I am thankful to José Luis Gómez Ribelles and his research team, including Ms. Carmen Antolinos Turpin and the biomaterials and tissue engineering center at Universidad Politécnica de Valencia, for their contribution with polymers and scaffold processing, in the context of Ms. Antolinos Turpin's research.

This proyect has been possible thanks to the support and financial aid of the Spanish Ministry of Science and Innovation (MCINN-MAT2010-21611-C03), as a part of coordinated labors to develop tissue engineered scaffolds for the regeneration of articular cartilage. Dr. Gomez Ribelles, as the coordinator of this project, together with Dr. Carda, as the manager of the

subproject MCINN-MAT2010-21611-C03-03, in joint efforts have designed the strategic approach for the present investigation. I, the author of this thesis however, received no funding from this project.

I would also like to acknowledge my orthopedic colleagues, Doctor Francisco Forriol and Doctor Pablo Gastaldi, for their contribution on early stages of this research, by leading the surgical and implantation procedures of the scaffolds.

I am especially grateful to my wife Cris, for her dedication, always having a word of encouragement when most needed. Her love and support all throughout the process has been invaluable. In her absence, this project would have not been feasible.

Finally and without a doubt, I would like to express my gratitude to my parents, Celso and Anabel, who with unconceivable dedication have offered their children the best of the legacies; a solid education, essential in the quest for knowledge.

Abstract

The purpose of this research is to assess *in vivo* articular cartilage regeneration induced by tissue engineered scaffolds.

These scaffolds were designed and manufactured previous to this investigation at the biomaterials center, by molding poly(ethyl acrylate-co-hydroxyethyl acrylate) copolymer with 90% of ethyl acrylate monomeric units, along with various cross-linker concentrations, obtaining 4 study groups with different stiffnesses.

Biomaterials in form of discs were implanted in a 3 mm chondral defect on adult rabbit knees, previously injuring subchondral bone to allow proper blood flow for cell repopulation purposes. Controls were submitted to similar layout, with no disc implantation. As part of this investigation, animals were allowed to heal for 3 months. Regeneration was assessed through a modified cartilage repair score, morphometric analysis and histomorphological procedures, using immunohistochemistry.

Implanted scaffolds induced articular cartilage regeneration on injured surface as well as cell colonization. An inverse association with the stiffness of the scaffold was observed, featuring increased fibrous tissue in harder scaffolds. Overall, developing cell population within the scaffolds in all study groups was immature, not well differentiated, forming cartilage and bone clusters, together with scarce blood vessels and

multinucleate cells. Morphometric scrutiny revealed cartilage predominance at repaired sites and immunohistochemistry confirmed hyaline cartilage presence in selected samples. Controls originated articular cartilage with fibrous appearance when compared to native hyaline cartilage.

In conclusion, tissue engineered scaffolds induced cartilage regeneration on the injured articular surface, holding an inverse correlation with the stiffness of the biomaterial. Furthermore, cell colonization and integration with surrounding tissue was more fitting with softer biomaterials.

El objetivo de este trabajo es estudiar la regeneración *in vivo* de cartílago articular inducido por scaffolds manufacturados mediante técnicas de ingeniería tisular, evaluando la formación de neotejido inducido por diferentes andamiajes, mediante técnicas histológicas y morfométricas.

Previo al presente trabajo, en el centro de biomateriales se han diseñado y fabricado scaffolds bioestables compuestos por copolímeros de poli-etilacrilato e hidroxietil-acrilato p(EA-co-HEA), con 90% unidades monoméricas de etilacrilato, en los que se ha variado la cantidad de entrecruzador, obteniendo así 4 grupos con distintas durezas.

Estos biomateriales, en forma de discos, se han implantado tras perforar una cavidad de 3 mm de diámetro hasta el límite del hueso subcondral, dejando un lecho cruento para estimular repoblación celular, en la articulación de la rodilla de conejos New Zealand. Los controles recibieron igual tratamiento, sin implante. Como parte de este trabajo, después de 3 meses, se sacrificaron los animales y se realizó el análisis de la regeneración tisular mediante un puntaje modificado para cartílago regenerado, cuantificación morfométrica y técnicas de histolomorfología, incluyendo la inmunohistoquímica.

En los discos implantados en profundidad, la regeneración del cartílago articular y la cantidad de anidación son inversamente proporcionales a la dureza del disco, presentando más tejido

fibrótico cuanto mayor sea la dureza. En general, las células anidadas dentro de los scaffolds de todos los grupos fueron mayoritariamente indiferenciadas, formando nichos de células óseas y cartilaginosas, con presencia de neovasos y ocasionales células multinucleadas. La cuantificación morfométrica evidencia un predominio de cartílago en las superficies reparadas y ensayos inmunohistoquímicos confirmaron la presencia de cartílago hialino en muestras seleccionadas. En los controles, se regeneró el cartílago articular, pero teniendo un aspecto de fibrocartílago en superficie, comparado con cartílago nativo.

En conclusión, los scaffolds sintéticos indujeron la regeneración del cartílago en la superficie articular, de una manera inversamente proporcional a su dureza. La anidación celular e integración con el entorno también fue mejor cuanto menor fue la dureza del disco implantado.

Glossary

AB	Alcian blue
AC	Articular cartilage
ACI	Autologous chondrocyte implantation
AFSCs	Amniotic fluid derived stem cells
BGS	Bone Graft Substitute
BMP	Bone morphogenetic protein
BRU	Bone remodeling unit
CACI	Collagen autologous chondrocyte implantation
CBIT	Biomaterials & tissue engineering center
CFU-F	Fibroblast colony forming unit
CI	Confidence interval
CS	Chondroitin sulfate
DAB	Diaminobenzidine
ECM	Extra-cellular matrix
EGDMA	Ethylene glycol dimethacrylate
FC	Fibrocartilage
FGF	Fibroblast growth factor
FDA	Food and drug administration
GAGs	Glycosaminoglycans
HA	Hyaluronic acid
HC	Hyaline cartilage
HE	Hematoxylin-Eosin
ICRS	International cartilage research society
IGF	Insulin-like growth factor
IL-1	Interleukin-1
KS	Keratan sulfate

MACI	Matrix-induced autologous chondrocyte implantation
MCRS	Modified cartilage repair score
M-CSF	Macrophage colony stimulating factor
MMPs	Matrix-degrading metalloproteinases
MSCs	Mesenchymal stem cells
MT	Masson's trichrome
NZ	New Zealand
OA	Osteoarthritis
PACI	Periosteum autologous chondrocyte implantation
PBS	Phosphate buffered saline
PCL	Polycaprolactone
PEA	Poly-ethyl-acrylate
PGs	Proteoglycans
PGE_2	Prostaglandin E_2
PHEA	Poly-hydroxyl-ethyl-acrylate
PMMA	Poly-methyl-methacrylate
ROI	Region of interest
SEM	Scanning electron microscope
SZP	Superficial zone protein
TE	Tissue engineering
TGF-β	Transforming growth factor-β
TIMPs	Tissue inhibitors of metalloproteinases
TNFα	Tumor necrosis factor-α
TJR	Total joint replacement
UV	Ultra violet

Table of Contents

1. Introduction

Cartilage is a highly specialized connective tissue that delivers structural support. There are three main types of cartilage, elastic cartilage, fibrocartilage and hyaline cartilage. The later, covers bone endings at articular surfaces, where it has a typical organization, forming the articular cartilage. Such tissue provides specific mechanical weight bearing properties. Nonetheless, given its avascular, aneural physiology, its healing and repair proficiency is very limited[1].

The orthopedic community has sought to heal articular cartilage injuries through different techniques, however, the repair scar tissue, having a more fibrous content lacks, among others, mechanical load distribution characteristics, which is essential for articular purposes[2,3].

Motivated by this challenge, the innovative science branch of biotechnology through tissue engineering is in search for answers. Alternatives for cartilage repair tissue to be as analogous to original hyaline cartilage as possible are being developed. Recently, artificial biocompatible scaffolds have been designed, in order to provide a provisional mechanically stable structure that will enable cartilage matrix producing cells to build up new cartilage[4]. Experimental layouts have approached several alternatives, combining different biomaterials as well as biological and biochemical processes in hope of a repair tissue growth with similar composition and functional features comparable to original articular cartilage[5].

Our research team is composed of joint efforts between Biomaterials & tissue engineering center (CBIT) and Universidad de Valencia (UV) headed and represented by Dr. Jose Luis Gómez Ribelles and Dr. Carmen Carda respectively. Based on conclusions drawn by previous trials of our research team, where several biomaterials were tested[6-8], we have selected co-polymers poly-ethyl-acrylate and poly-hydroxyl-ethyl-acrylate (PEA-co-PHEA) at specific concentrations as scaffold polymers, which gave the best preliminary results of cartilage regeneration on *in vivo* experiments with similar experimentation subjects[9].

In addition, these previous trials addressed an issue still being object of research, regarding the use of pre-seeded cells in scaffolds, due to the chondrogenic and osteogenic potential of bone marrow cells[10-12]. In their observations, a similar repair potential obtained by pre-seeded cells in scaffolds in contrast to those not pre-seeded, was perceived. Consequently, in the present investigation, bone marrow stimulation was performed, yet no cells were seeded in the scaffolds. Moreover, it focuses on the hardness of the biomaterial by varying the amount of cross-linker concentration that ultimately resulted in different scaffold stiffnesses, while maintaining the same composition.

The foremost aim of this research is to assess the ability of tissue engineered scaffolds, to repair or regenerate articular

cartilage and subchondral bed injuries in an experimental animal model. In this thesis, a qualitative as well as a quantitative evaluation of repair tissue and scaffolds was carried out after animal sacrifice in order to assess which stiffness is most appropriate for tissue regeneration.

1.1 Osteochondral Biology

1.1.1 Cartilage Overview

Cartilage is an exceptionally specialized connective tissue derived from the intermediate embryonic layer, the mesoderm, which will originate mesenchymal condensations, at about week 5 of the fetus, where it is to develop. Eventually one of three varieties found in the human body: elastic, fibrous or hyaline cartilage. Each type of cartilage has a cellular constituent, namely chondroblasts as well as chondrocytes and an extra-cellular matrix (ECM) composed by proteoglycans (PGs), glycosaminolycans (GAGs) and fibers (collagen and/or elastic).

Elastic cartilage is present in the ear, larynx and epiglottis. It features a yellowish color and it has more elasticity and flexibility than its counterparts, due to its dense network of fine elastic fibrils that stain basophilic with HE. Additionally, fibrils of collagen are also observed, even in larger quantities than elastic fibers. Additionally, while containing primarily collagen type II, some filling of types IX, X, XI collagen can also be found[13].

Fibrocartilage (FC), a more dense variety, contains mainly type I collagen, yet type II collagen can also be present. It can be

found on intervertebral discs, menisci and bone insertions of ligaments and tendons. It can be considered as a transition between dense connective tissue and hyaline cartilage since it has dense collagenous fibers and cartilage cells within lacunae, yet its structure is similar to broad connective tissue.

Hyaline cartilage (HC) is the most common variety, and can be found on adult population mainly in traquea, bronquii as well as in mobile synovial joint surfaces; the later usually known as articular cartilage. On a regular basis it has a more firm, whiter macroscopic presentation and a predominant (90–95%) type II collagen content, although some fibrils of types VI, IX, X and XI collagen may be present as well[14,15].

1.1.2 Articular Cartilage

Articular cartilage (AC) plays a vital role in joint morphology. An understanding of articular cartilage anatomy and physiology will enable the physician to fully appreciate its function and necessity. AC serves as a load-bearing elastic material that is responsible for the frictionless movement of the surfaces of synovial articulating joints (except for sternoclavicular and temporomandibular joints composed of fibrocartilage).

Likewise, most joints are surrounded by a thick fibrous capsule, also known as articular capsule. Its outer layer (*stratum*

fibrosum) is composed of avascular white fibrous tissue and its inner layer (*stratum synoviale*) which is a secreting layer, usually described separately as the synovial membrane. Synoviocytes contained in this membrane are specialized cells that secrete synovial fluid, complementing AC function. However, the ability of AC to undergo reversible deformation depends on its structural organization, including the specific arrangement of the matrix macromolecules and the chondrocytes.

Articular cartilage development starts from early mesenchymal stages forming dense cellular clusters or cartilage nuclei, also known as chondrification centers. Cells gradually mature, protected by an outer layer, the perichondrium. Within these centers, AC growth takes place by one of two ways. Either by interstitial growth, where mitotic divisions of one differentiated cartilage cell take place within a lacuna (forming isogenic groups) or by appositional growth, where different mesenchymal stem cells around the cartilage nucleus differentiate into chondrocytes. These growth forms are present until early puberty and are diminished with increasing age[1].

Articular cartilage is composed mainly by an ECM, containing 60-80% of its weight in water and chondrocytes (within lacunes). Due to its avascular nature, it is nourished by passive diffusion of nutrients from the synovial fluid[16-18]. In a similar

fashion, nerve supply is also absent from the tissue, leading to the non-perception of injury.

The ECM is of viscous or gelatinous nature. It comprehends a dense network of type II collagen fibers, PGs and GAGs. These components interact in a molecular level, to confer precise mechanical properties ideal for weight bearing and load distribution[19-21].

The main GAGs present in the articular cartilage ECM are three: Hyaluronic acid (HA), Chondroitin sulfate (CS) and Keratan sulfate (KS). Aggrecan, on the other hand, is the most important PG. It is composed of CS and KS, joined by a core protein. They are correspondingly linked by covalent bonds to a polypeptide backbone of HA (Fig. 1). Its key feature is its hydrophilicity, which enables water retention and therefore load distribution. Furthermore, its electronegative charge also contributes in the movement of water in order to ensure electroneutrality[22-24]. This water flow modulation confers articular cartilage its viscoelastic properties. ECM homeostasis is commanded by chondrocytes, not only through the synthesis of structural components but also by the action of matrix-degrading metalloproteinases (MMPs)[25].

During the growth period, synthesis of structural molecules (collagens, PGs, proteins) is stimulated by growth factors, including Insulin growth factor (IGF-1) and Transforming

growth factor (TGF-β). ECM breakdown on the other hand, is mediated by a variety of citokines such as Interleukin (IL-1) and Tumor necrosis factor (TNFα). Complex molecular regulation of choncrocyte function has been associated with osteoarthritic degradation. MMPs and proinflamatory factors are balanced by the action of Tissue inhibitors of metalloproteinases (TIMPs), which among other molecules contribute to the regulatory mechanisms[26,27].

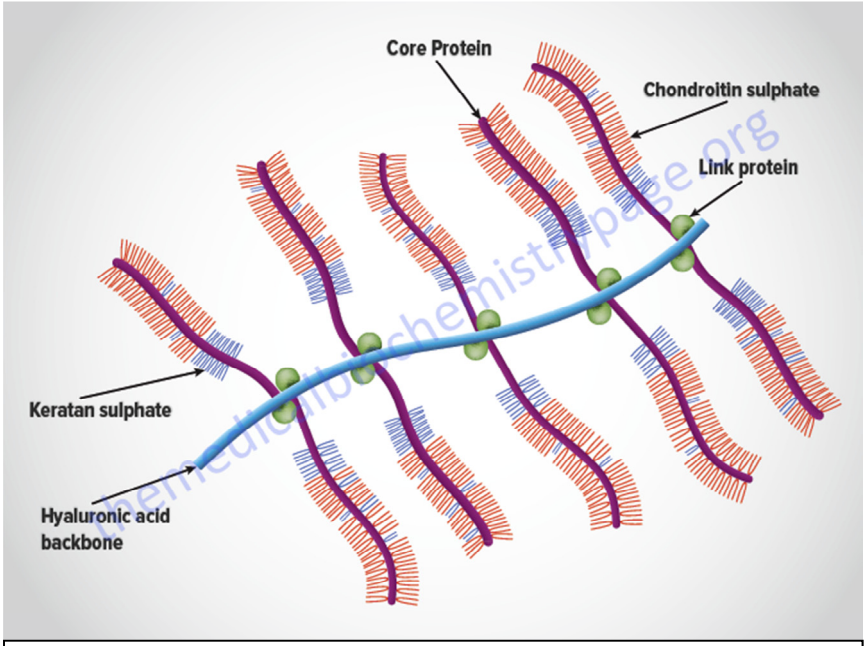

Fig. 1: Proteoglycan (Aggrecan) molecular structure. Image withdrawn from www.themedicalbiochemistrypage.org.

Cell content in articular cartilage is mainly chondroblasts and chondrocytes, which derive from mesenchymal stem cells that will be later described in bone physiology.

Chondroblasts are less differentiated cartilage cells, that originate from non-differentiated mesenchyme; they have a flattened shape and a well-developed rough endoplasmic reticulum in a basophilic cytoplasm. Their function is the elaboration of cartilage intercellular matter; under certain circumstances chondroblasts are capable of producing matrix-degrading enzymes for instance collagenase, elastase, hyaluronidase. Chondroblasts reside in the internal layer of periosteum and in the depth of matrix, within lacunes, where they mature into chondrocytes.

Chondrocytes on the other hand, are differentiated cartilage cells. They adapt to the form of the lacune that contains them, depending on the cartilage zone they are positioned. When observed through optical microscopy, they are often contracted by dehydration. Nuclear shape also varies correspondingly. As chondrocytes mature from chondroblasts, the basophilic features gradually turn into acidophilic and rough endoplasmic reticulum is retracted. Often, mature chondrocytes contain larger glycogen inclusions and small lipid droplets[1].

Regarding structure of AC (Fig. 2), it is divided into four functional zones: superficial, intermediate, deep and calcified

layers. The superficial zone has flattened chondrocytes that secrete a protein called the superficial zone protein (SZP) also known as lubricin[28,29]. This protein has been acknowledged to contribute in the lubrication at joint sites. The middle zone, composed of intermediate and deep zones, with more spherical chondrocytes, is responsible for the production of types II, IX collagen and aggrecan[30]. Usually collagen fibrils are thicker in this zone, and can be up to 110nm[31]. The calcified zone is composed of a mineralized ECM, producing the tidemark, which is a basophilic line that straddles the boundary between calcified and uncalcified cartilage. Chondrocytes are smaller than chondroblasts and have less metabolic activity. The thin calcified cartilage zone acts as a transitional zone from HC to bone, and establishes the boundary with the subchondral bone[32].

Moreover, collagen fibrils are arranged forming columns oriented vertically on the deeper layers, sustaining an arch form in the intermediate layer and assuming a horizontal pattern in the superficial zone[33,34]. Such disposition plays an important role on supporting and protecting the tissue under load bearing conditions[35].

Cartilage thickness varies depending on physiological load concentration. Under compression, articular cartilage disipates load forces by displacing water at compression site, not doing so with PGs, due to its tight network configuration with

collagen fibrils. This increases PG concentration at load bearing location. Upon removal of load, relaxation occurs as water re-expands tissue. Equilibrium is restored when swelling pressure of PGs matches tensile forces in collagen fibrils[36].

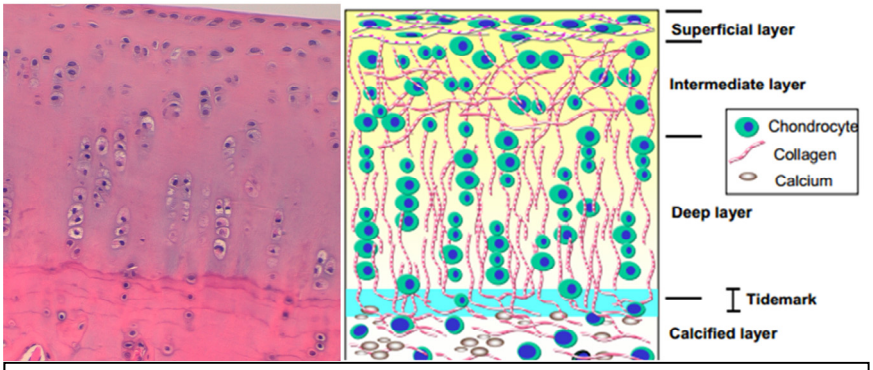

Fig. 2: Normal articular cartilage. Four functional layers are noted. Scheme from Chiang Mai University, faculty of veterinary medicine.

1.1.3 Bone Anatomy and Physiology

Bone is a variety of molded dense connective tissue, materializing the mechanical framework of the body. It is composed by organic molecules and mineralized inorganic salts that confer stiffness and rigidity. Macroscopically there are two types of bone tissue, the compact and the spongy bone. In the femoral head, for instance, both types of bone can be found directly under the cartilage coating.

Compact bone is in the outer layer of long bones, except on articular surfaces, enabling them to bear the load of body weight. Its basic unit is the osteon, also known as Haversian system. Each unit consists of concentric layers of bone (lamellae) surrounding a central canal, the Haversian canal. Inside this canal, blood supply and nerve terminals can be found. Osteocytes are located in lacunae, which are small spaces between the lamellae, and are interconnected by canaliculi for metabolic exchange. Furthermore, Volkmann's canals connect osteons to each other and the periosteum.

In contrast to compact bone, spongy bone is composed of thin columns of bone, trabeculae, containing bone marrow (cellular component). The osteon configuration is not comprehended, although most of its components are also present. This honeycombed bone is termed cancellous or trabecular, located

mostly near ends of long bones also called metaphysis, and beneath the articular surface. Given this anatomical feature, the layer of trabecular bone that is in contact with articular cartilage is also known as the subchondral bone, which will be exposed if a segment of cartilage should be lost. In mature bone, trabeculae are arranged in an orderly pattern that provides continuous units of bony tissue aligned parallel with the lines of major compressive or tensile force. Trabeculae thus provide a complex series of cross-braced interior struts arranged so as to provide maximal rigidity with minimal material[37].

The periosteum is a fibrous connective tissue that surrounds the outer layer of the bone in most of its surface, excluding the joints, which are covered by articular cartilage. Sharpey's fibers tightly attach the periosteum to the bone, and its role as bone matrix regulator is being considered[38]. The endosteum covers the inner surface of the bone, also providing nutrient exchange[39].

Bone ECM contains an organic constituent and a mineral component. The organic osteoid matrix is formed mainly by collagen (typically type I), GAGs and PGs. In adults, collagen represents 90% of this matrix, conferring bone its elastic and distraction resistant properties[1].

Mineralization, accountable for bone stiffness and compression resistance, is based on the precipitation of calcium phosphate in form of crystals of hydroxyapatite [Ca_{10} $(PO_4)_6(OH)_2$] and its subsequent growth. An increase of concentration of these components will result in precipitation, which can be down regulated by pyrophosphate, inhibiting mineral growth by storage of phosphate[40].

Cellular content in bone tissue can be categorized into 5 types: osteoprogenitor or mesenchymal stem cells (MSCs), osteoblasts, osteocytes, superficial or lining cells and osteoclasts.

Osteoprogenitor cells derive from primitive mesenchymal or pluripotent stem cells that also have the potential of differentiating into fibroblasts, chondrocytes, adipocytes, myocytes and endothelial cells. It is also known as Fibroblast colony forming unit (CFU-F). It is identified in bone marrow cultures by the colonies it originates and its capability for inducing new bone growth by connective tissue conversion [1]. Mesenchymal stem cells are fibroblast-like due to their oval, pure nucleus and clear cytoplasm with irregular limits. During bone formation, MSCs develop bone building cells during growth stages; however in adults they play an important role in bone and cartilage healing[41,42].

Osteoblasts are bone building cells in the sense that they synthesize and secrete organic bone matter (collagen fibers, PGs and GAGs, such as osteonectin, and osteocalcin). Its nucleus is usually situated at a domain in opposition to new bone formation. Cytoplasm is very basophilic and through electronic microscopy, a developed rough endoplasmic reticulum as well as a noticeable Golgi apparatus is distinguished. Osteoblasts synthesize osteoid which will be mineralized by dephosphorylation through the action of alkaline phosphatase.

Osteocytes are the actual bone cells. They play an important role in communicating the state of bone tissue to superficial bone lining cells and osteoclasts. They arise from trapped osteoblasts inside newly formed osseous matrix. Transformation into mature osteocytes features a gradual degradation of rough endoplasmic reticulum and Golgi apparatus. Once at their mature state, they do not possess the ability of further cell division[43,44].

Bone lining cells originate from osteoblasts that have finished bone remodeling and cover like a squamous epithelium all external and internal bone surfaces where there is no osteoblast or osteoclast activity. Consequently, they are disperse along the tissue. Such layer of inactive cells is critical since they lie on a thin osteoid layer (non-mineralized matrix) where bone resorption does not occur. It is therefore necessary to eliminate this layer before osteoclasts can have direct

contact with mineralized bone content and bone resorption can occur. Bone lining cells are activated (possibly by osteocyte signaling) and secrete the collagenase required to remove the non-mineralized matrix, and allow osteoclast activity [1].

Osteoclasts are bone breakdown cells. They are giant multinuclear cells with variable size and shapes. Commonly they contain 5-10 nuclei, but up to 50 in a single cell may be found. Cytoplasm in young osteoclasts is basophilic, but eventually it turns acidophilic. It contains various Golgi complexes, numerous mitochondria and primary lysosomes, that possess the ability of secreting acid phosphatase.

Bone remodeling is a process by which new bone is formed or removed respectively, depending on mechanical and/or metabolic requirements. Sequential coordination between osteoclast mediated resorption and osteoblast facilitated synthesis of new bone is achieved by means of signaling factors[45-47]. This synchronized activity is carried out by a bone remodeling unit (BRU) (Fig. 3). Upon compact bone remodeling, this unit works based on a leading edge (cutting cone) rich in osteoclasts, creating a tunnel through the calcified matrix, and a trailing edge (closing cone) where osteoblasts fill the tunnel with concentric bone lamellae[48,49].

Such complex signaling pathway, involves the release of soluble factors (Macrophage colony stimulating factor (M-CSF) and

osteoprotegerin) produced by the bone lining cells and their interaction with recruited osteoclasts[50,51]. Also, through the action of cytokines (IGF-1, PGE2), parathyroid hormone, Vitamin D and calcitonin, among other molecules, osteoblasts are stimulated to either build or resorb bone. Their counterpart, the osteoclasts are stimulated by cathepsin K and other molecules to break down bone whenever necessary to maintain calcium homeostasis.

Angiogenesis on the other hand, is also known to contribute in the process of bone remodeling and fracture healing. The lack of oxygen and the subsequent generation of angiogenic factors have shown to be critical in achieving successful bone regeneration. This area however, has not been properly explored[52].

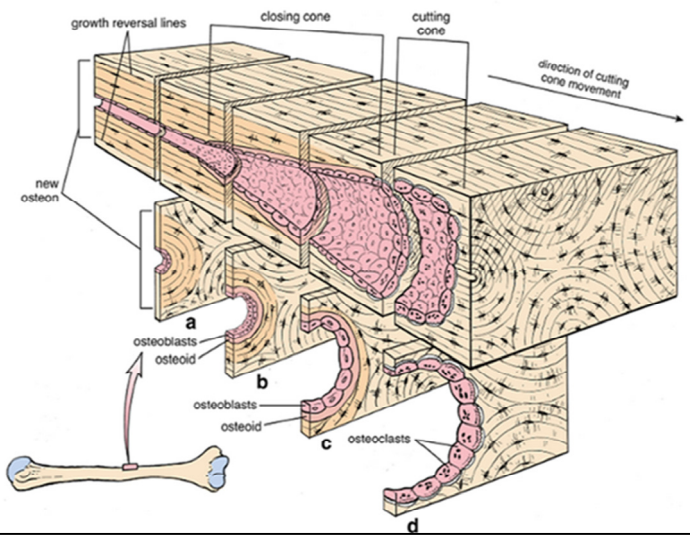

Fig. 3: Compact bone remodeling unit; Cutting and closing cone. (Histology 6th ed, Michael H. Ross and Wojciech Pawlina)

1.2 Articular cartilage injuries

Cartilage injury can be mainly originated by 3 entities: Traumatic injury, subchondral bone pathology and/or degenerative/inflammatory arthritis.

Direct cartilage trauma, or bone trauma with extension to the joint surface results in damage of cartilage microstructure. Shear forces are particularly harmful to cartilage integrity[53]. Fractures and cartilage injuries frequently comprise larger joints, such as shoulder, hip or knee, even though smaller joints are also susceptible of damage[54,55].

Subchondral bone provides a structural support for articular cartilage. Given their close relation, any pathological event in one end, distresses the other. Such is the case of avascular necrosis, or osteochondritis dissecans, where articular cartilage is damaged secondary to bone necrosis[56,57].

Arthritis is an inflammation of the joint, concerning all of its constituents, including articular cartilage. It can be classified in two main groups, according to its etiology: degenerative, or inflammatory. The later can be induced by microorganisms (bacteria, virus, fungi), and it is known as septic arthritis. Reactive arthritis is related to bacterial infection at a remote site with a following aseptical inflammation in a given joint

mediated by a cross reaction of a linked antigen present at joint site.

Autoimmune arthritis refers to rheumatoid related backgrounds. Finally, microcrystals usually of sodium urate or calcium pyrophosphate, have the potential to generate an inflammatory state as well.

Degenerative arthritis, commonly known as osteoarthritis (OA) is mostly linked to a mechanical cause, but it is also multifactorial. Additionally it is more prevalent in women than men and in increases with age[58,59]. Associated factors such as limb malalignment or menisci resections increase load forces on focal points, contributing to the prompter deterioration of cartilage.

On an experimental model of OA, changes in the appearance and distribution of the chondrocytes preceded damage to articular surfaces. A slight increase in cell density and occasional lacunae with two nuclei were evident one week after the operation inducing OA. Fibrillation of cartilage gradually progresses with time, until, after seven weeks, deep clefts are evident. By sixteen weeks, the cartilage matrix was highly cellular, clones of two or more cells were abundant particularly around severely fibrillated sites, the lacunae were enlarged compared with controls and many vacant lacunae were evident; erosion of the articular surface layer was complete[60].

Despite these histological findings in animals, most of epidemiologic studies are based on radiologic analysis. Some authors even sustain that OA is the most common joint disease in the world, with 80% of population older than 75 years showing degenerative changes[61].

Cartilage injuries are described according to different criteria, including localization, severity, size and morphology. Injuries at load-bearing sites are of particular clinical relevance, being the focus of reconstruction on clinical settings. In order to establish the severity of cartilage injury, clinicians often use the Outerbridge classification or the recently published classification by the International cartilage research society (ICRS)[62,63]; (Table 1). Partial thickness injuries are distinguished from full-thickness ones, that also include subchondral bone. Staging is usually performed during arthroscopy procedures, where a real-time morphologic description is feasible however and classification through non-invasive imaging techniques are also possible[64-66].

Cartilage injury has been focus of intense research over the years, due to its vast prevalence and limited healing potential. Physiological repair mechanisms are limited by age and affected joint among other factors. Spontaneous growth of scar tissue, or fibrocartilage, covers injured area, lacking mechanical properties for load bearing. Under these conditions, cartilage develops degenerative changes that eventually require clinical

intervention. Moreover, a critical injury size of 6 mm has been described, where no spontaneous healing is observed and even extended degeneration is detected[67].

Even though partial-thickness damages are less severe than full-thickness cartilage injuries, the healing potential of the former is limited. Due to the lack of blood supply of AC, in a superficial injury, chondrocytes through activation can generate a mixed scar tissue of poor quality. In contrast, when subchondral bone is exposed, repair process is favored by bone marrow pluripotent cells as well as the cascade of healing events provided by blood flow. Such repair tissue partakes a still high content of collagen I, present in fibrocartilage, which will begin degradation after 24 months[68].

Grade	Outerbridge	ICRS
0	Normal cartilage	Normal cartilage
I	Softening and swelling of cartilage	Nearly Normal (soft indentation and/or superficial fissures and cracks
II	Fragmentation and fissuring, less than 0.5-inch diameter	Abnormal (lesions extending down to <50% of cartilage depth)
III	Fragmentation and fissuring, greater than 0.5-inch diameter	Severly Abnormal (cartilage defects >50% of cartilage depth)
IV	Erosion of cartilage down to exposed subchondral bone	Severly abnormal (through the subchondral bone)

Table 1: Classification of cartilage injury. Adopted from www.eorif.com

1.3 Current articular cartilage repair techniques

Clinicians have sought different strategies to treat AC injuries with mainly two objectives. First, decrease general symptoms and second, prevent or slow down the degenerative process of joint surface. The ideal repair technique would not only fulfill the initial objectives, but would return mechanical properties of HC. Different attempts and approaches have been suggested; nevertheless, the desired effects are not exactly encountered. While some techniques diminish clinical symptoms, not only the degenerative process lingers, but ultrastuctural characteristics of HC have not yet been fully reproduced. From a conservative approach by means of joint lavage, science has developed remarkable strategies like subchondral bone stimulation and osteochondral repair in an attempt to stimulate natural healing. Recently, a tissue engineering approach has not only complemented former knowledge, but it also withholds an exciting promise for tissue regeneration[69].

1.3.1 Joint lavage

Joint lavage is a technique that seeks the elimination of cartilage break-down products (debris), enzymes or crystal remnants present in joint space. Lavage is performed by

injecting the joint with saline, along with the drainage of joint fluid. The cycle of injection and drainage may be repeated several times. Through this procedure chondrocytes might be able to regulate the catabolic process at initial OA stages. Theoretically, removal of debris in the joint would decrease inflammation and thus joint pain. Different hypothesis postulate that the renewal of synovial fluid and joint capsule pressure variations might also contribute to the improvement of symptoms, especially in rheumatoid patients[70].

Tidal irrigation uses one point of entry into the joint to inject sterile fluid and draw fluid out. Non-arthroscopic joint lavage uses two points of entry into the joint, one to inject fluid and the other to draw fluid out; no visual inspection of the joint occurs. Nowadays, arthroscopic joint lavage is most commonly used, with visual real-time inspection of the joint and the possibility to repair other structures such as meniscus or unstable cartilage flaps simultaneously. A more recent point of discussion has been if to remodel cartilage by mechanical or electrothermic techniques[71,72].

The effectiveness of joint lavage has been questioned and studied. According to Cochrane's review of 7 clinical trials involving 567 patients[73], joint lavage does not produce a significant benefit for patients with knee osteoarthritis with regard to pain relief or improvement in joint function. Three of the 7 trials involved arthroscopic joint lavage. Two of the

studies involved non-arthroscopic joint lavage, and two were tidal irrigation. In 2008, the American Academy of Orthopedic Surgeons published 22 recommendations for the treatment of symptomatic knee osteoarthritis[74]. However, arthroscopy with debridement or joint lavage was not recommended to treat symptomatic knee osteoarthritis since there was no evidence of significant benefit[75]. Due to the lack of scientific support, other techniques have been explored.

1.3.2 Subchondral bone marrow stimulation

Subchondral bone stimulation is based on the healing potential of full-thickness AC injuries, where subchondral bone is exposed. Pluripotent stem cells could lead to a better cartilage repair, nevertheless, the resultant fibrocartilage is mainly built by type-I collagen. Around the mid 50's, Kenneth Pridie described a method of resurfacing knee joints, by perforating the subchondral bone with a Kirschner wire[76,77]. This technique has evolved to modern alternatives with electrical drills, maintaining the same principle of stimulating blood flow from bone marrow. Microfracture, drilling, and abrasion arthroplasty are considered marrow stimulation techniques[78,79].

Some technical challenges have risen in the process; angle and depth of perforation, speed of drills and thermic effects are still

being discussed. Nevertheless, this approach is widely accepted and performed in small diameter cartilage injuries. It is also a valid approach in degenerative cartilage injuries given the fact that it stimulates the repair process. Clinical outcomes have been acceptable in the sense that there is a symptomatic improvement in 3 out of 4 patients, even though the scar tissue has a mixed cartilage component.

1.3.3 Osteochondral repair

More recent surgical strategies pursue the repair or regeneration of cartilage, particularly in weight-bearing surfaces. Osteochondral allograft is a piece of tissue taken from human donors, processed and cryopreserved by bone and tissue banks in order to decrease the immune response once implanted. This process has led to increased susceptibility of chondrocytes to cell death and consequently, graft failure[80,81].

Autografts, on the other hand, do not have this problem, since they are harvested from the same patient; ideally from the same joint, to avoid donor site morbidity. Theoretically, osteochondral tissue can be harvested from non-load-bearing sites, transferring and implanting it at weight-bearing locations such as femoral condyles. This process was described as mosaicplasty (Fig. 4). This technique was proposed for injuries up to 4 cms, to be used in patients younger than 50 years old.

Indications also exclude any mechanical or inflammatory disease of the joint, including dysplasia or neoplastic growth[82-85].

Histologically, HC is observed at transplanted site at eight weeks, with a support of trabecular subchondral bone and FC can be identified at harvest site. Even though there is morbidity at donor site, it is trivial; however success rates have been associated with less weight of patients[86].

This technique is easily accomplished by placing the greater diameter allografts in a lesser diameter bed in a press-fit fashion. Even though osteochondral grafts achieve good stability, mosaicplasty is limited to a few autogenous donor sites that in most cases are unable to fill the entire injured surface. Remaining space should be supplemented with additional techniques.

Periosteum and perichondrium transplants have also been proposed as alternatives to repair the injured osteochondral surface[87]. Several difficulties have been encountered, including the attachment or suture to host uninjured cartilage[88]. The rapid decrease in biologic potential of cells and cartilage component macromolecules has led to inconsistent results[89,90].

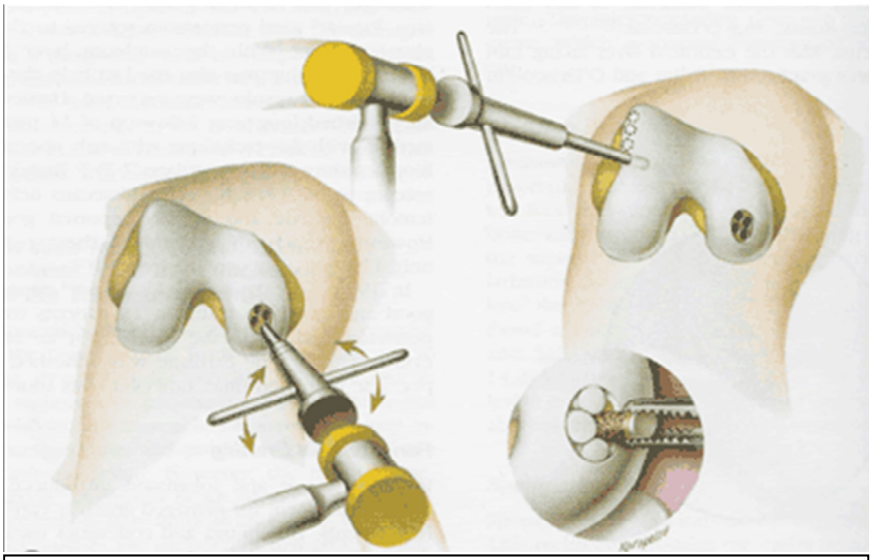

Fig. 4: Mosaicplasty. Note press-fit implantation. (Image from kneejointsurgery.com, Leeds, Yorkshire)

In 1994, Brittberg *et al.* introduced the concept of autologous chondrocyte implantation (ACI) with good clinical and histological results. This technique consists of three phases. In the first phase, during arthroscopy, harvested a minimum amount of autogenous cartilage is performed. In the second phase, chondrocytes are isolated from harvested cartilage tissue, cultured and expanded *in vitro*. On a third and last phase, chondrocytes are injected and seeded onto the defect that has been covered with a periosteum flap [Periosteum autologous chondrocyte implantation (PACI)] and sealed with a fibrin cloth[91].

Problems of abrasion force leads to suture failure and an unsuccessful outcomes. Furthermore, donor site morbidity at

periosteum flap and graft hypertrophy encouraged the development of the second generation of ACI techniques. By replacing the periosteal flap with a porcine collagen membrane as a graft covering, the Collagen-covered ACI (CACI) was introduced[92]. Even though promising, several problems were later encountered. Even cell distribution could not be ensured by either ACI generations, which require chondrocyte suspension to be injected under the chosen covering. Likewise, both methods require the graft to be sutured in place, which had later been associated with poor outcomes.

Matrix-induced autologous chondrocyte implantation (MACI) was developed as a third generation of ACI, where cells are seeded onto a biodegradable porous matrix to create cartilage. Biomaterial adapts entirely and in a press-fit manner to the cartilage injury, while maintaining a structure for tissue regeneration[93,94].

A general weakness of these therapeutic strategies is that the newly formed tissue lacks the structural organization of articular cartilage and has inferior mechanical properties compared to native tissue, and is therefore prone to failure. The contribution that cartilage tissue engineering can make, is to create a more durable and functional replacement of the degenerated tissue, or to stimulate regeneration of new hyaline cartilage tissue, which is therefore more likely to bear the mechanical conditions in a joint after implantation. One

ultimate goal in this field of research is to develop a replacement tissue that has a structure and composition resembling native cartilage, yielding similar mechanical behavior and which fully restores joint functionality.

Each joint has different mechanical demands, and behaves in a particular manner depending on forces acting upon it. Still, any joint is mechanically a very demanding environment. During joint loading, a normal stress is uniformly imparted to the chondrocytes.

As the tissue undergoes a compressive load, the pressurization of the fluid phase initially supports the applied load, because water is trapped within the solid matrix of the tissue. Although theoretically the total stress from pressurization is uniform, the stress may vary throughout the cartilage on a joint surface, thus leading to gradients in total stress and pressure, particularly near the joint surface. Eventually, fluid is expelled from the tissue, and the frictional force between the fluid and solid phases of the tissue dissipates energy from the applied load. In the joint, cartilage is typically exposed to stresses between 3 and 10 MPa[95], with stress as high as 18 MPa having been reported in the hip joint[96].

These stresses should be translated to hydrostatic pressure due to fluid phase pressurization, as described above. Additionally, the human walking cadence generally is up to 1 Hz[97]. As such,

tissue engineering efforts have generally focused on magnitudes and frequencies within these physiologic ranges[98].

An evolution in scientific rationale and improved clinical outcomes has made of these techniques a valid strategy to treat greater cartilage injuries in high-demand patients. Nonetheless, a satisfactory healed hyaline cartilage tissue has not been able to be restored.

Current strategies in human medicine for treatment of diffuse joint degeneration rely on replacement of the whole degenerated joint with inert implants[99-102] (Fig. 5). Excellent treatment outcome has been achieved for up to 15 to 20 years, but approximately 20% of treated patients require revision procedures after this time[103,104]. For younger patients this current state-of-the-art may translate to two or more revision surgeries during their lifetime. A biological solution to repair damaged cartilage that would provide life-long pain relief would be a major medical achievement.

On the whole, independent of surgical technique performed, the process of rehabilitation plays a critical role. Physiotherapy and continuous passive movement contribute to the integral management of cartilage injuries[105-107].

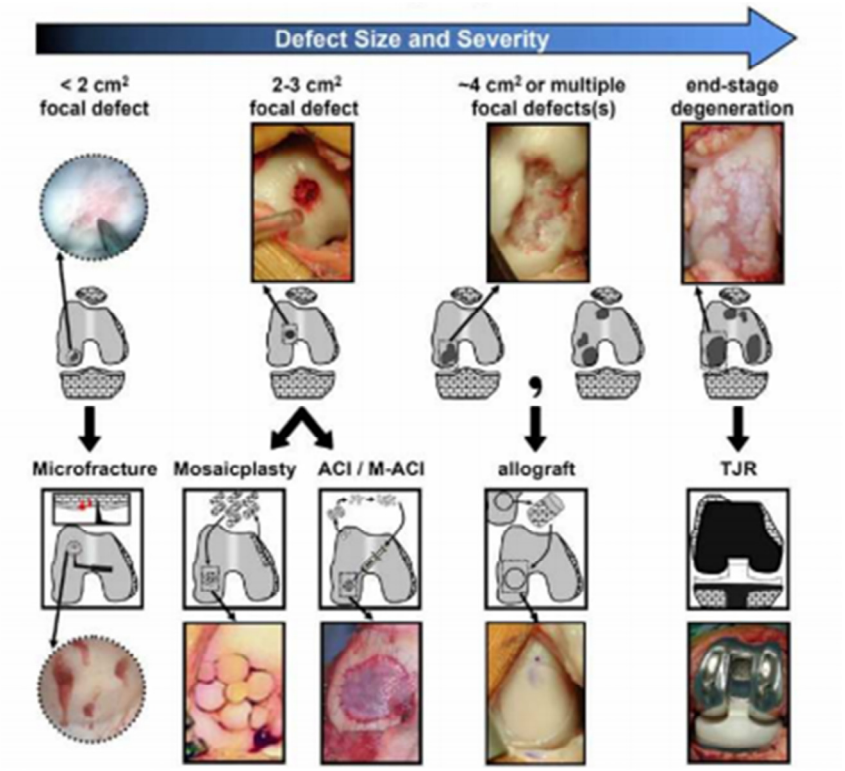

Fig. 5: Current treatment for articular cartilage degeneration. Printed from Williams *et al*. 2010[102].

1.3.4 Tissue engineering approach

Tissue engineering (TE) is an evolving interdisciplinary field that applies the principles of engineering and life sciences toward the development of biological substitutes that restore, maintain, or improve tissue function, providing permanent solutions to millions of people in distress caused by tissue damage and tissue loss[108]. The basic approach of tissue engineering involves the use of cells, scaffolds and signaling factors, also known as the TE triad. By means of controlled stimulation of selected target cells, contained in a support structure which may be a scaffold, a matrix, or a membrane, through a systematic combination of molecular and mechanical signals, new tissue can be regenerated.

The optimal cell source for cartilage tissue engineering is still being identified. Chondrocytes, fibroblasts, stem cells and genetically modified cells have all been explored for their potential as a viable cell source for cartilage repair[109-112]. Chondrocytes are found in native cartilage and have been extensively studied to assess their role in producing, maintaining and remodeling the cartilage ECM. Fibroblasts are easily obtained in high numbers and can be redirected toward a chondrogenic phenotype. Recent work has focused on stem cells, which have multi-lineage potential and can be isolated from a variety of tissues. These progenitor cells can be expanded through several passages without loss of

differentiation potential[113]. Additionally, all of these cells can be modified genetically to induce or enhance chondrogenesis. The goal in cartilage TE is to find an ideal cell source that can be easily isolated, capable of expansion and cultured to express as well as synthesize cartilage specific molecules (e.g., type II collagen and aggrecan)[114,115].

Scaffolds provide the mechanical support necessary for cells to settle and synthesize new tissue. The primary focus has been on polymeric materials, in forms of hydrogels, sponges and fibrous meshes. Scaffolds provide a 3D environment that is desirable for the production of cartilaginous tissue[116,117]. It should have certain properties such as: have directed and controlled degradation, allow for the diffusion of nutrients and waste products, adhere and integrate with the surrounding native cartilage and provide mechanical integrity depending on the defect location, among others.

To date, a wide range of natural and synthetic materials have been investigated as scaffolding for cartilage repair. Synthetic polymers include: poly(α-hydroxy esters), poly(ethylene glycol/oxide), poly(propylene fumarate), poly(urethane), poly(vinyl alcohol), poly(lactic-co-glycolic acid), among others[118-125]. Natural polymers that have been explored as bioactive scaffolds for cartilage engineering include: alginate, agarose, fibrin, HA, collagen, gelatin, chitosan, chondroitin sulfate, and cellulose[126-134].

In scaffold designing, the hydrophilic/hydrophobic balance in the material influences the adherence of cells to the scaffold walls and confers the scaffold biodegradable properties[7,135-139].

Naturally derived polymers for cartilage regeneration have good cell interaction and hydrophilicity but they are mechanically too fragile to maintain the desired shape until newly formed tissue matures. However, biodegradable polymers need to improve the hydrophilicity to hinder cell attachment and protein adsorption on their surface. It is widely accepted that if chondrocytes adhere to the pore walls of a scaffold, despite the 3D environment, they tend to dedifferentiate[140-143]. For an adequate regeneration, cell arrangement should be more similar to what occurs in nature, where chondrocytes are situated in lacunae embedded into a hydrophilic ECM. In fact, recent strategies have been described to modify biomaterials in order to increase hydrophilicity[144]. Likewise, previous work in our group recognized the best suitable hydrophilic/hydrophobic proportions of acrylate polymers that stimulate cartilage cell growth[7,137,145-147].

Not only the nature of scaffolds influences the healing role of the implant, but also the percentage of porosity and pore dimensions. Depending on biomaterial origin and characteristics, interconnected pores from 200 to 400 μm diameter and 90% porosity provide a reasonable environment for chondrogenesis[148].

As the third component of the tissue engineering triad, stimulating factors have been employed to induce, accelerate, and enhance cartilage formation[149-151]. Growth factors such as TGF-β, fibroblast growth factor (FGF), bone morphogenetic protein (BMP), and IGF, along with other soluble factors like HA, CS, and insulin, have been explored for their effects on cartilage tissue engineering. BMPs in particular, impact both chondrogenesis and osteogenesis, as they can assist osteochondral integration at the implant site. These morphogens regulate chondrocyte differentiation states and ECM composition. Specifically, BMP-2 and -7 act synergistically and have been shown to increase matrix production in chondrocytes and progenitor cells[152]. In addition, gene therapy has developed as another method of local delivery, where cells can be engineered to over-express bioactive molecules[153]. Finally, mechanical signals have also been explored, through loading regimes such as hydrostatic or dynamic compression. All of these methods have led to enhanced cartilage production[154,155].

Bone tissue, as a vital and functional support of AC has also been subject of research. As for cartilage TE, bone TE relies on the same areas of focus, such as cell sourcing, scaffolds design and stimulating agents. Bone marrow derived mesenchymal stromal cells, endothelial cells isolated from umbilical cord, and adipose stem cells have been explored[156,157].

In bone TE, scaffolds provide support in the formation of tissue, also playing an essential role in cell growth and differentiation. Various biomaterials and bioactive ceramics have also been subject of research[158]. The recommended pore size for a scaffold is 200-500 μm. Relatively larger interconnected pores favor direct osteogenesis, since they allow migration of cells, vascularization and high oxygenation. Nonetheless, an uncontrolled increase in the void volume results in a reduction in mechanical strength of the scaffold, which can be critical for regeneration in load-bearing bones[159,160].

Recently, TE research has proposed the osteochondral repair as an alternative to the cartilage repair strategy[161-165]. The assembly of bi or multilayered structures has been described[166,167]. These bilayer scaffolds should be suitable to incorporate two different tissues, satisfying the different biological requirements. Thus, heterogeneous structures are being built, in which one of the sides promotes cartilage regeneration and the other region, exhibiting different properties, encourages bone integration[167-173]. Recently, commercial products such as the Smith & Nephew TRUFIT™ Bone Graft Substitute (BGS) Plug, manufactured from POLYGRAFT® material, a blend of poly DL-lactide-co-glycolide, calcium sulfate, polyglycolide fibers and surfactant, has been indicated for use in filling bony voids or gaps caused by trauma or surgery that are not intrinsic to the stability of the bony structure. TRUFIT BGS Plugs are indicated to be gently packed

into bony voids or gaps of the skeletal system[174,175]. These defects may be surgically created osseous defects or osseous defects created from traumatic injury to the bone. TRUFIT BGS Plugs provide a bone void filler that resorbs and is replaced with bone during the healing process. However, the overall short-term clinical and MRI outcome of the osteochondral scaffold plug for cartilage repair in the knee is modest. In a pilot study a modest clinical improvement became apparent at 12 months of follow-up. MRI data showed no deterioration of the repair tissue, but 20% of the patients had persistent clinical symptoms after surgery[176].

1.4 Morphometric analysis in histopathology

The histopathological analysis of samples has traditionally been completed through a series of qualitative descriptions made by qualified pathologists[177]. However, characterization of certain pathological entities sometimes requires not only qualitative description, but also quantitative evaluation, an thus morphometry is especially useful for quantitative assessment that escapes trained discrimination[178].

Morphometry epistemologically means the "measurement of shapes". It is defined as a quantitative description or the techniques used to characterize dimensional properties of objects. Moreover, it is able to quantify different parameters such as area, perimeter, diameter, texture, or relationship with contiguous structures[179].

Depending on its particular use, static measures should undergo validation and standardization of assessment criteria, which could decrease intra and inter-observer variability, increasing sensitivity on identifying minimal cell changes and lower laboratory costs[180,181].

Morphometry has been used for several purposes, but most of all the study of cancer, where quantification of cells and nuclear

categorization becomes a key issue[182-184]. Moreover, morphometry, by computer-aided image analysis, can form a simple, relatively less expensive, and an effective diagnostic tool to sort out malignant cells by evaluation of various parameters, especially nuclear and cytoplasmic variables of the atypical cells. With the advent of image analysis and automatic softwares, various cell measurements can be carried out in a more objective, time-conserving manner, with reproducible results in the form of selected digital images. A range of cellular parameters, including nuclear shape, area, and optical density can be evaluated[185].

The studies on articular cartilage have been traditionally based on individual observations but this approach is limited by its subjectivity and bias, yielding considerable variability. Computerized morphometric analysis provides a simple, reliable, and reproducible method for improved and consistent results. Image analysis software for quantitative analysis of articular cartilage is one of the tools that has been explored in various research works. Articular cartilage has been approached on New Zealand rabbits as experimental models, as well as humans. Rubin describes the effects on prednisolone on rabbit chondrocytes[186], while Goyal, for instance, makes an interesting approach on typifying AC morphology according to age difference for the study of osteoarthritis[187]. In contrast, no studies that we are aware of have been published using the morphometric approach to scrutinize cartilage tissue

regeneration on tissue engineered scaffolds. Our research team however, has shown preliminary results on the use of morphometry for assessment of cartilage regeneration in local scientific meetings.[188]

The general process of measurement begins at histological slides, which implies a 2 dimension interpretation. Third dimension and volume estimates involve a series of complex mathematical calculations called stereology that are limited by the nature of the biologic sample itself.

The digital analysis of histologic images consists of specialized software that processes digitalized information captured from microscope. Internal calibration and standardization by an expert observer can considerably reduce errors. Each pixel stores image data in lines and columns. Histogram reveals different peaks ideally with a normal distribution. At this point, not only visual control of measured elements is promising, but also data banks can be uploaded based on epidemiologic standards[189]. Once image has been captured, it is important to have an optimum contrast which enables distinction of objects of interest from background.

Afterward, the process of separation or segmentation, is completed by assigning reference color values to a certain label and selecting all pixel matrix values. The matching pixel values will be ordered to the allotted group of interest. Finally, a

region of interest (ROI) is outlined and object quantification is possible[190]. Techniques may vary depending on subject studied; for our purposes, we did not count objects but rather measured areas occupied by previously identified tissues.

In spite of various investigations using morphometric tools[180,191], particularly in cartilage tissue[192-194], it is important to highlight that morphometry is an important assessment tool for diagnostic and research purposes, however it should not be interpreted as a substitute of traditional methods.

1.5 General and specific objectives

1.5.1 General objective

The central aim of our research is to assess *in vivo* articular cartilage regeneration induced by tissue engineered [P(EA-co-HEA)] scaffolds with different stiffnesses and porosities on a rabbit experimental model, based on histomorphological studies.

1.5.2 Specific objectives

- Morphological typification of repair tissue by means of routine and special histological techniques, including immunohistochemical methods.
- Histological analysis and correlation with conditioning factors of repair tissue growth at injury site as well as within implants.
- Morphometric quantification of growth tissue relative to implantation site and biomaterial characteristics.
- Based on histological and morphometric evaluations, determine the optimum cross-linker concentration that best enables acrylate polymer scaffolds heal cartilage injuries.

1.6 Hypothesis

Biological repair tissue of articular cartilage injuries has suboptimal mechanical properties. Through tissue engineering techniques, poly-ethyl-acrylate and poly-hydroxyl-ethyl-acrylate co-polymers [P(EA-co-HEA)] scaffolds have been implanted on experimental animals to investigate the repair tissue growth and their relation to biomaterial stiffness.

Our hypothesis postulates that P(EA-co-HEA) scaffolds will induce a suitable biological response similar to native articular cartilage. Furthermore, based on scaffold structure, we presume a close correlation of the stiffness and porosity of the biomaterial with the type and characteristics of repair tissue growth.

2. Methodology

2.1 Scaffold manufacturing for tissue engineering

Biomaterial selection and scaffold synthesis were made by Polytechnic University of Valencia, through the Biomaterials and Tissue Engineering Center (CBIT), under the direction of Dr. Jose Luis Gómez Ribelles. This part of the project was not made by the author, and it is a part of Ms. Antolinos Turpin's thesis, not a part of the present thesis.

Among factors that affect protein adsorption and cell adhesion are composition of biomaterial and its mechanical properties. According to Pérez Olmedilla *et. al.*[7], the spatial distribution of hydrophilic domains in a polymer substrate can be crucial for the cell adhesion, viability and proliferation of human chondrocytes cultured in vitro. Good biological response was obtained in monolayer culture on a p(EA-co-HEMA), presenting phase separation with hydrophobous domains of nanometric dimensions dispersed in a hydrophilic matrix consisting in a copolymer richer in PHEMA than the average composition. This among other former research led by this group, in joint efforts with our research group, led us to focus on poly(ethyl acrylate-co-hydroxyethyl acrylate) [P(EA-co-HEA)], copolymer with 90% of ethyl acrylate monomeric units[8,9,139,145,147].

A 10% fraction of total polymer weight adds a Hydroxyl group, which will react with variable quantities of a cross-linking substrate, ethylene glycol dimethacrylate (EGDMA); thus conferring different stiffnesses to the polymer, according to the cross-linking concentration.

At CBIT, manufactured by Ms Antolinos Turpin, a porous structure was generated from a template (negative scaffold) using poly(methyl methacrylate) (PMMA), microspheres of known size, 90 ± 10 μm as porogen (Lucite PMMA Colacryl dp 300). Templates were synthesized by using a press under constant pressure and temperature above vitreous transition of PMMA on three stages. First stage, at 150ºC, 100 Bar, during 8 minutes. Second stage at 150ºC, 100 Bar during 4 minutes. Third stage at 150ºC, 200 Bar, during 25 seconds. Microspheres were placed under conditions to allow slight deformation and adhesion. Interconnection of pores was controlled due to constant pressure applied[195]. Two mm thick templates were cooled down and prepared for polymerization.

Precursor monomers (EA and HEA) were weighed and proportionally mixed the mass percentage to fit the 90%-10% protocol of P(EA-co-HEA). Afterward, 1%, 2%, 5% and 7% respectively, of EDGMA as cross linker and 0,5% benzoin as polymerization reaction starter were added.

Calculations to find the mass of necessary monomer were performed at CBIT, starting from a total mass (m_T) of 10 gr. Afterwards, monomer solution was poured by means of a pipette over the porous template and packed in sealed glass frames for polymerization. Next, it was polymerized during 24 hours under UV rays at room temperature. Then, postpolymerization was carried out during additional 24 hours at 90ºC. Templates were at that point retrieved from glass frames and washed by a sohxlet washer using acetone to eliminate the PMMA porogen. (Fig. 6). This process was done through 4 washing cycles of 8 hours each, changing the acetone residue between each cycle.

Subsequently, acetone was progressively displaced by distilled water to avoid scaffold template collapse, maintaining desired dimensions. After a 48 hour vacuum drying period at room temperature, 3-4 mm diameter and 1 mm thick rounded molds were punched out from the template. Finally, all discs were sterilized by 25 kGy Gamma radiation.

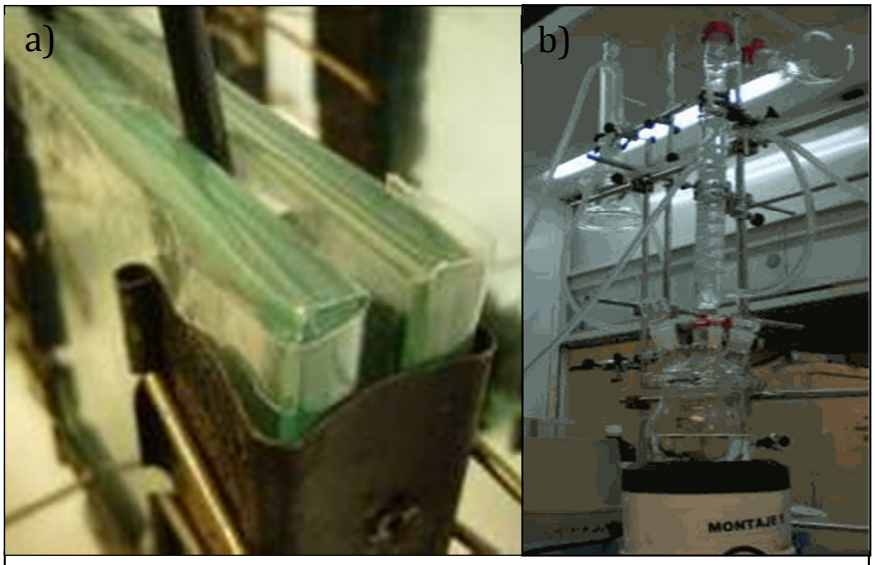

Fig. 6: Scaffold manufacturing. a) Sealed glass frames for polymerization. b) Sohxlet washer. Courtesy of biomaterials and tissue engineering center, UPV.

Four groups of scaffolds were manufactured, all of them with the same copolymer composition P(EA-co-HEA) and different cross-linking concentrations (Table 2). Each scaffold group was assigned to experimental animals according to study protocol.

Group	EA	HEA	EGDMA	Porosity	Solid Biomaterial
A	90%	10%	1%	82%	18%
B	90%	10%	2%	84%	16%
C	90%	10%	5%	88%	18%
D	90%	10%	7%	67%	23%

Table 2: Composition and porosity of scaffold groups.

Concerning scaffold characterization, PEA is hydrophobic, while P(EA-co-HEA) has slightly decreased hydrophobicity due to the hydrophilic component of HEA.

The porosity of the resultant scaffold (Table 2) was calculated through a series of formulas and measurements at CBIT during the manufacturing process.

The morphology of scaffolds assigned to the 4 trial groups (Fig. 7) was detailed through a cryogenic scanning electron microscope (CryoSEM) (JEOL JSM 5410).

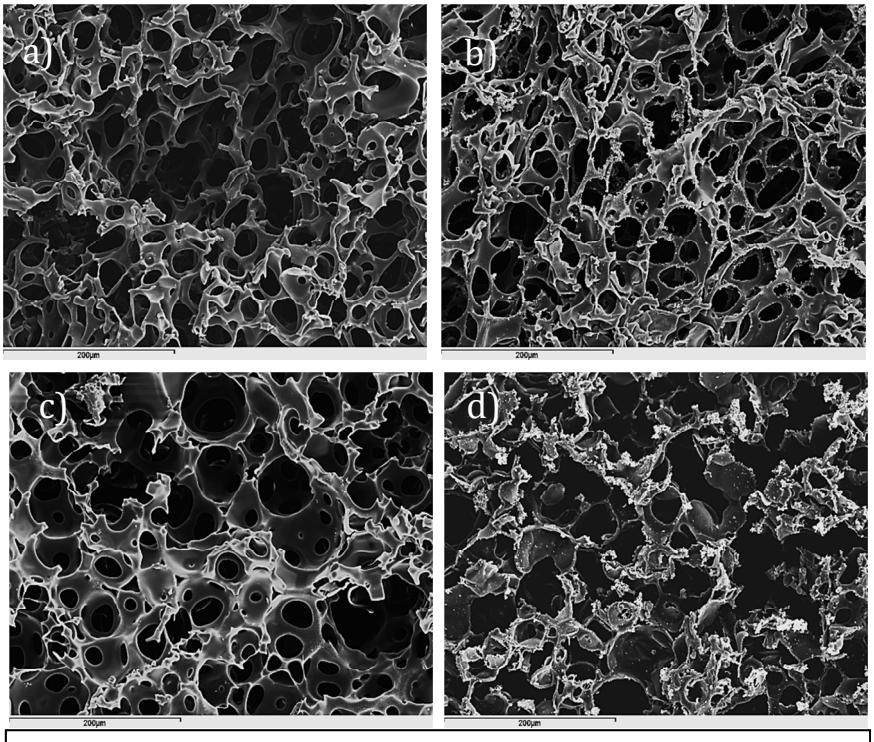

Fig. 7 : Scanning electron microscope (SEM) photography a) Group A, b) Group B, c) Group C, d) Group D. All pictures were taken at 250x. Courtesy of biomaterials and tissue engineering center, UPV, as part of Ms. Antolinos Turpin's thesis.

2.2 Experimental population

2.2.1 Animal characterization

To carry out our research we have chosen the rabbit as an experimentation animal, due to its anatomical resemblance to human knees, accessible stabling, costs and high volume of previous published literature[196-199].

Rabbits were obtained from Granja San Bernardo de Tulebras (Navarra, Spain). Research protocol was approved by Universidad de Valencia ethics committee according to laws 86/609/EEC; 214/1997 & 164/1998 from state territory Generalitat Valenciana. Previous experimentation with the same biomaterial composition proved biocompatibility[9]. A total of 35 samples were processed. However, 4 samples were lost during process due to lack of scaffold attachment for further analysis. Therefore 31 samples were analyzed. However, due to early animal decease (two at operating room and one for digestive pathology 3 weeks after surgery), three samples have been described, but not included for statistical analysis, which results in a final n of 28.

New Zealand (NZ) rabbits (Fig. 8) have been our focus, due to their size and docile behavior, ideal for pre and post operatory management. We used white fur coat rabbits given they are the

most common color. Typically they have a rounded head, short neck and red eyes. The adult animal can weigh 4 – 5 thousand grams and measure 60 cms long. Our experimental population was 20 weeks old at the time of the surgery. Animal stabling was carried out according to law; RD 1201/2005 on experimental animal protection. Rabbit characteristics require sufficient stabling space (2,200 cm^2 x 40 cm high) for growth and free movement until scheduled sacrifice. Animals were stabled at least 72 hours prior to procedure on individual cages for environment adaptation. Identification marks were placed on internal right ear as well as the corresponding stabling cage.

2.2.2 Surgical procedure

All surgical procedures were carried out by the same orthopedic group of physicians, Doctors Forriol and Gastaldi, at the research central unit of the school of medicine and odontology of Universidad de Valencia. Hand surgery instruments were employed, fitting proportionally the surgical animal site.

Dimensions of NZ rabbits were fitting for anesthetic and surgical purposes. Thirty minutes before surgical procedure, intramuscular sedatives [Ketamine (Pfizer) 15 mg/Kg & Metomidine (Pfizer) 0,1 mg/Kg] and antibiotic profilaxis [Cefazolin (Normon) 20 mg/Kg] were provided. An intravascular access was kept on the auricular vein with

maintenance saline infusion. Knee fur at surgical site was removed immediately before entering operating room. Anesthetic procedure was carried out by veterinary staff of the central research unit. After initial sedatives, inhalatory anesthesia was maintained with 1,5% Isoflurane (Abbott Laboratories) through respiratory mask. Intramuscular ketoprofen [Sanofi-Aventis (1mg/Kg)] was provided as anti-inflammatory agent. Rabbit was placed face upward on the operating table, securing both posterior extremities to the table, with knees at 110º flexion. Aseptic standard surgical techniques and antiseptic measures with Iodine solution were taken. With the flexed knee, we identified anatomical repairs such as patella, quadriceps tendon and patellar tendon. A 20 mm medial parapatellar incision was performed, ensuring a 5 mm proximal margin from internal superior pole of the patella and 3 – 5 mm distal margin from tibial tubercle. The fine subcutaneous tissue was dissected and superior medial genicular artery was ligated for hemostatic purposes. Subsequently, medial arthrotomy was performed (longer than skin window), and we found a variable venous blood bed at Hoffa fat pad, which was controlled by a hemostatic clamp. Once hemostatic control was achieved, with extended knee, patella and extensor mechanism was subluxated laterally. At the center of femoral trochlear notch, a 3 mm round cartilage injury (Fig. 9) was made with a dermatologic biopsy devise, through gentle circular movements.

Depth was freehand completed until subchondral blood bed from bone was identified. Native cartilage was extracted, leaving a round 3 mm diameter x 1 mm deep cartilage injury. Then, scaffold disc was press fit implanted to fill the cavity. Blood coming from subchondral bone marrow soaked the scaffold. Stability and anchorage of implant was confirmed by various intraoperatoty flexo-extension cycles with extensor mechanism reduced in place. Surgical site was cleaned from debris and hemostasis was ensured. Successively, it was sutured with Dexon 3/0 (Braun) and wound covered with Nobecutan (Inbisa) adhesive dressing. Postoperative care consisted in temperature rising with an electric cover in animal cage and oral anti-inflammatory [Meloxicam 0,3 – 0,6 mg/Kg (Boehringer Ingelheim)] once daily for 3 days. Additional daily wound inspection was carried out until fur completely concealed surgical site.

Animal sacrifice was performed 12 weeks after implantation, according to veterinary protocol. Preoperative sedatives were delivered [Ketamine (Pfizer) 15 mg/Kg & Metomidine (Pfizer) 0,1 mg/Kg]. Once under anesthetic narcosis, euthanasia was performed by means of intravenous sodium tiopenthal (Braun) overdose (500 mg) through auricular vein access. Once animal was deceased, mid femur and tibia cross fractures were executed and knees were extracted. According to study design and protocol, some animals had two knees with scaffold implants; on others others, contralateral knee was used as non-

treated control. Soft tissue was scraped and distal femur was placed in marked bottles with 10% buffered Formaldehyde for further histological processing. Photographs with digital camera (Cannon SX20) were taken all throughout surgical procedure.

Fig. 8: New Zealand white rabbit.

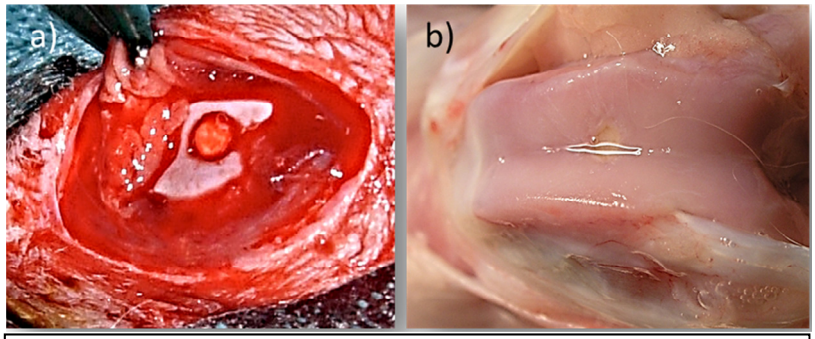

Fig. 9: a) Intraoperatory cartilage injury and disc placement b) Post- mortem sample of distal femur to be processed.

2.3 Histological Study

2.3.1 Histology

Histological assessment was carried out through several stains that, when interpreted together, complement and provide valuable data. According to study protocol, samples were stained with Hematoxylin-Eosin, Masson's trichrome, Alcian blue and Picrosirius red stains (Table 3).

Once a five day period of Formaldehyde inclusion has lapsed, samples were placed on a decalcifying solution (Osteosoft, Merck) for five weeks at room temperature. After distal femur was decalcified, a sagittal cut was made, obtaining two halves "a" and "b". These two halves were photographed with a magnifying glass camera (Leica DFC 320). They were placed into paraffin wax cassettes, each one labeled with the sample number followed by the corresponding letter "a" or "b" respectively. Samples with letter "a" preferably, and when necessary those with the letter "b" were sliced in 5μm thick sections with a microtome (Leica). Samples were placed on glass microscope slides and left at 37ºC for 48 hours until dry. Then, they were stained according to protocol using different techniques as specified in table 3. When samples were stained, they were photographed by means of a digital microscope

camera (Leica; DMD108). Polarized light microscopy was performed for picrosirius stains.

Hematoxylin-Eosin (H-E) stains cytoplasm in pink, nuclei in blue, while connective tissue stains in red to pink tones.

Masson's trichrome (MT) on the other hand, stains cells in red – pink tones, erythrocytes in red and collagen fibers in blue. The amplified spectrum of color provides a better contrast that enables component discrimination.

By using Alcian blue (AB), strongly acidic sulfated mucosubstances will be stained blue, nuclei in stained pink and cytoplasm in pale pink. To better suit our purposes, the counterstain was made with Hematoxylin, resulting in a darker overview, but stating a higher contrast between cartilage and bone tissue, useful for morphometric scrutiny.

Picrosirius red is one of the best understood techniques of collagen histochemistry. Stained sections viewed under polarized light microscopy present a light birefringence and a wide color spectrum that can be identified, depending on collagen fibril alignment, diameter and packing density[200]. Furthermore, different collagen types can be characterized by the picrosirius – polarization method. Type I collagen shows up as thick, strongly birefringent, yellow or red fibers, while type III collagen appears as thin, weakly birefringent greenish fibers.

type II collagen, present in hyaline cartilage, does not form fibers and displays a weak birefringence of varying color[201,202].

Stain	Protocol
H-E	1. Deparaffinize slides and hydrate to distilled water 2. Stain in Hematoxylin for 5 min 3. Wash in tap water and differentiate with 0,5% chloridric acid 4. Neutralize with sodium bicarbonate 5. Wash with distilled water and stain with Eosin during 3 min 6. Wash with distilled water 7. Dehydrate through 95% alcohol, 2 changes of absolute alcohol, 3 min each 8. Clear in Xylene 9. Mount with resinous mounting medium
Masson's Trichrome	1. Deparaffinize slides and hydrate to distilled water 2. Wash in distilled water 3. Stain in Harris Hematoxylin for 5 min 4. Wash in running tap water 5. Wash with 1% acetic water 6. Stain with Ponceau Fuchsin for 5 min 7. Wash with 1% acetic water 8. Stain with Orange G for 5 min 9. Wash with 1% acetic water 10. Stain with Aniline Blue for 10 min 11. Wash with 1% acetic water 12. Wash with distilled water 13. Dehydrate, clear in Xylene and mount
Alcian Blue	1. Deparaffinize slides and hydrate to distilled water 2. Stain in Alcian Blue for 20 min

Table 3: Histological staining protocols.

	3. Wash in running tap water for 2 min 4. Rinse in distilled water 5. Counterstain with Hematoxylin for 5 min 6. Wash in running tap water for 1 min 7. Dehydrate, clear and mount
Picrosirius Red	1. Deparaffinize slides and hydrate to distilled water 2. Running tap water rinse for 1 min 3. Stain with Weigert´s Hematoxylin for 8 min 4. Rinse in running tap water for 10 min 5. Stain with Picrosirius red solution for 60 min 6. Acidified water for 5 min (2 times) 7. Dehydrate, clear and mount

Table 3 (Continued): Histological staining protocols.

2.3.2 Immunohistochemistry

Immunohistochemical assessment was achieved by identifying type I and II collagen and Osteocalcin content. The presence of bone tissue was observed when type I collagen and/or Osteocalcin (synthesized by osteoblasts) were detected. Hyaline cartilage was acknowledged when type II collagen was present. Fibrocartilage, on the other hand, was identified where collagen type I was predominant.

After deparaffinization and rehydration, following standard methods, sections were pretreated with 100UI/mL hyaluronidase in Phosphate buffered saline (PBS) at 37°C

during 30 min, for antigen retrieval. Then, sections were incubated overnight at 4°C with 1:100 dilution of mouse monoclonal anti- type I collagen (Sigma; C2456), 1:100 dilution of mouse monoclonal anti- type II collagen (Calbiochem; CP18) or 1:50 dilution of mouse monoclonall anti-osteocalcin antibody (RD Systems; MAB1419) respectively in PBS containing 0.1% bovine serum albumin. Sections were subsequently incubated with LSAB-2 Kit (Dako) at room temperature. Finally, samples were immunostained with diaminobenzidine (DAB) as chromogen according to manufacturer´s instructions and counterstained with Mayer´s Hematoxylin. As a negative control, sections were incubated with PBS instead of specific primary antibodies and stained according to protocol[203,204].

2.3.3 Score

Cartilage repair has been assessed by means of a modified cartilage repair score (MCRS), based on a histologic scoring system used to grade 12-week specimens, developed by Solchaga *et al.*[205]; the score evaluates 10 items and has a maximum score of 29 (Table 4). Evaluation criteria include: Percentage of HC, surface regularity, degenerative changes given by hypercellularity or cell clusters, structural integrity, thickness of repair tissue compared to normal cartilage, integration of superior and inferior margins (of scaffold), bone filling (inside scaffolds), presence of a tidemark and

degenerative changes present in adjacent cartilage. Our group has modified the criteria, by evaluating tissue growth within scaffolds.

Percentage of HC	
80 - 100%	8
60 - 80%	6
40 - 60%	4
20 - 40%	2
0 - 20%	0
Surface regularity	
Smooth and intact	3
Superficial horizontal lamination	2
Fissures	1
Severe disruption, including fibrilation	0
Degenerative changes	
Severe hypercellularity	1
Mild or moderate hypercellularity	2
Normal cellularity, no clusters, normal staining	3
Normal cellularity, mild clusters, moderate staining	2
Mild or moderate hypocellularity, slight staining	1
Severe hypocellularity, poor staining	0
Structural integrity	
Normal	2
Slight disruption, including cysts	1
Severe desintegration	0

Table 4: Histologic scoring system used to grade the 12-week specimens. Modified Cartilage Repair Score (MCRS), based on Solchaga *et al*, 2000.

Thickness	
121 - 150% of normal cartilage	1
81 - 120% of normal cartilage	2
51 - 80% of normal cartilage	1
0 - 50% of normal cartilage	0
Integration of superior margins (of scaffold)	
Bonded	2
Partially bonded	1
Not bonded	0
Integration of inferior margins (of scaffold)	
Bonded	2
Partially bonded	1
Not bonded	0
Bone filling (inside scaffolds)	
101 - 125%	2
76 - 100%	3
51 - 75%	2
26 - 50%	1
0 - 25%	0
Tidemark	
Present	1
Absent	0
Degenerative changes in adjacent cartilage	
Normal cellularity, no clusters, normal staining	3
Normal cellularity, mild clusters, moderate staining	2
Mild or moderate hypocellularity, slight staining	1
Severe hypocellularity, poor staining	0

Table 4 (continued): Histologic scoring system used to grade the 12-week specimens. Modified Cartilage Repair Score (MCRS), based on Solchaga *et al*, 2000.

2.4 Morphometric approach

Morphometric software, Image pro Plus 7.0 (Media Cybernetics) has been run on Alcian Blue stained samples, in order to objectively quantify repair tissue on injured surface as well as within scaffold limits. Alcian blue stain has been selected, due to the gross color contrast between cartilage and bone tissue.

First of all, Images with 4x magnification were selected. Once the picture was uploaded, the software was calibrated by means of the scale bar to match the magnification of the microscopic image originally taken. Next, the contrast was sharpened through best fit, in order to enhance tissue discrimination. A designated region of interest (ROI) was assigned to repair tissue contained within limits of tangent lines from lateral borders of the scaffold to joint surface (Fig. 10). Inside each scaffold, ROIs divide the area into three sectors: superior, inferior and periphery. A longitudinal line divides the sample studied into superior and inferior halves. Likewise, vertical lines from lateral left and right margins confine periphery area to approximately 1/5 of total area (Fig. 11). A total of 5 ROI sections per sample were scrutinized

Segmentation was performed by using default color settings of software. Colors have been coded into: red = cartilage, yellow =

bone, green = scaffold (biomaterial and pore) and aquamarine = undifferentiated tissue. Software scrutinized and quantified by color pixels the area and therefore, the amount of tissue assigned to each variable. Furthermore, picrosirius, trichrome and H-E staining complemented tissue evaluation. Data was exported to excel books to be analyzed.

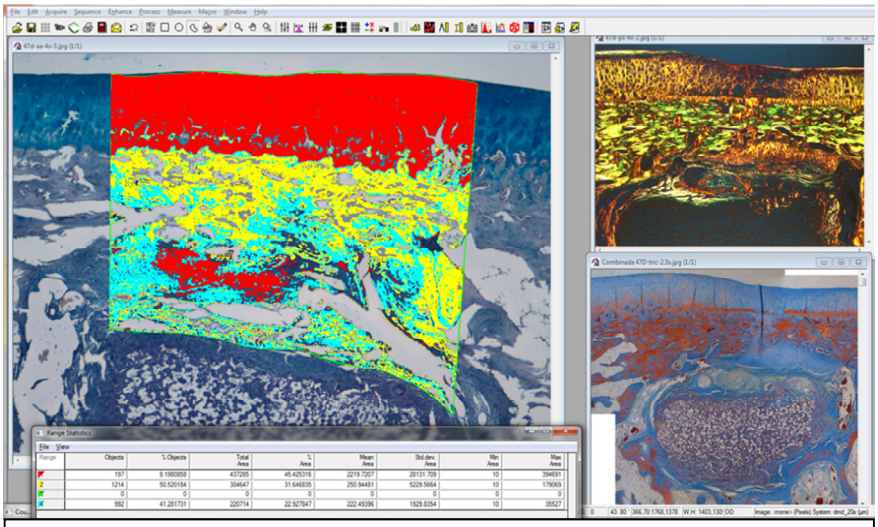

Fig. 10: Morphometric analysis using Image Pro Plus 7.0. Repair tissue ROI. Picrosirius and Trichrome stains complement tissue scrutiny.

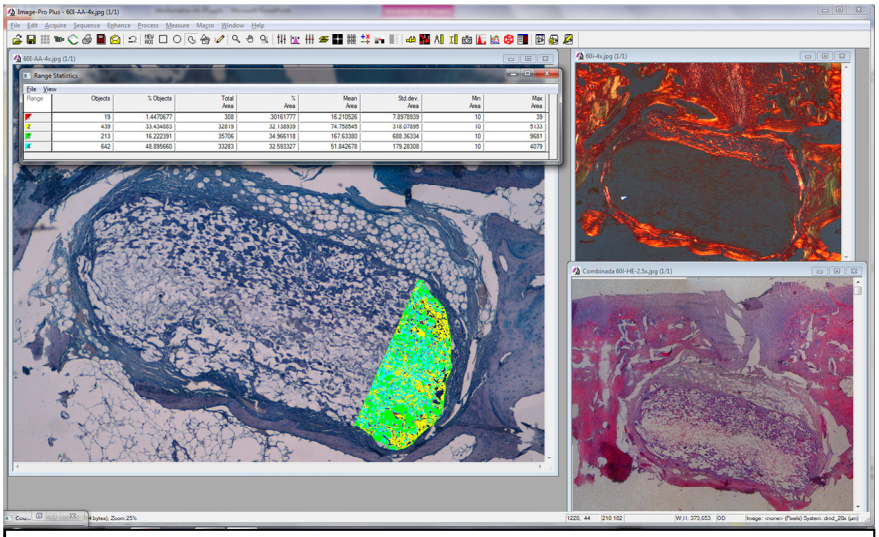

Fig. 11: Morphometric analysis using Image Pro Plus 7.0. Right periphery ROI. Picrosirius and H-E stains complement tissue scrutiny.

2.5 Statistical analysis

Database of Image pro plus 7.0 (media Cybernetics) software was exported to Microsoft office Excel (Version 2010). Synthesis of information was processed and translated into variables for statistical interpretation.

Statistical analysis was performed with the use of IBM SPSS Statistics for Windows, Version 19.0. (Armonk, NY: IBM Corp). Since a normal distribution could not be established, given the number of samples available (n=28), the non-parametric test Kruskal-Wallis was used. This increased the accuracy of interpretation. P values less than 0,05 were considered statistically significant.

Histologic criteria to measure regeneration of cartilage were statistically assessed by means of a descriptive analysis of the MCRS score and selected relevant histologic parameters. Such analysis of trial group variables included mean values, typical error and confidence interval (CI).

Repair tissue at joint surface was expressed as the percentage of each tissue, which is cartilage, bone and undifferentiated tissue contained in the ROI specified above. Furthermore, inside the scaffolds, solid biomaterial was excluded in order to avoid misinterpretation. (Table 2). Repair tissue inside the

scaffolds is expressed as the percentage of the area occupied by each tissue, which is cartilage, bone, undifferentiated tissue and remaining empty pore space, relative to total scaffold area, once the solid biomaterial component was excluded.

Morphometric statistical analysis was done by means of bilateral bivariate correlations of descriptive variables measuring repair tissue and repair cartilage growth in the articular surface, with those variables quantifying tissue inside the scaffolds. Further, sections within the scaffolds (superior, inferior and peripheral) were analyzed by type of repair tissue growth. This data was analyzed by means of Pearson's correlation coefficient.

Additionally, this tool established a relationship (r) between the mean values of histologic variables measured for cartilage repair at joint site and the amount of cross-linker contained in each trial group of scaffolds (A,B,C,D). Control groups were not included in the statistical analysis since no cross-linker was used.

3. Results

3.1 Sample characterization and morphometric scrutiny

A total of 31 samples were assigned to 6 different study groups and, four of which vary the amount of cross-linker concentration and one control group (further subdivided into two subgroups: injured and uninjured cartilage). Each group has an average of 5,50 (± 0,50) samples. Out of the total sample (n=31), three trials (49D, 49I, 50D) were not analyzed in context of assigned group, due to premature rabbit loss, however they are also described in detail. Final n to be analyzed is 28. (n=28) (Table 5)

There is a common distribution pattern of scaffold location. Three months after surgery, 6 samples (n=6) (at least one from each trial group) remain in close contact with the joint cavity, presenting a more superficial behavior. In contrast, the majority of scaffolds (n=12), present a profounder location, conditioning the repair tissue to the depth of establishment.

Each sample has been processed by means of several histological techniques (H-E, MT, AB) as well as picrosirius red stain (Fig. 12a). They were then histologically evaluated using a modified cartilage repair score (MCRS) in order to assess the quality of repair tissue. Different criteria applied by the modified cartilage repair score (MCRS) define the quality of

repair tissue. Additionally, morphometric software, Image pro Plus 7.0 (Media Cybernetics) has been employed to quantify repair tissue on injured surface as well as within scaffold limits.

Cross analysis between all the stains was done during the morphometric assessment for complementary information. Moreover, in selected samples, immunochemistry assays have verified the presence of collagen type I, II and osteocalcin, contributing to the overall examination (Fig. 12b).

Group	Sample	Deceased
A	45D	t = 3 months
	51D	t = 3 months
	51I	t = 3 months
	54D	t = 3 months
	50D	t = 0
B	47D	t = 3 months
	57D	t = 3 months
	60I	t = 3 months
	46D	t = 3 months
	52D	t = 3 months

Table 5: Sample distribution; I = left, D = right, t = time.

C	48I	t = 3 months
	52I	t = 3 months
	57I	t = 3 months
	58D	t = 3 months
	48D	t = 3 months
	54I	t = 3 months
D	58I	t = 3 months
	59D	t = 3 months
	53D	t = 3 months
	49I	t = 3 weeks
	49 D	t = 3 weeks
Control	21D	t = 3 months
	47I	t = 3 months
	53I	t = 3 months
	59I	t = 3 months
	60D	t = 3 months
	45I	t = 3 months
	46I	t = 3 months
	21I	t = 3 months
	20I	t = 3 months
	25I	t = 3 months

Table 5 (Continued): Sample distribution; I = left, D = right, t = time.

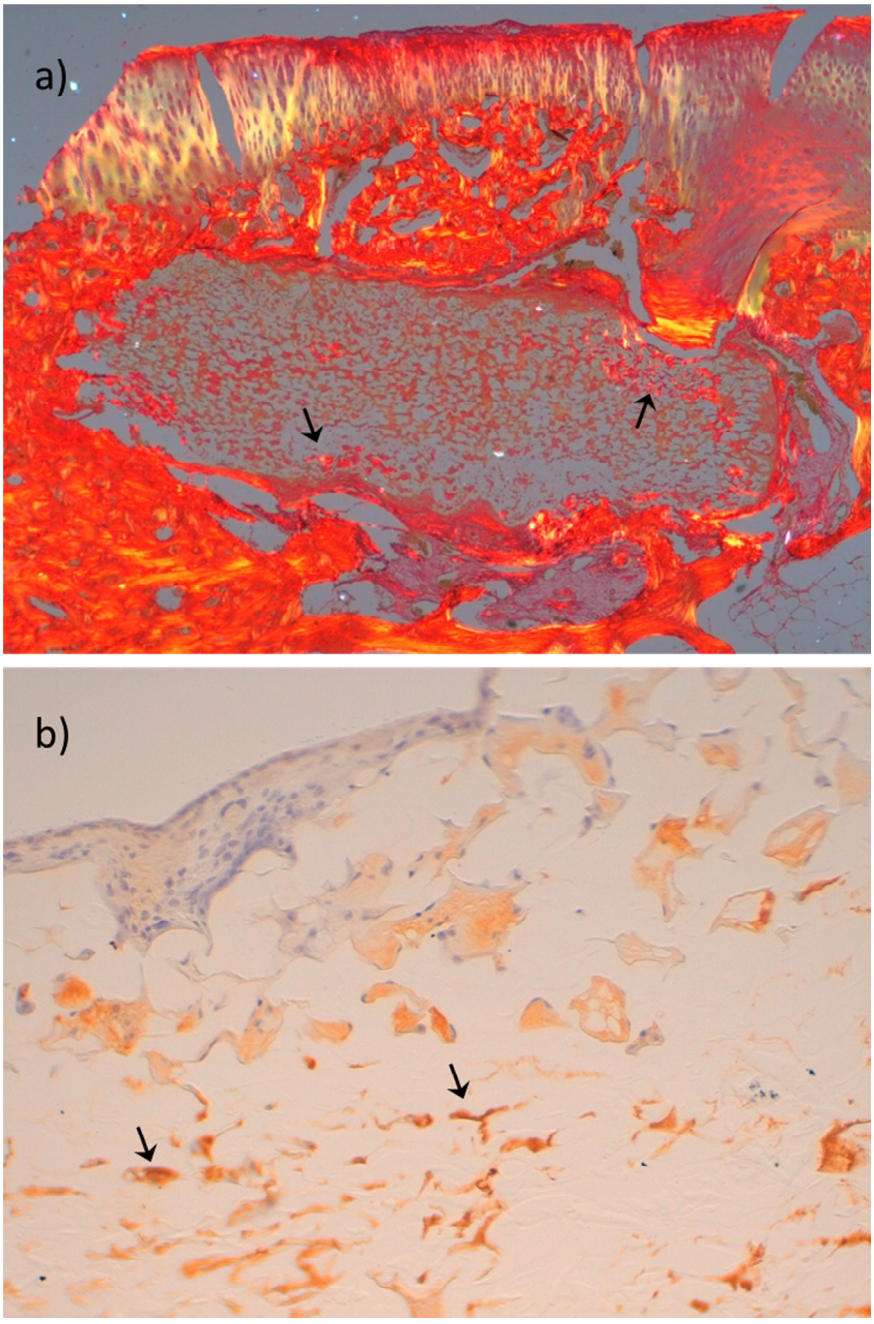

Fig. 12: Sample analysis. a) Picrosirius red stain complementing sample 57I assessment. Birefringence shown by arrows characterizes collagen type I, present in bone tissue and is found in some cells within scaffold b) Positive immunohistochemistry 1/100 dilution shown by arrows, confirming presence of regenerated collagen type II in sample 52D

3.1.1 **Group A** (1% cross-linker)

Experimental group A encompasses five samples (n=5), one of which has been excluded, for early rabbit loss. There is a predominant deep-seated scaffold pattern (n=3) that partially rebuilds the injury site, and one superficial-seated scaffold (n=1).

At superficial joint site (Fig. 13a), cartilage, as well as fibrous tissue and subchondral bone are present. Still, cartilage is the foremost repair tissue. The structure of former healthy cartilage has been achieved in most injured area, in all samples, as revealed on intermediate repair scores.

In the interior of scaffolds (Fig. 13b), most pores were filled with new cartilage and bone tissue, however, many cells have an undifferentiated feature.

The only superficial-seated scaffold managed to bond completely with the adjacent cartilage tissue, however one fourth of its area is still to be filled.

Repair tissue at joint surface (Fig. 13a):

- Morphometric quantification: Cartilage (HC+FC): 79,63%; Bone: 9,73%; Undifferentiated tissue:10,64%.
- Histological criteria: Out of 79,63% of the measured cartilage, 64% had hyaline cartilage appearance and

36% had fibrous characteristics; MCRS group average: 16,0 (CI: 14 - 20).

Repair tissue inside the scaffolds (Fig. 13b):

- Morphometric quantification (respect to total scaffold area): Cartilage: 14,88%; Bone: 8,46%; Undifferentiated tissue: 20,55%; Empty pores: 46,01%, Solid scaffold: 10,10%.

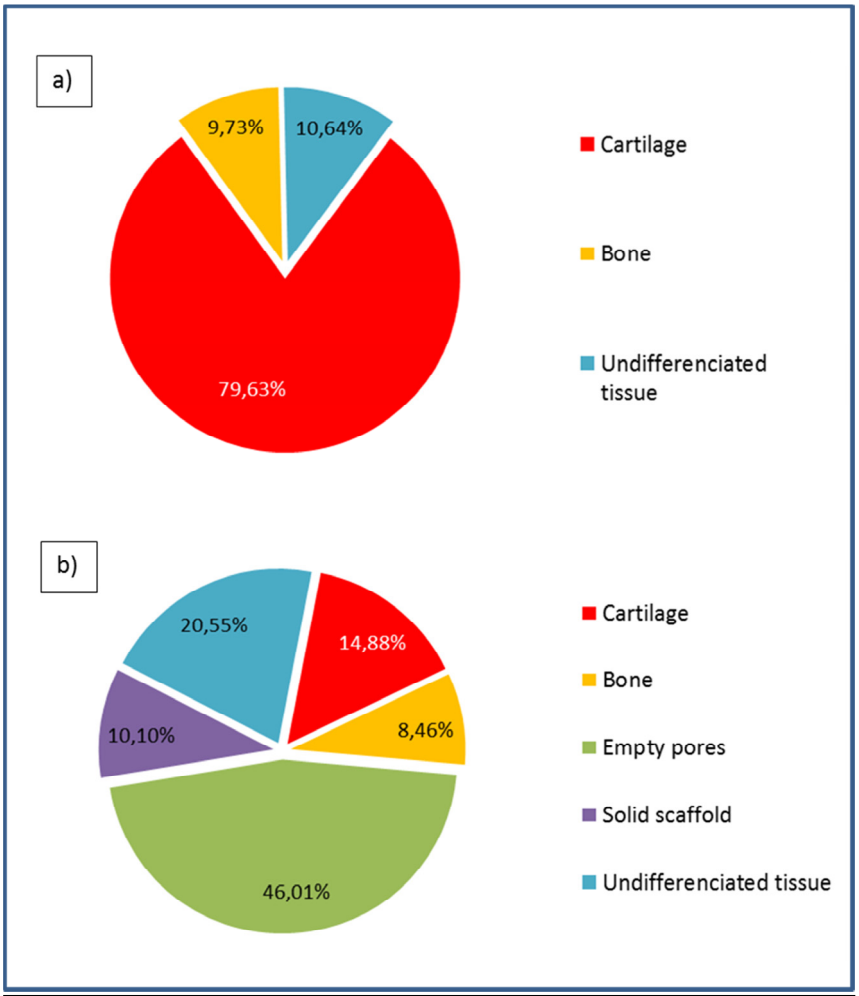

Fig. 13: Group A. Morphometric quantification of tissue distribution: a) At joint surface. b) Inside the scaffolds respect to total scaffold area.

The following section contains case by case analysis of group A samples. Detailed description of morphological features is displayed:

Sample 45D (Fig. 14)

On a macro view, a lack of fusion can be observed at the injury site. There is a large growth in one end of the cavity surface, but unfinished on its counterpart, resulting in an eccentric 1 mm diameter pore at the articular surface. Cartilage at joint surface has a smooth, glassy appearance that is partly white similar to native cartilage at the grown end and partly red at the other end (Fig. 14 a,b).

Histologically, repair tissue at articular surface shows a fibrous center with apparent hyaline cartilage laterally (Fig. 14d). This can be seen by the abundant collagen type I fibers that have been stained in blue with MT stain. There is a slight disruption of the structural integrity of repair tissue at joint surface and absence of the tidemark.

Overall, repair tissue at joint surface morphometrically is: 76,93% of cartilage (HC+FC); 19,98% of bone and 3,10% of undifferentiated tissue. Histologically: Out of the 76,93% of quantified cartilage, 50% has hyaline cartilage appearance and 50% fibrous cartilage features; MCRS: 14.

The scaffold displays an ovoid form (Fig. 14c), located at 250 μm from the joint cavity, having a total area of 1.318.295 μm^2. The scaffold pores are occupied by new formed tissue, mostly undifferentiated cells, with sporadic new vessels. In order to discriminate cells, we have compared features with native surrounding tissue, enabling us to identify cartilage and bone structures. Tissue not complying with such characteristics has been classified as undifferentiated. There is also partial scaffold integration with host tissue (Fig. 14d, e), especially in the inferior border; areas of new bone establishment are observed, with occasional multinuclear cells and no signs of rejection. In the superior portion of the scaffold, there is an area of fibrosis, although there is integration with native cartilage.

The morphometric quantification of tissue distribution inside the scaffold, excluding the solid biomaterial is:

ROI (%)	Cartilage	Bone	Empty Pores	Undifferentiated
Superior	7,25	1,70	67,72	23,33
Inferior	3,83	1,56	54,38	40,23
Periphery	7,70	1,02	51,66	39,62

Globally, there is a 5,36% of cartilage, 1,34% of bone and 29,32% of undifferentiated tissue content within total scaffold area, although 52,46% is still empty pore and 11,52% is solid scaffold biomaterial.

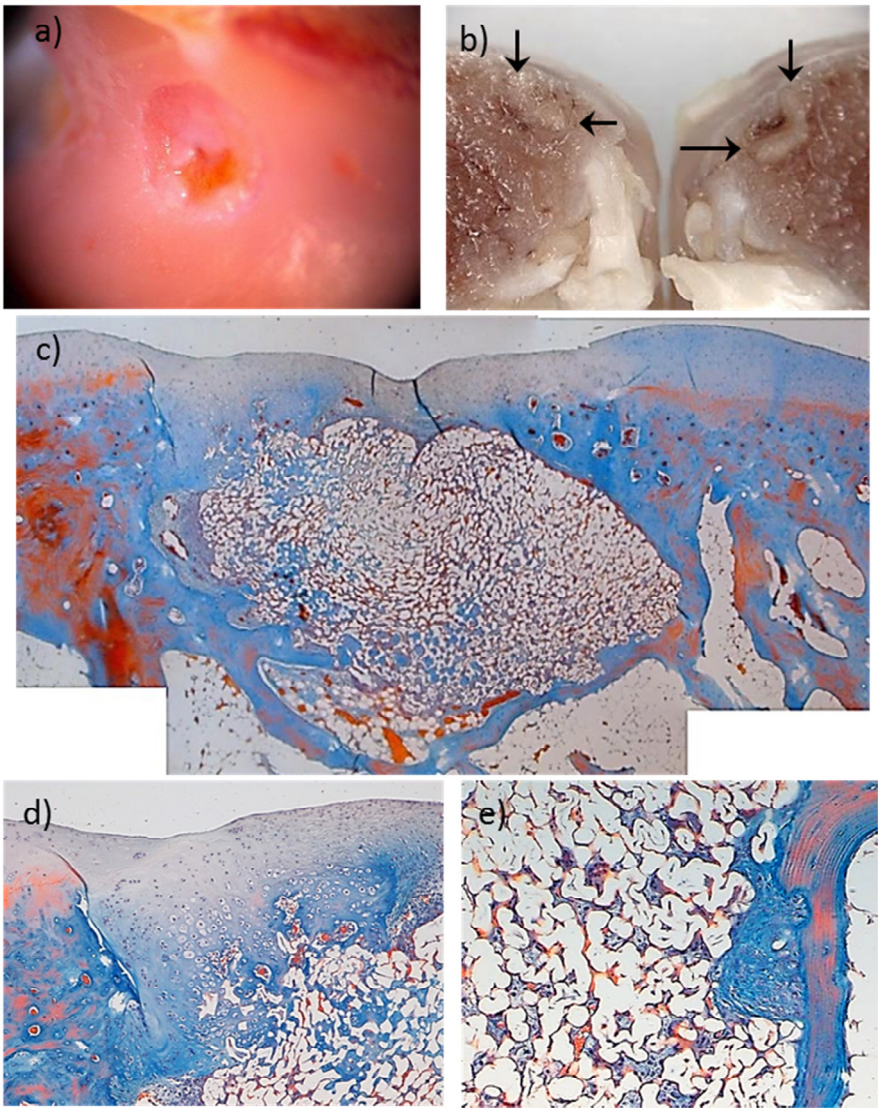

Fig. 14: Sample 45D. a) Macroscopic view after animal sacrifice. b) Sagittal cut of distal femur, following tissue decalcification, 4 weeks after sacrifice. Scaffold in place shown by arrows. c) Reconstruction by means of 3 images at 2,5x; panoramic view, MT stain. d) 10x close up; Integration with native cartilage; fibrous center. MT stain. e) 20x close up; clumps of new cartilage in scaffold; Integration with bone. MT stain.

Sample 51D (Fig. 15)

On a macro view of the distal femur, a lack of union can also be observed at the injury site. There is a symmetrical concentric growth at the articular surface, with a subsequent 0,3 mm opening. There is a procedure scar overlapping the study region. Cartilage at joint surface area has a rugged yet glassy appearance, which is white on the center and pink on the periphery (Fig. 15a, b).

Histologically, repair tissue at articular surface looks like immature hyaline cartilage, along with a fibrous tissue on the center (Fig. 15c). This can be appreciated by small and elongated chondrocytes and abundant collagen type I fibers that are densely packed and have been stained in blue with MT stain. The surface of this repair cartilage is disrupted, has fissures and cysts. There is also no tidemark present at reconstructed site.

Overall, repair tissue at joint surface morphometrically is: 86,32% of cartilage (HC+FC); 0,99% of bone and 12,63% of undifferentiated tissue. Histologically: Out of the 86,32% of quantified cartilage, 50% has hyaline cartilage appearance and 50% fibrous cartilage features; MCRS: 15.

The scaffold displays an elongated rectangular form (Fig. 15c), located at 1.100 μm from the joint cavity, with a total area of

1.629.808 μm². The scaffold pores are mostly filled by cartilage, bone and abundant undifferentiated cells, and is rich in new vessels. We have compared features with native surrounding tissue, enabling us to identify cartilage and bone structures. Tissue not complying with such characteristics has been classified as undifferentiated. There are also minor areas of scaffold integration, restricted by a fibrous band in lateral and inferior borders of the scaffold (Fig. 15d) and rare multinuclear cells. Ectopic bone has regenerated within HC and FC repair tissue (Fig. 15e).

The morphometric quantification of tissue distribution inside the scaffold, excluding the solid biomaterial is:

ROI (%)	Cartilage	Bone	Empty Pores	Undifferentiated
Superior	0,47	12,15	80,39	7,00
Inferior	0,45	21,22	69,23	9,10
Periphery	0,36	18,58	68,67	12,39

Globally, there is a 0,38% of cartilage, 15,12% of bone and 7,99% of undifferentiated tissue content within total scaffold area, despite the fact that 62,74% are still empty pores and 13,77% is solid scaffold biomaterial.

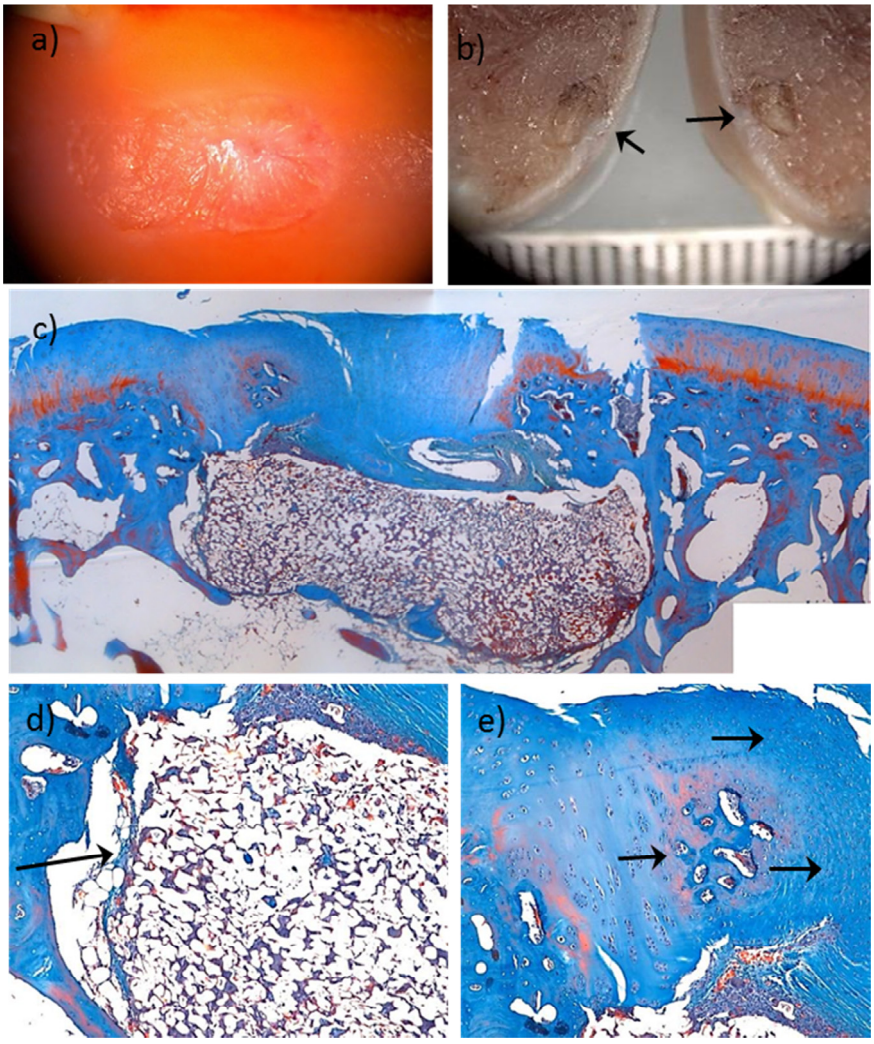

Fig. 15: Sample 51D. a) Macroscopic view after animal sacrifice. b) Sagittal cut of distal femur, following tissue decalcification, 4 weeks after sacrifice. Scaffold in place shown by arrows. c) Reconstruction by means of 5 images at 2,5x; panoramic view, MT stain. d) 10x magnification up of peripheral left margin; lack of integration; band of fibrosis signaled by arrow. MT stain e) 10x magnification of superior left quadrant; repair tissue growth shown by arrows can be detailed. MT stain.

Sample 51I (Fig. 16)

On a macro view, a lack of fusion between the new grown tissue edges can be observed at the injury site (Fig. 16a). There are four growth terminals developing unevenly at the articular surface, resulting in a 1mm H-shaped cleft (Fig. 16a. b). Cartilage at joint surface has a glassy appearance with white and red areas.

Histologically, repair tissue at articular surface appears fissured by a finger-like indent extending from the joint cavity (Fig. 16c). There are areas of cartilage where appropriate ECM, lacunae and rounded chondrocytes can be seen (Fig. 16d). Likewise, areas of fibrosis can be observed, especially at the center of the injured surface. Densely packed fibers and have been stained in lighter blue with MT stain. Similarly, moderate hypercellularity is found and the tidemark is absent.

Overall, repair tissue at joint surface morphometrically is: 72,19% of cartilage (HC+FC); 17,96% of bone and 9,85% of undifferentiated tissue. Histologically: Out of the 72,19% of quantified cartilage, 65% has hyaline cartilage appearance and 35% fibrous cartilage features; MCRS: 15.

The scaffold presents a slight V-shape trapezoid form (Fig. 16c), located at 900 μm from the joint cavity, having a total area of 2.903.843 μm^2. The scaffold pores are mostly occupied by

cartilage, bone as well as undifferentiated cells, with copious new vessels. Comparing features with native surrounding tissue, allowed us to classify cartilage and bone structures. Tissue not complying with such characteristics was classified as undifferentiated tissue. The scaffold is partially bonded to the adjacent tissue, restricted by fibrous tissue (Fig. 16d). Some multinuclear cells can be found in the center and periphery of the scaffold (Fig. 16d). At the inferior border, fibrosis, multinucleated cells and vessels can be found (Fig. 16e).

The morphometric quantification of tissue distribution inside the scaffold, excluding the solid biomaterial is:

ROI (%)	Cartilage	Bone	Empty Pores	Undifferentiated
Superior	0,45	18,77	50,91	29,87
Inferior	0,82	16,04	48,46	34,68
Periphery	0,20	16,28	58,93	24,58

Globally, there is a 0,53% of cartilage, 15,77% of bone and 27,59% of undifferentiated tissue content within total scaffold area, whereas 46,01% are still empty pores and 10,10% is solid scaffold biomaterial.

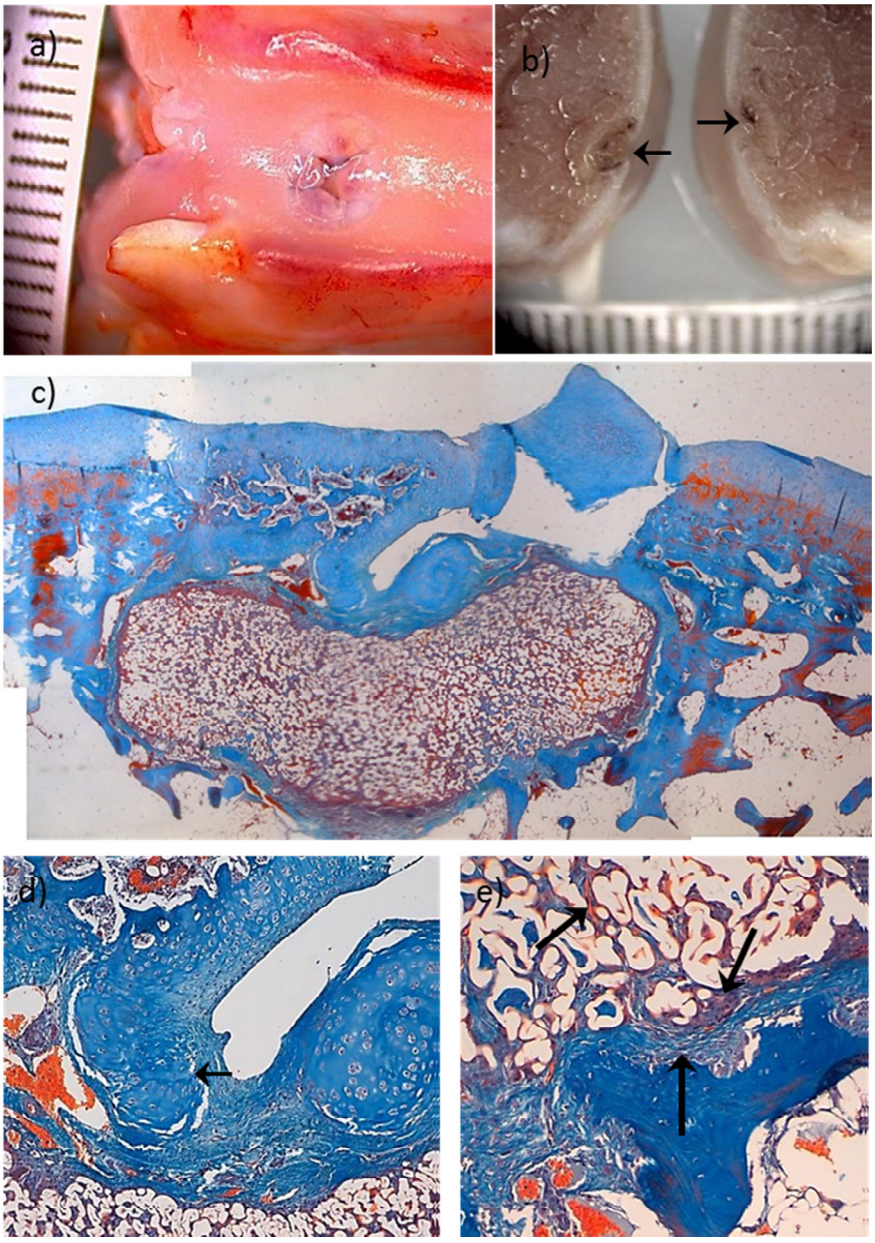

Fig. 16: Sample 51I. a) Macroscopic view after animal sacrifice. b) Sagittal cut of distal femur, following tissue decalcification, 4 weeks after sacrifice. Scaffold in place shown by arrows. c) Reconstruction by means of 6 images at 2,5x; panoramic view, MT stain. d) 10x magnification of superior margin; Indentation close-up. New immature cartilage is shown by arrow. MT stain. e) 20x magnification of inferior border; fibrosis, multinucleated cells and vessels shown by arrows. MT stain.

Sample 54D (Fig. 17)

On a macro view of the distal femur, a complete filling of repair tissue is observed (Fig 17a); however, at the articular surface a horizontal fissure and a subsequent flap can be noticed (Fig 17b). Non-flap cartilage at joint surface area has a smooth surface, with a white and glassy presence.

Histologically, scaffold is aligned with surface; located within native articular cartilage, in direct contact with joint cavity (Fig. 17c). At joint surface, the regularity is slightly altered and a mild hypocellularity can be observed. Scaffold barely touches tidemark, which is mostly present. However there is a complete bond of the scaffold with adjacent host tissues (Fig 17c, d).

Overall, repair tissue at joint surface morphometrically is: 83,04% of cartilage (HC+FC); 0% of bone and 16,96% of undifferentiated tissue. Histologically: Out of the 83,04% of quantified cartilage, 90% has hyaline cartilage appearance and 10% fibrous cartilage features; MCRS: 20.

The scaffold presents a rectangular shape (Fig. 17c), located at 0 μm from the joint cavity, having a total area of 317.356 μm^2. The scaffold pores are mostly occupied by cartilage cells (Fig. 17e), with no multinuclear cells or new vessel growth. When features were compared features with native surrounding tissue, allowed us to classify cartilage, bone or

undifferentiated tissue. As above mentioned, the scaffold is totally bonded to the adjacent host tissue plus no obvious fibrous tissue is observed (Fig. 17c, d).

The morphometric quantification of tissue distribution inside the scaffold, excluding the solid biomaterial is:

ROI (%)	Cartilage	Bone	Empty Pores	Undifferentiated
Superior	44,64	0,28	29,38	25,71
Inferior	59,97	2,64	23,34	14,05
Periphery	62,77	1,53	19,08	16,62

Globally, there is a 53,26% of cartilage, 1,59% of bone and 17,29% of undifferentiated tissue content within total scaffold area, even though 22,84% are still empty pores and 5,01% is solid scaffold biomaterial.

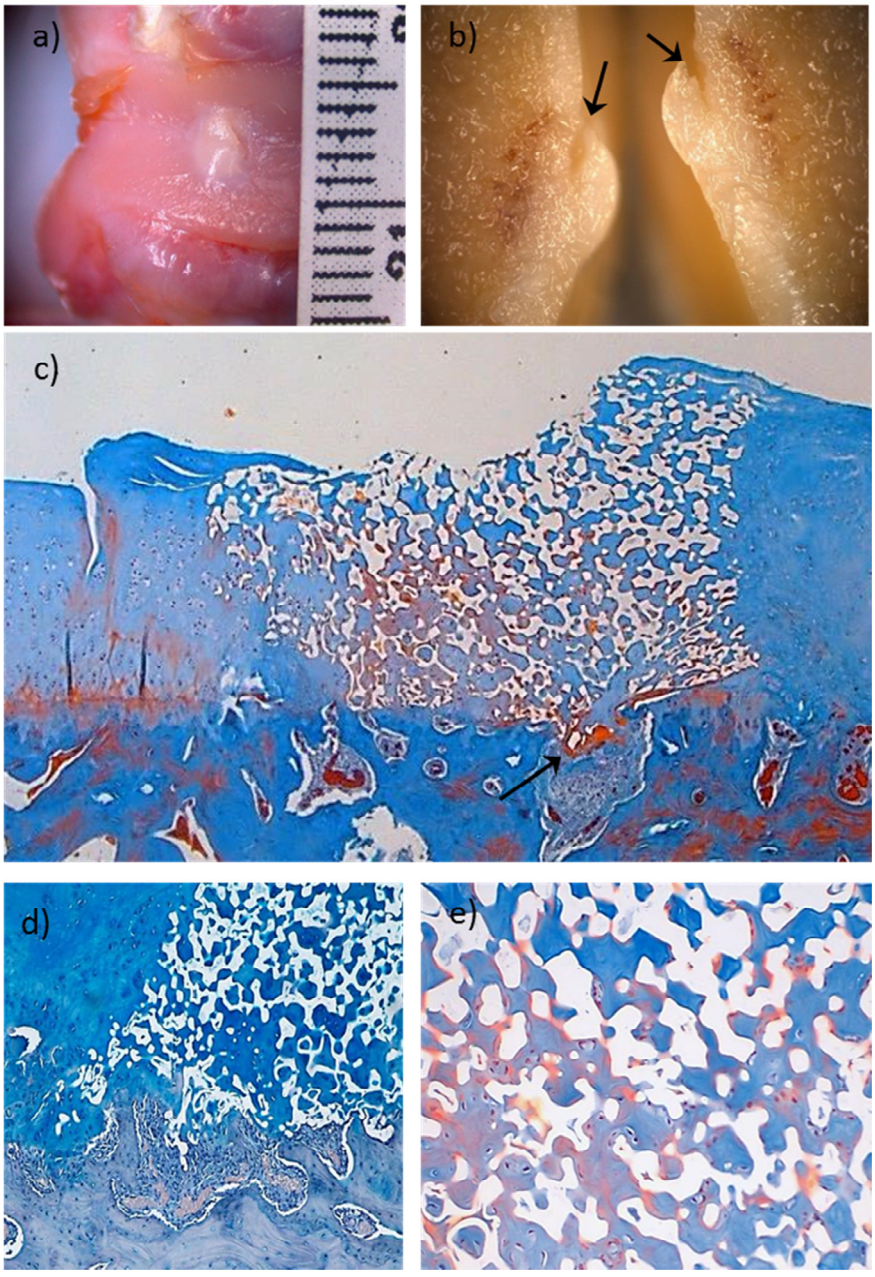

Fig. 17: Sample 54D. a) Macroscopic view after animal sacrifice. b) Sagittal cut of distal femur, following tissue decalcification, 4 weeks after sacrifice. Scaffold in place. Horizontal fissure and flap shown by arrows. c) Image at 2,5x; panoramic view. Scaffold barely in contact with tidemark shown by arrow, MT stain. d) 10x magnification, alcian blue stain; integration of inferior margin. e) 20x magnification of center scaffold in MT stain; abundant cell occupation is observed.

Sample 50D* (Fig. 18)

**Sample deceased at 0 weeks at operating room, therefore not considered for group performance*.

On a macro view, it is observed that the disc is not aligned with the articular surface. There is a lack of continuity with adjacent tissue and implanted disc is uncovered. A dark red color prevails (Fig. 18a, b).

Histologically, as mentioned, there is no repair tissue on the surface. Injury limits are regular and well defined. Tidemark is absent. MCRS: Not quantified

The scaffold presents rectangular shape, located at 600 μm from the joint cavity (Fig. 18c), having a total area of 959.234 μm^2. The scaffold pores are mostly occupied by erythrocytes (Fig. 18d) and there are no signs of vascularization or multinuclear cells. There is no fibrous tissue development or bond to the adjacent tissue. Altogether, there is no tissue growth within the scaffold, merely isolated erythrocytes scattered in a vacant scaffold.

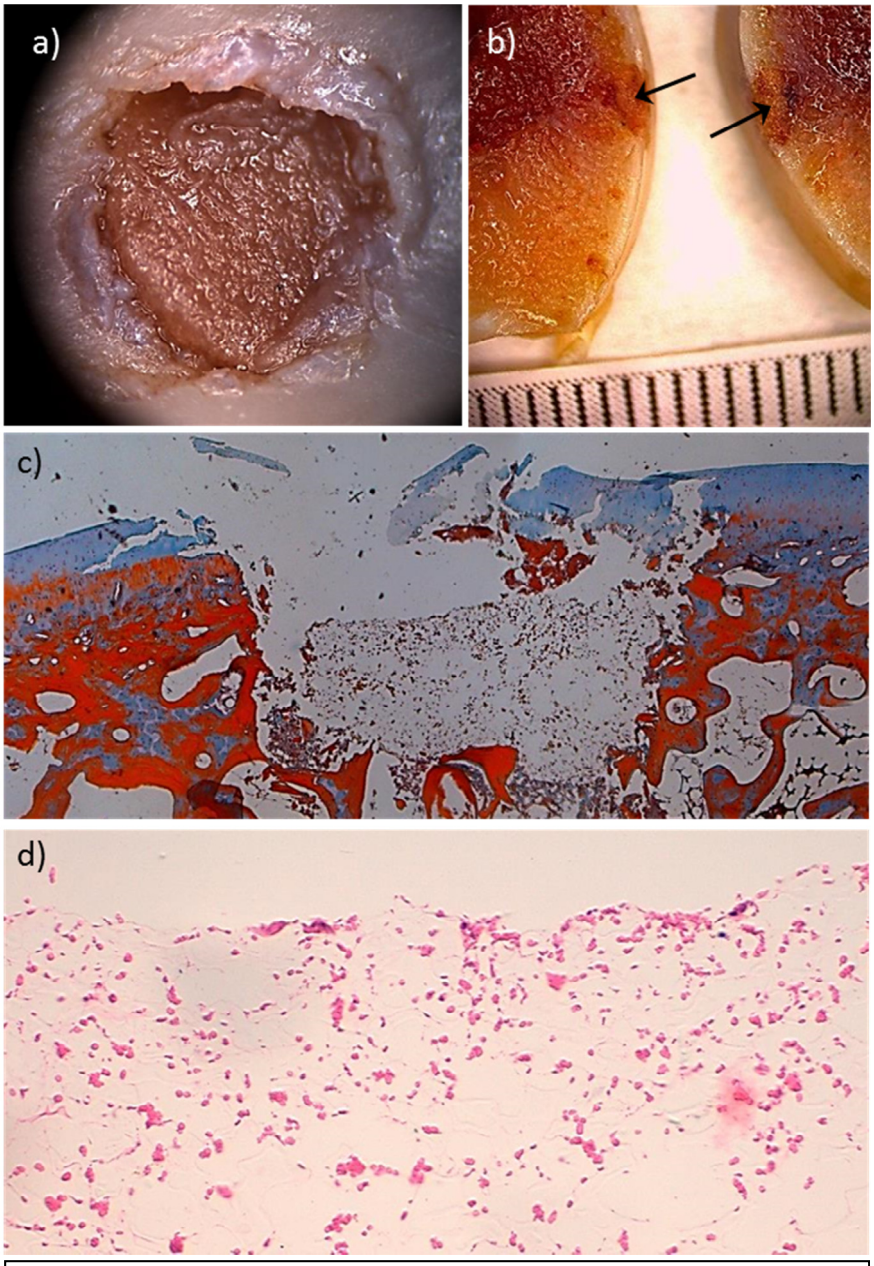

Fig. 18: Sample 50D. a) Macroscopic view after animal decease at operating room. b) Sagittal cut of distal femur, following tissue decalcification, 4 weeks after procedure. Scaffold in place shown by arrows. c) Reconstruction by means of 2 images at 2,5x; panoramic view, MT stain. d) 20x magnification of superior implant margin; Multiple erythrocyte occupation is observed on H-E stain.

3.1.2 **Group B** (2% cross-linker)

Experimental group B covers five samples. Although a more balanced proportion exists, there is still a prevalence of deep (n=3) to superficial-seated (n=2) scaffold pattern. In general, the structure of healthy cartilage has been partially reached; however, as exposed on repair scores, a wide pattern of behavior can be found. Different criteria applied by the modified cartilage repair scores (MCRS) define the quality of repair tissue.

At superficial joint site (Fig. 19a), repair tissue is predominantly cartilage and to a lesser extent, undifferentiated tissue.

Inside the scaffolds (Fig. 19b), despite a common pattern of central inoccupation, most scaffolds were filled with new cells. Three main tissues were identified, cartilage, bone and frequently undifferentiated tissue.

One deep-seated scaffold achieved excellent reconstruction site of injury; conversely, on the superficial-seated cases there was severe disintegration of structural integrity.

Repair tissue at joint surface (Fig. 19a):

- Morphometric quantification: Cartilage (HC+FC): 57,36%; Bone: 20,38%; Undifferentiated tissue: 22,26%.

- Histological criteria: Out of the 57.36% of measured cartilage, 55% had hyaline cartilage appearance and 45% fibrous characteristics; MCRS group average: 12,0 (CI: 5 - 17).

Repair tissue inside the scaffolds (Fig. 19b):

- Morphometric quantification (respect to total scaffold area): Cartilage: 12,02%; Bone: 9,17%; Undifferentiated tissue: 26,01%; Empty pores: 44,85%, Solid scaffold: 7,95%.

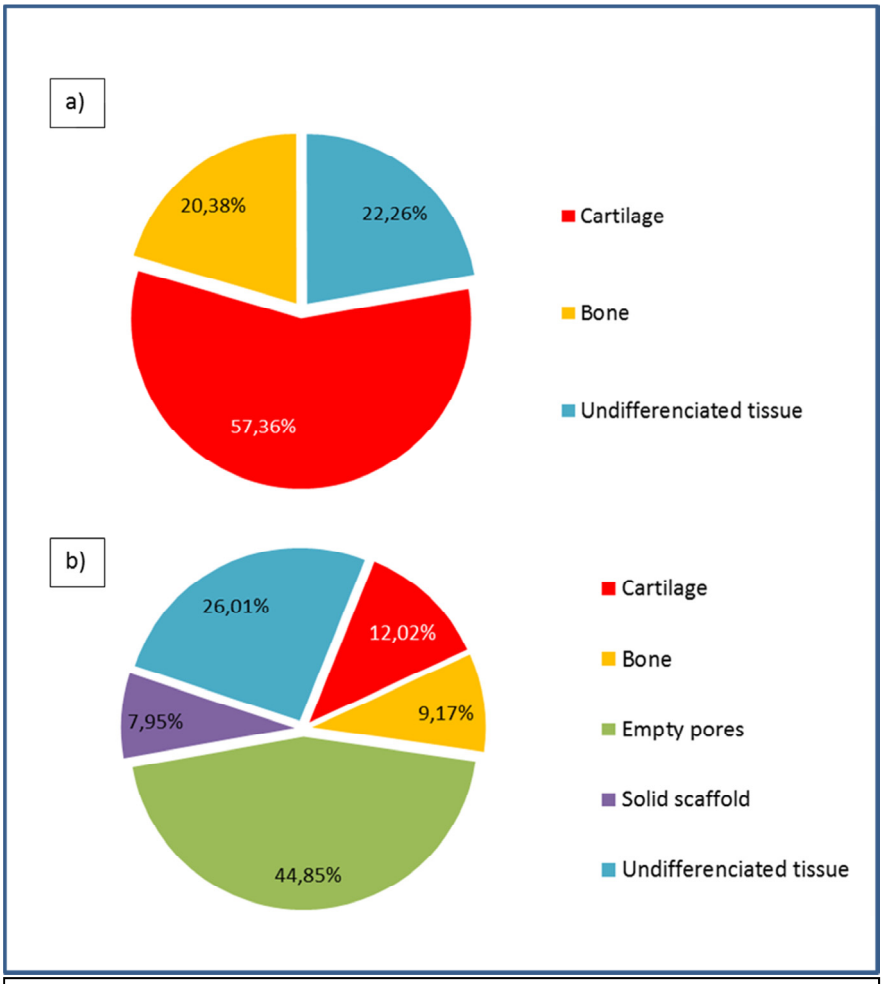

Fig. 19: Group B. Morphometric quantification of tissue distribution:
a) At joint surface. b) Inside the scaffolds respect to total scaffold area.

The following section contains case by case analysis of group B samples. Detailed description of morphological features is displayed:

Sample 47D (Fig. 20)

On a macro view of the distal femur, a lack of fusion between the margins of tissue that has grown towards the center of the injury site can be observed. At the articular surface there are certain growth terminals developing unevenly, causing a 1mm fissure (Fig. 20a, b). Cartilage at joint surface has a glassy presentation with some whitish but predominantly reddish areas.

Histologically, repair tissue at articular surface has a mature hyaline articular cartilage appearance, covering the surface of the injured cavity (Fig. 20c). There are areas of cartilage where appropriate ECM, lacunae and rounded chondrocytes can be observed. There is a smooth surface regularity; nonetheless there is a mild hypercellularity. Tidemark is present, under which lies an area of subchondral bone of 750 μm, between superficial cartilage and the scaffold. Beneath this bone layer, a second cartilage area (250 μm x 1.500 μm) is observed, forming a “bone tissue sandwich” (Fig. 20c).

Overall, repair tissue at joint surface morphometrically is: 45,43% of cartilage; 31,65% of bone and 22,93% of undifferentiated tissue. Histologically: Out of the 45,43% of quantified cartilage, 100% of it had HC features; MCRS: 17.

Scaffold shows an elongated ovoid form, located at 1.500 μm from the joint cavity (Fig. 20c), with total area of 1.788.884 μm^2. The scaffold pores are mostly filled by undifferentiated cells, with isolated zones of ostensible bone matrix. New vessel growth can be found all throughout the scaffold. Compared its features with native surrounding tissue, enabled us cartilage and bone classification. Tissue not adjusting to such characteristics was classified as undifferentiated tissue. Scaffold integration with host tissue is restricted by a fibrous band encapsulating most of the framework (Fig. 20c, e). Rarely multinuclear cells are found in the center of the scaffold, yet there are plentiful near the periphery (Fig. 20e).

The morphometric quantification of tissue distribution inside the scaffold, excluding the solid biomaterial is:

ROI (%)	Cartilage	Bone	Empty Pores	Undifferentiated
Superior	0,00	3,03	34,97	62,00
Inferior	0,00	4,76	27,65	67,59
Periphery	0,00	4,34	34,14	61,52

Globally, there is no cartilage inside the scaffold, whereas there is a 3,72% of bone and 60,00% of undifferentiated tissue

content within total scaffold area, while 30,48% are still empty pores and 5,80% is solid scaffold biomaterial.

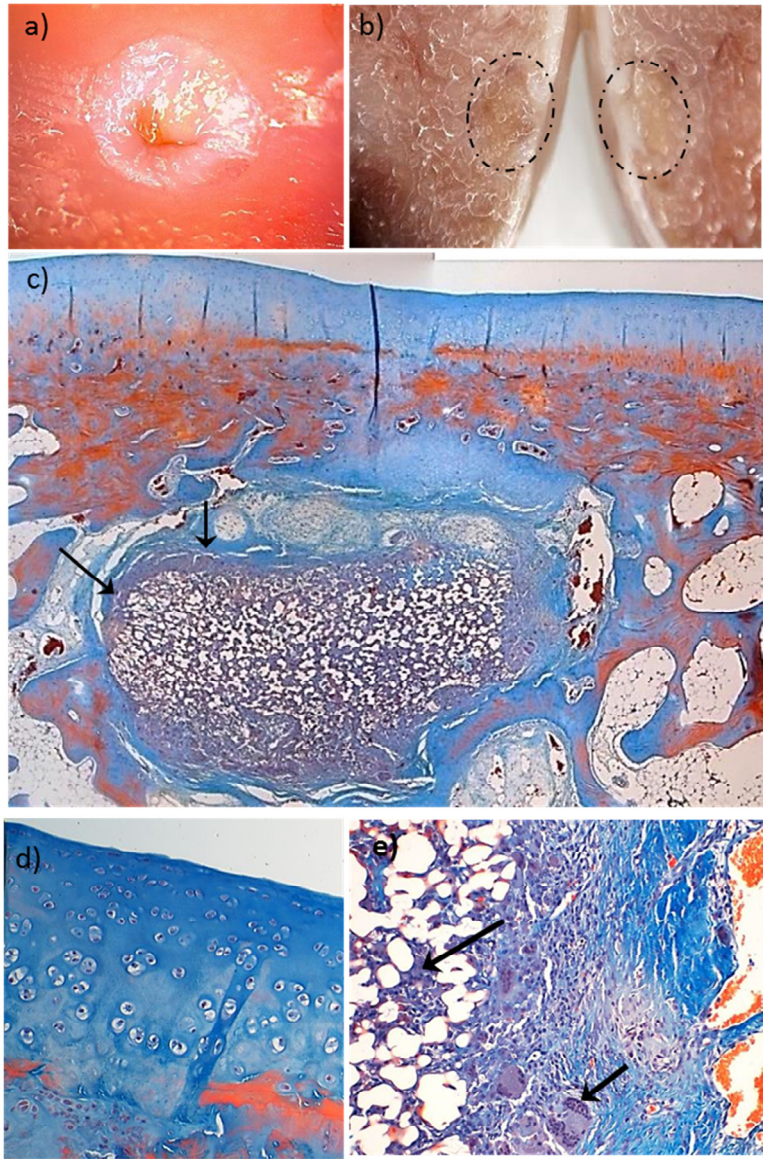

Fig. 20: Sample 47D. a) Macroscopic view after animal sacrifice. b) Sagittal cut of distal femur, following tissue decalcification, 4 weeks after sacrifice. Scaffold in place enclosed in ovals c) Reconstruction by means of 4 images at 2,5x; panoramic view, arrows show fibrosis encapsulation. d) 20x magnification of superficial repair cartilage. e) 20x magnification of right peripheral margin; multinucleated cells shown by arrows and fibrosis are present. All histologic slides in MT stain.

Sample 57D (Fig. 21)

On a macro view, a complete repair of injury site is displayed. The articular surface at the injury site is smooth, with a white and glassy presence (Fig. 21a, b).

Histologically, repair tissue at articular surface appears fissured. Hyaline cartilage proliferation is seen from two ends joined together at the center by a fibrous tissue (Fig. 21c). There are mostly areas of hyaline cartilage, a slight hypercellularity (Fig. 21d), and a bone tissue sandwich: that is, a layer of 300 μm of bone tissue, between cartilage stratums (Fig. 21c). Tidemark has not been reconstructed.

Overall, repair tissue at joint surface morphometrically is: 89,60% of cartilage (HC+FC); 1,50% of bone and 8,90% of undifferentiated tissue. Histologically; Out of the 89,60% of quantified cartilage, 60% has hyaline cartilage appearance and 40% fibrous cartilage features; MCRS: 15;

The scaffold presents an elliptical form, located at 650 μm from the joint cavity (Fig. 21c), having a total area of 1.772.211 μm^2. The scaffold pores are mostly empty, especially in the center (Fig. 21c), where no porous structure is observed. It is partially bonded to surrounding bone and cartilage tissue (Fig. 21d), although few clusters of cartilage and bone cells are found at peripheral locations

(Fig. 21e). Scarce multinuclear cells and vessels can be found near the inferior border of the scaffold.

The morphometric quantification of tissue distribution inside the scaffold, excluding the solid biomaterial is:

ROI (%)	Cartilage	Bone	Empty Pores	Undifferentiated
Superior	13,66	0,02	74,96	11,35
Inferior	20,77	0,18	73,10	5,95
Periphery	20,92	0,60	61,00	17,48

Globally, there is a 15,82% of cartilage; 0,18% of bone and 8,97% of undifferentiated tissue content within total scaffold area, however 63,02% are still empty pores and 12,00% is solid scaffold biomaterial.

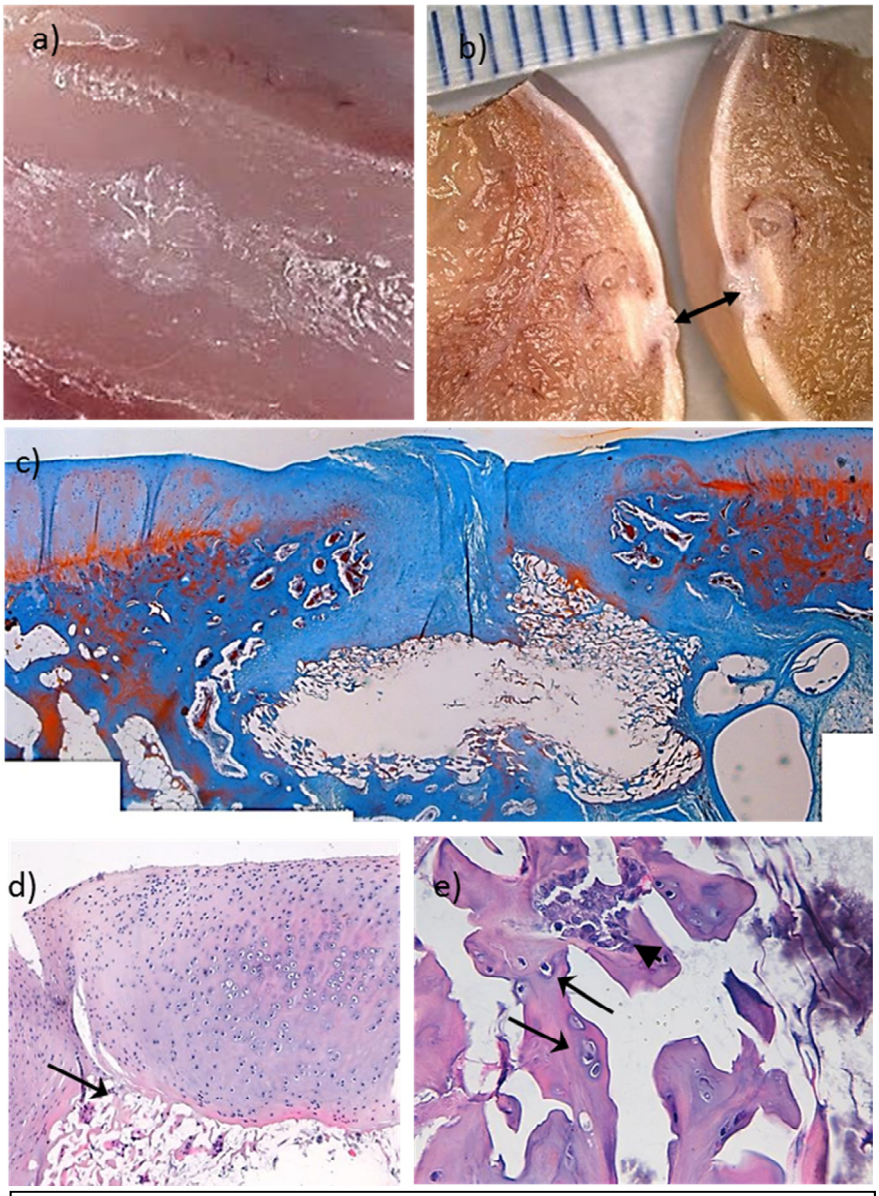

Fig. 21: Sample 57D. a) Macroscopic view after animal sacrifice. b) Sagittal cut of distal femur, following tissue decalcification, 4 weeks after sacrifice. Scaffold in place shown by arrows. c) Reconstruction by means of 4 images at 2,5x; panoramic view, MT stain. d) 10x magnification of superior border; mature repair hyaline cartilage integrating with scaffold shown by arrow. H-E stain. e) 40x magnification, osteoblast (arrowhead) and chondrocyte occupation shown by arrows. H-E stain.

Sample 60I (Fig. 22)

On a macro view of the femur, no complete union is revealed at the injury site (Fig. 22a, b). At the articular surface, there are uneven growth fragments, resulting in a central fissure of 1 mm. Tissue growth over disc surface has a glossy appearance.

Histologically, there is a severe disruption of the articular surface mostly at the center of injury (Fig. 22c). Also, an associated moderate hypercellularity of the new grown tissue is observed (Fig. 22c). There is a 750 μm fragile fibrous band that attempts to joins the loose ends of the injury (Fig. 22d), descending perpendicular to the surface and reaching the scaffold (Fig. 22c). There is no tidemark presence. Moreover, ther is an area of bone and an adipocyte band of 1.985 x 251 μm that lie just above the scaffold.

Overall, repair tissue at joint surface morphometrically is: 64,56% of cartilage (HC+FC); 29,38% of bone and 6,06% of undifferentiated tissue. Histologically: Out of the 64,56% of quantified cartilage, 35% has hyaline cartilage appearance and 65% fibrous cartilage features; MCRS: 10.

The scaffold displays an elongated egg-shape, located at 1.400 μm from the joint cavity (Fig. 22c), having a total area of 626.988 μm^2. The scaffold pores are mostly filled by bone tissue and undifferentiated cells in the superior and inferior

thirds, leaving a vacant band in the middle third of the scaffold (Fig. 22c). There are few areas of integration since a fibrous band is encapsulating most of the framework (Fig. 22c). Occasional multinuclear cells and vessels are found in the superior and inferior thirds (Fig. 22e). Picrosirius stain (Fig. 22d) expresses birefringency at new cartilage, confirming a fibrous nature that contains collagen type I, in contrast to HC.

The morphometric quantification of tissue distribution inside the scaffold, excluding the solid biomaterial is:

ROI (%)	Cartilage	Bone	Empty Pores	Undifferentiated
Superior	1,04	37,47	34,00	27,49
Inferior	0,18	20,09	45,06	34,67
Periphery	0,45	27,86	34,44	37,25

Globally, there is a 0,49% of cartilage; 26,34% of bone and 30,62% of undifferentiated tissue content within total scaffold area, though 35,74% are still empty pores and 6,81% is solid scaffold biomaterial.

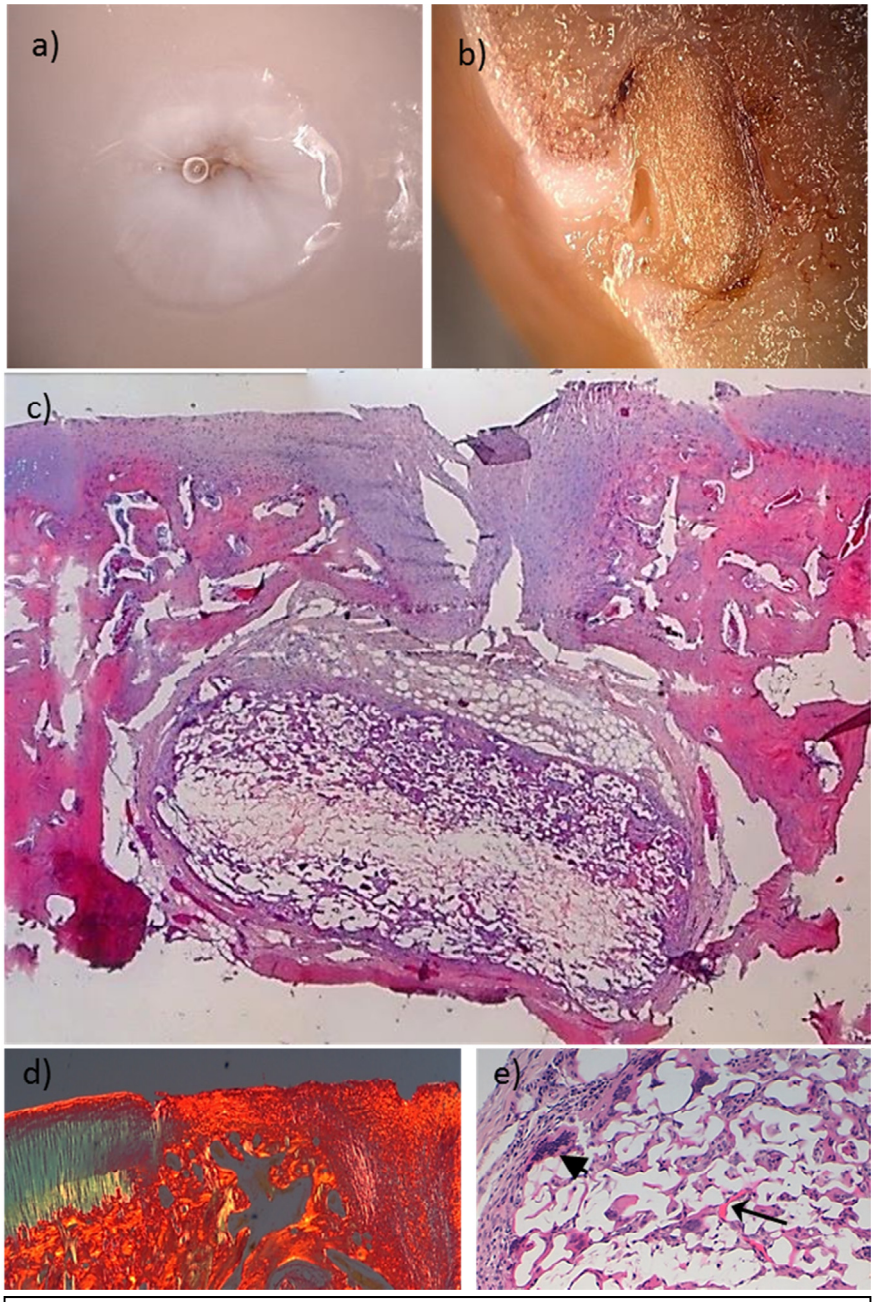

Fig. 22: Sample 60I. a) Macroscopic view after animal sacrifice. b) Sagittal cut of distal femur, following tissue decalcification, 4 weeks after animal sacrifice. Scaffold in place. c) Reconstruction by means of 4 images at 2,5x; panoramic view, H-E stain. d) Polarized light picrosirius stain, 10x magnification; hyaline and fibrous cartilage. e) 20x magnification H-E stain; fibrous tissue, multinuclear cells (arrowhead), and new vessels (arrow) are observed.

Sample 46D (Fig. 23)

On a macro view, a complete repair tissue growth at the injury site is witnessed (Fig. 23a, b). Nevertheless, at articular surface, there is no peripheral integration with the native tissue. Over the disc, the surface area is homogeneous, soft, glassy and whitish.

Histologically, it can be observed that the scaffold is aligned with articular surface, located within native cartilage tissue, in direct contact with joint cavity (Fig. 23c). There is a severe disruption of the surface regularity and structural integrity, due to the fact that the periphery of the disc has not been integrated with surrounding tissue peripherally, creating steep fissures (Fig. 23a, c), however, there is a partial bond of the scaffold with adjacent host tissue in the inferior border (Fig. 23d). Scaffold clearly protrudes over tidemark, which has not been repaired.

Overall, repair tissue at joint surface morphometrically is: 75,89% of cartilage (HC+FC); 5,08% of bone and 19,04% of undifferentiated tissue. Histologically: Out of the 75,89% of quantified cartilage, 60% has hyaline cartilage appearance and 40% fibrous cartilage features; MCRS: 13.

The scaffold presents an inverted trapezoid shape, located at 0 μm from the joint cavity (Fig. 23c), having a total area of

406.212 μm^2. The scaffold pores are mostly occupied by cartilage cells and no multinuclear cells, or new vessel growths are observed (Fig. 23d, e). Additionally, there is a central band of unoccupied pores, where a pattern in the form of a transverse undulating band can be appreciated (Fig. 23c). There is also a complete bond of the scaffold with adjacent host tissue in the inferior border, but no bond in the superior left or right borders whatsoever (Fig. 23c, d). Nevertheless, on the center of the superior margin, fibrosis and hyaline cartilage can be observed (Fig. 23e).

The morphometric quantification of tissue distribution inside the scaffold, excluding the solid biomaterial is:

ROI (%)	Cartilage	Bone	Empty Pores	Undifferentiated
Superior	29,92	1,69	46,44	21,94
Inferior	69,15	2,24	23,90	4,71
Periphery	26,91	5,72	62,62	4,76

Globally, there is a 39,51% of cartilage; 2,64% of bone and 9,91% of undifferentiated tissue content within total scaffold area, though 40,27% are still empty pores and 7,67% is solid scaffold biomaterial.

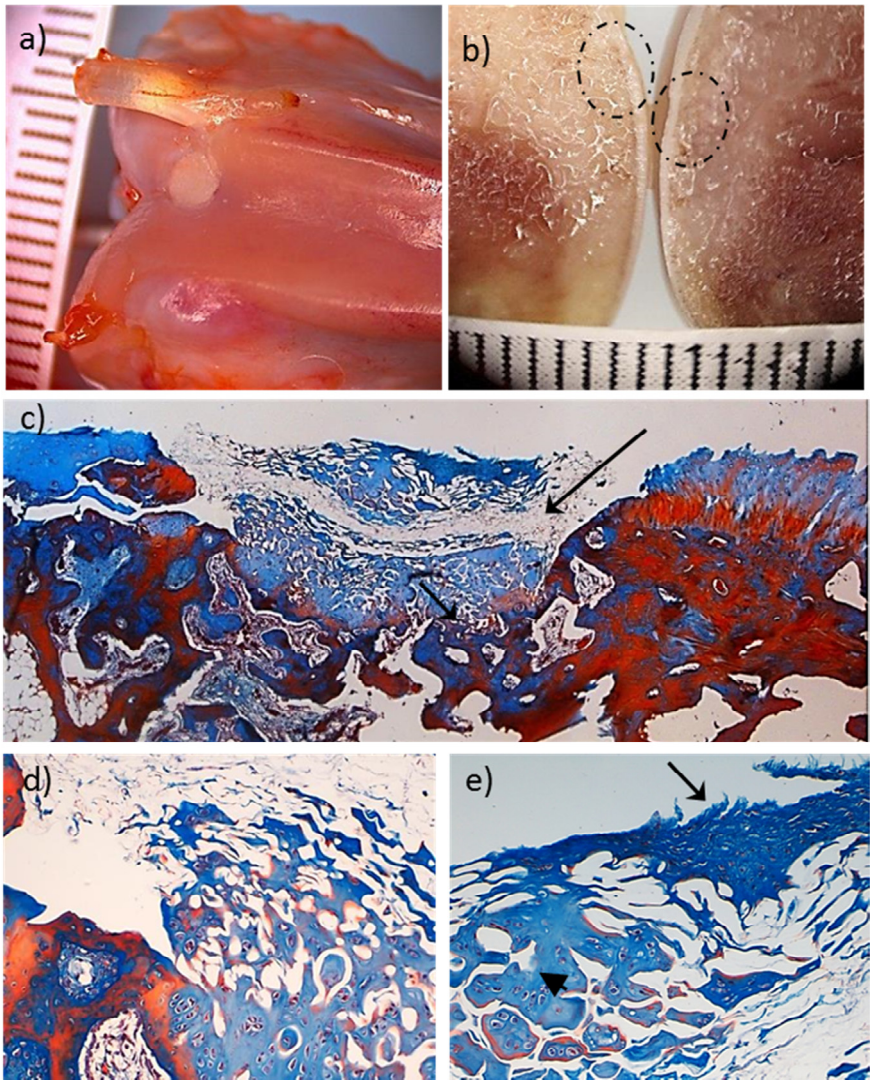

Fig. 23: Sample 46D. a) Macroscopic view after animal sacrifice. b) Sagittal cut of distal femur, following tissue decalcification, 4 weeks after sacrifice. Scaffold in place enclosed in dotted circles. c) Reconstruction by means of 2 images at 2,5x; panoramic view. A pattern of central inoccupation in the form of a transverse undulating band can be noted (arrow). d) 20x magnification; integration with inferior border, in contrast, no integration on lateral side. e) 20x magnification of superior margin; fibrosis (arrow) and hyaline cartilage (arrowhead) can be seen. All histologic slides in MT stain.

Sample 52D (Fig. 24)

On a macro view a small indent is observed at the repaired surface (Fig. 24a, b). At articular surface, there is an outlying repair tissue growth over the disc, which surface has an irregular white arrangement.

Histologically, the scaffold is observed aligned with the surface; located within native cartilage tissue, in direct contact with joint cavity (Fig. 24c). There is a severe disruption and fibrillation of the surface, with a lack of integration of the scaffold, and associated to a severe hypocellularity (Fig. 24c). However, there is a thin fibrous band that attempts to cover the superior margin of the scaffold (Fig. 24d). The tidemark, on the other hand is absent. The scaffold is protruding into deeper tissues. Still, there is a partial bond with adjacent host tissue.

Overall, repair tissue at joint surface morphometrically is: 11,32% of cartilage (HC+FC); 34,29% of bone and 54,39% of undifferentiated tissue Histologically: Out of the 11,32% of quantified cartilage, 20% has hyaline cartilage appearance and 80% fibrous cartilage features; MCRS: 5.

The scaffold has a rectangular shape, located at 0 μm from the joint cavity (Fig. 24c), with a total area of 2.450.150 μm^2. The scaffold pores are mostly occupied by undifferentiated tissue, although bone and cartilage clusters are observed near the

inferior margin (Fig. 24e). There is also a wide unoccupied central band. Partial bonding of the scaffold with adjacent host tissue occurs in the inferior border, principally with bone tissue (Fig. 24e), where scarce vessels and multinucleated cells are found; nonetheless no bond in the superior left or right margins with cartilage are observed.

The morphometric quantification of tissue distribution inside the scaffold, excluding the solid biomaterial is:

ROI (%)	Cartilage	Bone	Empty Pores	Undifferentiated
Superior	2,15	7,17	61,81	28,86
Inferior	7,16	26,78	53,48	12,57
Periphery	5,51	4,85	57,73	31,91

Globally, there is a 4,28% of cartilage; 12,96% of bone and 20,55% of undifferentiated tissue content within total scaffold area, though 54,75% are still empty pores and 7,47% is solid scaffold biomaterial.

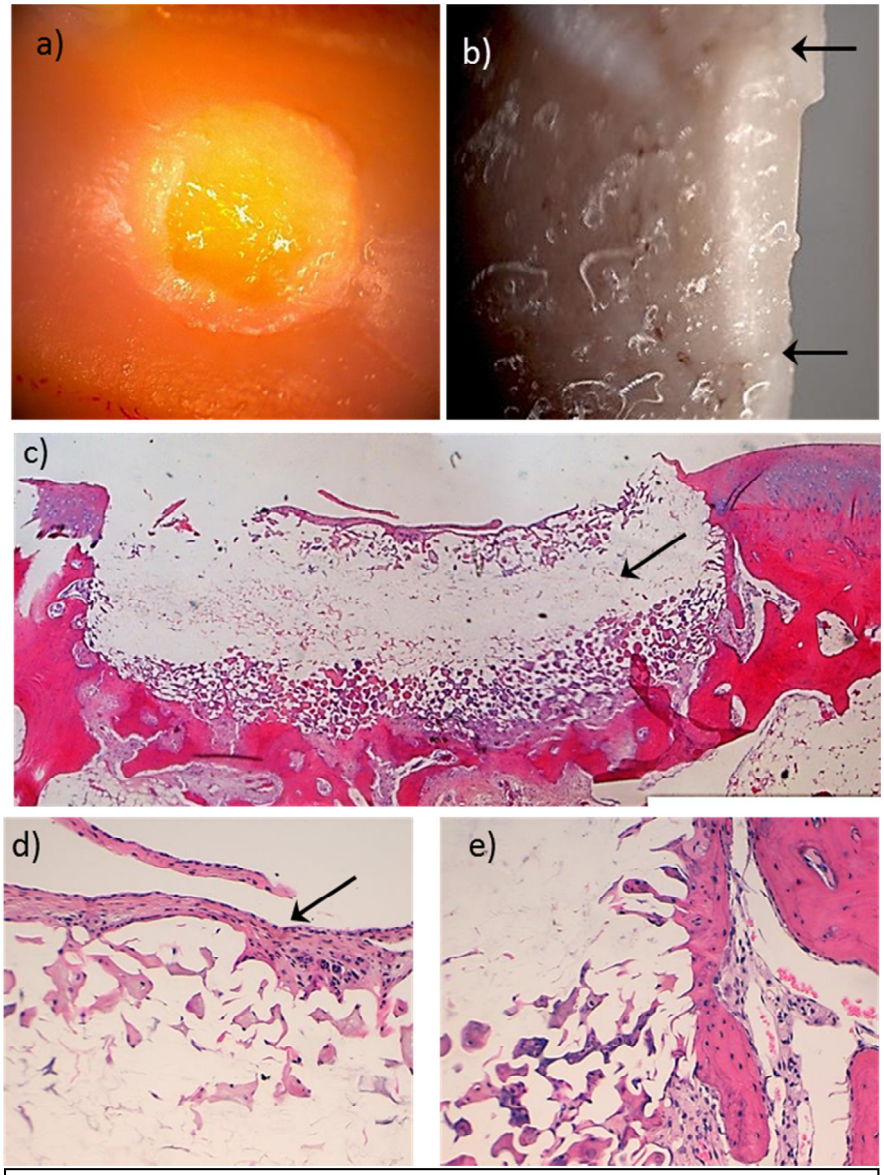

Fig. 24: Sample 52D. a) Macroscopic view after animal sacrifice. b) Sagittal cut of distal femur, following tissue decalcification, 4 weeks after animal sacrifice. Scaffold in place shown by arrows. c) Reconstruction by means of 3 images at 2,5x; panoramic view. A pattern of central band inoccupation can be noted (arrow) d) 20x magnification of superior border; fibrous band on surface (arrow). e) 20x lateral margin; scaffold integration with adjacent tissues, middle third unoccupied. All histologic slides in H-E stain.

3.1.3 **Group C** (5% cross-linker)

Experimental group C comprises six samples. There are two patterns of scaffold behavior. There is also a predominance of deep (n=4) to superficial-seated (n=2) scaffold pattern. The general structure of uninjured cartilage has been partially reconstructed by repair tissue; however, repair scores reveal a wide dispersion of data.

At superficial joint site (Fig. 25a), repair tissue is predominantly cartilage, with 74,48% of the total repair area above the scaffold. Bone and undifferentiated tissue is present in similar proportions.

In the interior of scaffolds (Fig. 25b), pores have been mostly occupied, when compared to other trial groups. Three main tissues were identified, cartilage most frequently, followed by undifferentiated tissue and bone with similar proportions. High content of vessels and multinuclear cells is observed, which suggests high turnover cellular activity.

Both one superficial and one deep-seated scaffold achieved best results; on the other hand, other scaffolds performed poor tissue regeneration.

Repair tissue at joint surface (Fig. 25a):

- Morphometric quantification: Cartilage (HC+FC): 74,48%; Bone: 12,98%; Undifferentiated tissue: 11,94%.
- Histological criteria: Out of 74,48% of the measured cartilage, 41% had hyaline cartilage appearance and 59% had fibrous characteristics; MCRS group average: 12, 0 (CI: 5 - 20).

Repair tissue inside the scaffolds (Fig. 25b):

- Morphometric quantification (respect to total scaffold area): Cartilage: 25,62%; Bone: 20,13%; Undifferentiated tissue: 20,26%; Empty pores: 29,91%, Solid scaffold: 4,08%;

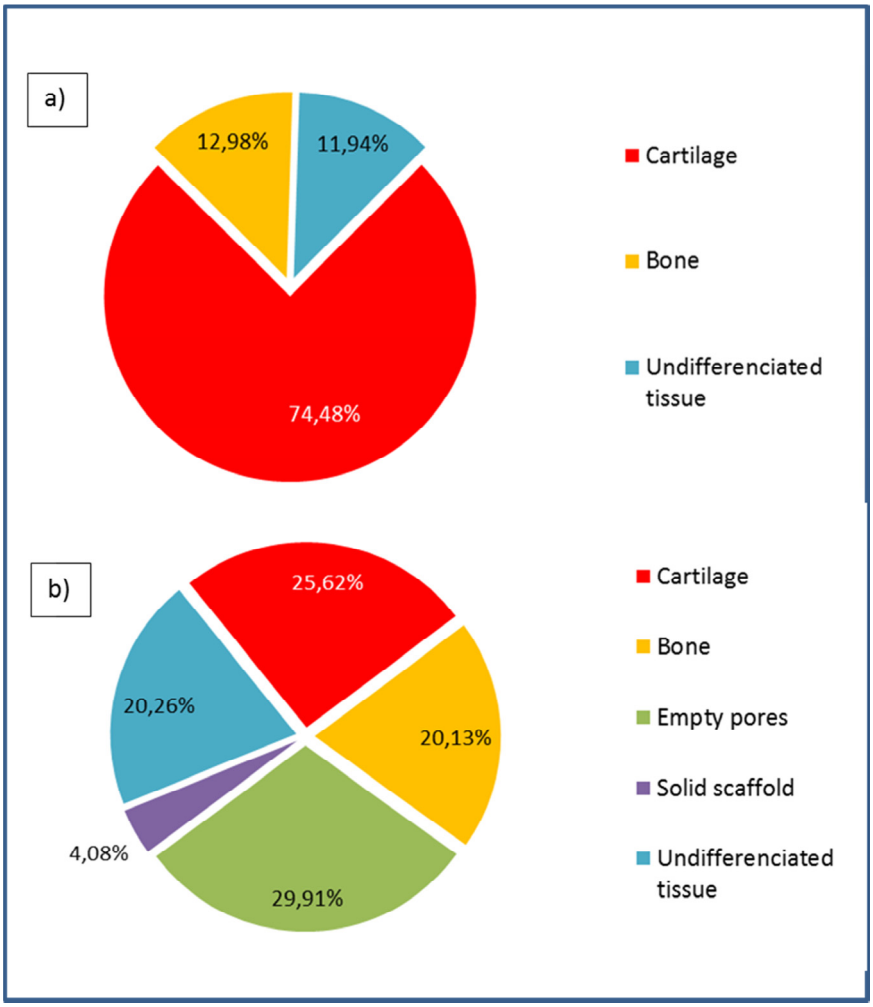

Fig. 25: Group C. Morphometric quantification of tissue distribution: a) At joint surface. b) Inside the scaffolds respect to total scaffold area.

The following section contains case by case analysis of group C samples. Detailed description of morphological features is displayed:

Sample 48I (Fig. 26)

On a macro view of the distal femur, the disc is observed underneath the surface, in a profounder interval. At the articular surface, there is a marginal growth of repair tissue, with an irregular small profile, yet similar to adjacent articular cartilage (Fig. 26a, b).

Histologically, it is observed that the repair tissue has only partially covered the articular surface; roughly over half of the scaffold is uncovered by tissue (Fig. 26c). Additionally, there is severe discontinuity of the surface, given by a 1.680 μm gap (Fig. 26c). Mild cluster grouping at superficial repair site suggests degenerative changes (Fig. 26d). However, there is a wide band of hypercellular fibrous tissue sheltering the uncovered part of the scaffold (Fig. 26c). Tidemark has not been reconstructed.

Overall, repair tissue at joint surface morphometrically is: 45,11% of cartilage (HC+FC); 22,05% of bone and 31,90% of undifferentiated tissue. Histologically: Out of the 45,11% of

quantified cartilage, 15% has hyaline cartilage appearance and 85% fibrous cartilage features; MCRS: 5.

The scaffold has adopted an elongated, elliptical form, with oblique positioning with respect to articular surface (Fig. 26b, c). It is located at 0 – 1.000 μm from the joint cavity (Fig. 26c) and has a total area of 1.452.823 μm^2. The scaffold pores are almost entirely filled by cartilage, bone and undifferentiated cells, with scarce empty spaces (Fig. 26c). We compared its features with native surrounding tissue, in order to enable cartilage and bone classification. Tissue not adjusting to such characteristics was classified as undifferentiated tissue. Integration is restricted by a fibrous band capturing most of the scaffold's content (Fig. 26c, d), although 10% of the perimeter near the inferior margin demonstrates integration with host bone tissue. New vessel growth can be found all throughout the scaffold. Scarce unusually large multinuclear cells are found near the superior and inferior margins (Fig. 26e).

The morphometric quantification of tissue distribution inside the scaffold, excluding the solid biomaterial is:

ROI (%)	Cartilage	Bone	Empty Pores	Undifferentiated
Superior	3,82	36,60	34,52	25,07
Inferior	11,66	25,04	36,67	26,63
Periphery	3,79	37,96	36,07	22,18

Globally, there is a 6,71% of cartilage; 30,68% of bone and 23,92% of undifferentiated tissue content within total scaffold

area, while 34,04% are still empty pores and 4,64% is solid scaffold biomaterial.

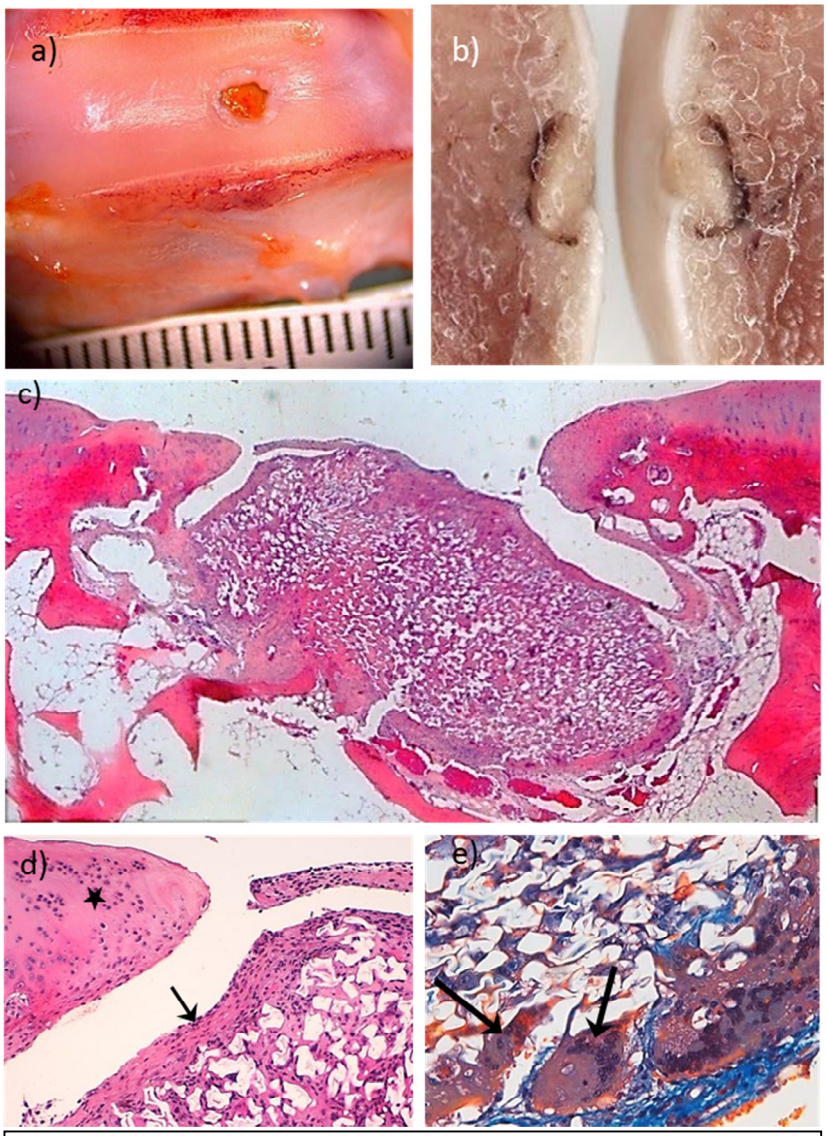

Fig. 26: Sample 48I. a) Macroscopic view after animal sacrifice. b) Sagittal cut of distal femur, following tissue decalcification, 4 weeks after sacrifice. Scaffold in place. c) Reconstruction by means of 4 images at 2,5x; panoramic view, H-E stain. A surface gap can be noticed. d) 20x magnification of superior border; cartilage growth end separated by fissure and fibrous tissue (shown by arrow) from scaffold. Mild cellular clusters are observed in repair tissue (shown by star). H-E stain. e) 40x magnification of inferior margin; giant multinuclear cells shown by arrows and surrounding fibrous tissue are observed. MT stain.

Sample 52I (Fig. 27)

On a macro view, it is observed that the two sides of the disc have had an uneven development; one side, with repair tissue growth covering half of injury site, whereas the other side, leaving scaffold exposed to the surface (Fig. 27a, b). At the articular surface, repair tissue is pale, while uncovered disc presents a more pinkish color.

Histologically, an uneven growth of both sides of the disc can be seen, as grasped macroscopically (Fig. 27c). Repair tissue of the articular surface appears with fissures, due to the incomplete integration of the superficial part of the scaffold (Fig. 27c). There is a slight disruption of the structural integrity and mild cell clustering yet there are several areas of immature hyaline cartilage (Fig. 27d). A 2.000 μm long portion of the surface (which contains scaffold in the interior) separates the completely repaired cartilage borders (Fig. 27c), hence the disrupted surface. Tidemark is absent and has not been reconstructed.

Overall, repair tissue at joint surface morphometrically is: 96,01% of cartilage (HC+FC); 1,29% of bone and 1,08% of undifferentiated tissue. Histologically: Out of the 96,01% of quantified cartilage, 50% has hyaline cartilage appearance and 50% fibrous cartilage features; MCRS: 16.

The scaffold presents a unique oblique form, and it is located at 0 - 500 µm from the joint cavity (Fig. 27c), having a total area of 1.544.791 μm^2. This sloping inlay of the scaffold grants it a partial superficial and a partial deep-seating behavior. The scaffold pores are mostly occupied by new repair tissue (Fig. 27c). Cartilage and bone, as well as undifferentiated tissue are identified. Some areas, particularly in the superficial portion, have essentially cartilage features (Fig. 27d). It is completely bonded to surrounding tissue, both the superficial, as well as the deep-seated shares (Fig. 27d, e). Frequently multinuclear cells and vessels can be found near the inferior border (Fig. 27e).

The morphometric quantification of tissue distribution inside the scaffold, excluding the solid biomaterial is:

ROI (%)	Cartilage	Bone	Empty Pores	Undifferentiated
Superior	22,02	2,61	41,98	33,39
Inferior	18,96	17,90	40,85	22,29
Periphery	47,47	8,17	27,79	16,57

Globally, there is a 25,49% of cartilage; 8,41% of bone and 24,58% of undifferentiated tissue content within total scaffold area, however 36,54% are still empty pores and 4,98% is solid scaffold biomaterial.

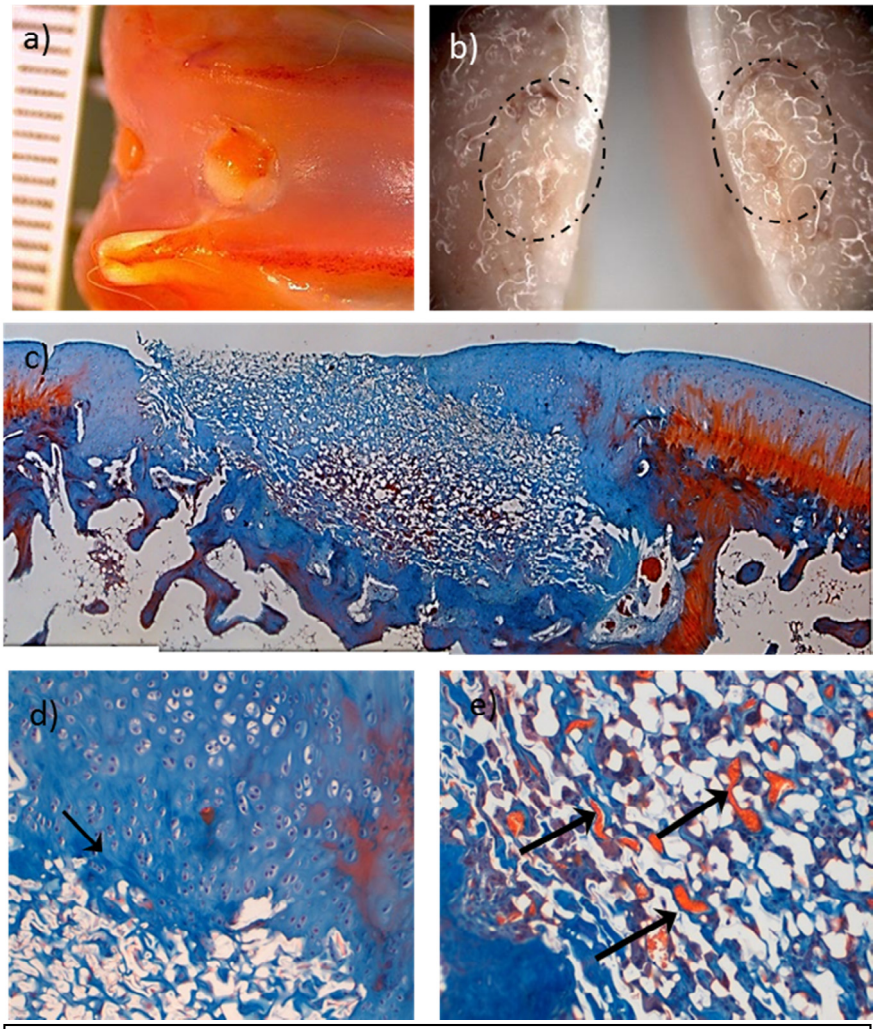

Fig. 27: Sample 52I. a) Macroscopic view after animal sacrifice. b) Sagittal cut of distal femur, following tissue decalcification, 4 weeks after sacrifice. Scaffold in place enclosed in dotted circle. c) Reconstruction by means of 3 images at 2,5x; panoramic view. A deep and superficial pattern of scaffold establishment is observed. d) 20x magnification of superior border; immature cartilage integrating with scaffold (arrow). e) 20x magnification of inferior margin; integration with bone tissue, abundant new vessel growth shown by arrows. All histological slides with MT stain.

Sample 57I (Fig. 28)

On a macro view of the distal femur, a complete repair tissue growth over the injury site is beheld; surface area of the disc is somewhat uneven and whitish (Fig. 28a, b).

Histologically, repair tissue of the articular surface appears with a slight disintegration given by clefts and fissures (Fig. 28c). An associated cell cluster formation is also observed within new formed cartilage. The 400 μm thick cartilage has immature, but hyaline characteristics. Underneath, a 700 μm thick osseous band above the scaffold position (Fig. 28c). The tidemark has not been reconstructed.

Overall, repair tissue at joint surface morphometrically is: 65,51% of cartilage (HC+FC); 33,15% of bone and 1,33% of undifferentiated tissue. Histologically: Out of the 65,51% of quantified cartilage, 70% has hyaline cartilage appearance and 30% fibrous cartilage features; MCRS: 17.

The scaffold displays an elongated oval shape, located at 1.100 μm from the joint cavity (Fig. 28c), having a total area of 1.036.188 μm^2. The scaffold pores are mostly filled by cartilage and bone tissue. However, copious undifferentiated cells are observed in the superior two thirds, leaving a less occupied band in the bottom third of the scaffold (Fig. 28c). There are some areas of integration with adjacent tissue (Fig. 28d),

restricted by a fibrous band on 25% of the frame perimeter (Fig. 28e). Occasional multinuclear cells and vessels are found all throughout the scaffold (Fig. 28d).

The morphometric quantification of tissue distribution inside the scaffold, excluding the solid biomaterial is:

ROI (%)	Cartilage	Bone	Empty Pores	Undifferentiated
Superior	2,02	34,27	61,35	2,36
Inferior	2,69	29,66	65,87	1,77
Periphery	5,96	39,72	51,85	2,47

Globally, there is a 3,12% of cartilage; 31,60% of bone and 2,03% of undifferentiated tissue content within total scaffold area, though 55,66% are still empty pores and 7,59% is solid scaffold biomaterial.

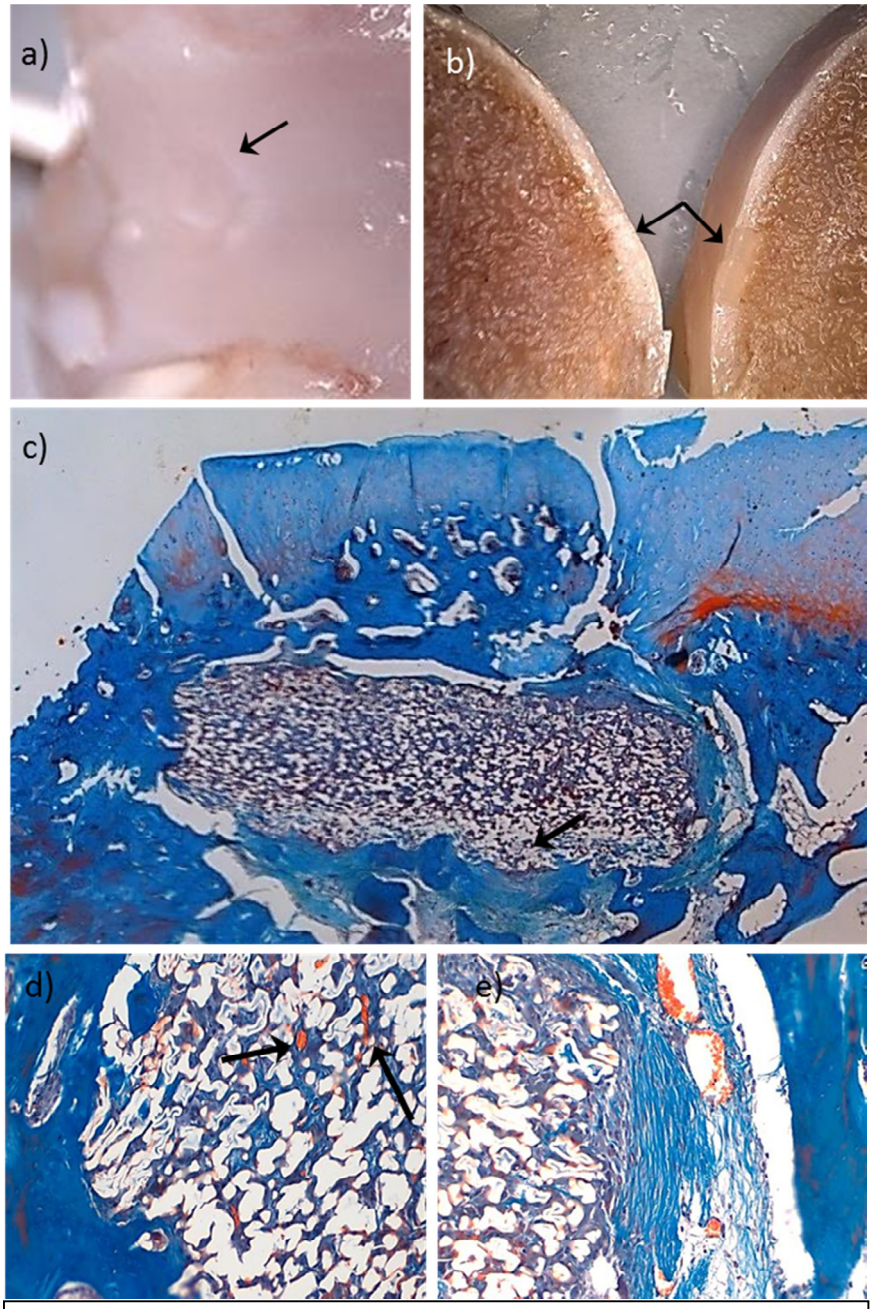

Fig. 28: Sample 57I. a) Macroscopic view after animal sacrifice. Scaffold in place shown by arrow. b) Sagittal cut of distal femur, following tissue decalcification, 4 weeks after sacrifice. Scaffold in place shown by arrows. c) Reconstruction by means of 5 images at 2,5x; panoramic view. A band of less tissue occupation at inferior third is shown by arrow. d) 20x inferior margin; integration and new vessel growth shown by arrows. e) 20x right border; surrounding fibrosis. All histological slides with MT stain.

Sample 58D (Fig. 29)

On a macro view, a lack of fusion between neocartilage fronts can be observed at injury site. There are several growth segments developing unevenly, resulting in a 1 mm cleft (Fig. 29a, b). Surface of the disc at articular site has different areas with matte and whitish appearance.

Histologically, a slight disruption of the surface structural integrity is observed (Fig. 29c), given the above mentioned cleft. Two cartilage tissue ends are separated by a 700 μm fibrous center (Fig. 29c, d). In these cartilage ends, there are mostly areas of hyaline cartilage, with mild hypocellularity content (Fig. 29c). Tidemark has not been reconstructed.

Overall, repair tissue at joint surface morphometrically is: 81,96% of cartilage (HC+FC); 4,59% of bone and 13,44% of undifferentiated tissue. Histologically: Out of the 81,96% of quantified cartilage, 20% has hyaline cartilage appearance and 80% fibrous cartilage features; MCRS: 7.

The scaffold presents a particular distorted shape (Fig. 29c) and different parts of the scaffold are located between 0 and 1200 μm from the joint cavity (Fig. 29c), having a total area of 1.898.516 μm^2. The scaffold pores are occupied by cartilage and bone, but mostly undifferentiated tissue (Fig. 29e). In order to discriminate cells, we have compared features with native

surrounding tissue, enabling us to identify cartilage and bone structures. Tissue not complying with such characteristics has been classified as undifferentiated. The scaffold is mostly encapsulated by fibrous tissue (Fig. 29c). It is also barely bonded to surrounding host tissue, especially osseous tissue. Sporadic multinuclear cells are observed (Fig. 29e), while numerous vessels can be found in the entire scaffold.

The morphometric quantification of tissue distribution inside the scaffold, excluding the solid biomaterial is:

ROI (%)	Cartilage	Bone	Empty Pores	Undifferentiated
Superior	29,38	24,42	16,05	30,15
Inferior	8,51	39,41	26,80	25,28
Periphery	19,60	39,31	22,91	18,19

Globally, there is a 18,80% of cartilage; 32,87% of bone and 24,50% of undifferentiated tissue content within total scaffold area, yet 20,97% are still empty pores and 2,86% is solid scaffold biomaterial.

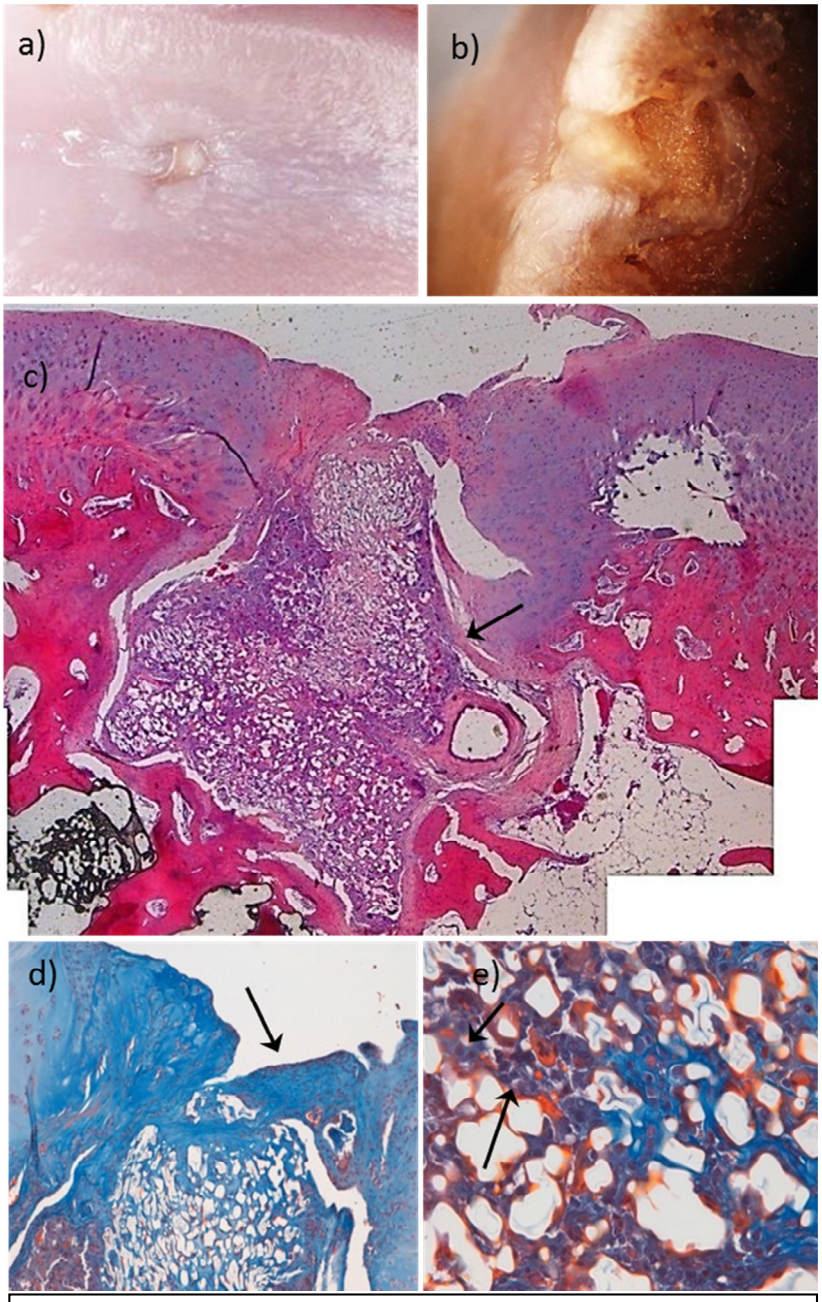

Fig. 29: Sample 58D. a) Macroscopic view after animal sacrifice. b) Sagittal cut of distal femur, following tissue decalcification 6 weeks after sacrifice. Scaffold in place c) Reconstruction by means of 5 images at 2,5x; panoramic view, H-E stain. A dismorphic scaffold can be noticed. Fibrosis is shown by arrow. d) 20x magnification of MT stain; repair fibrous, incomplete center shown by arrow. e) 40x magnification of central scaffold. Undifferentiated cells are shown by arrows. MT stain.

Sample 48D (Fig. 30)

On a macro view of the distal femur, a complete repair tissue growth over the injury site is observed (Fig. 30a, b). Nevertheless, zones with no peripheral integration with native tissue are identified (Fig. 30a). Disc surface area is mostly white; then again a marginal fold with a more pinkish color can be seen (Fig. 30a, b).

Histological study shows that, scaffold is aligned with surface, located within native cartilage tissue, in direct contact with joint cavity (Fig. 30c). There is horizontal lamination and a slight disruption of the surface integrity given by lack of integration of the left lateral margin (Fig. 30c). A fibrocartilage layer covers one fourth of the surface (Fig. 30c, d). Scaffold extends beyond tidemark, which is still absent (Fig. 30c).

Overall, repair tissue at joint surface morphometrically is: 64,29% of cartilage (HC+FC); 15,35% of bone and 18,73% of undifferentiated tissue. Histologically; Out of the 64,29% of quantified cartilage, 80% has hyaline cartilage appearance and 20% fibrous cartilage features; MCRS: 20.

The scaffold presents a trapezoid shape; it is located at 0 μm from the joint cavity (Fig. 30c) and has a total area of 1.881.727 μm^2. The scaffold pores are mostly occupied by cartilage cells (Fig. 30d, e), however, bone and undifferentiated cells are also

present, concentrated near the inferior margin (Fig. 30e). There is a complete bond with the adjacent tissues, especially with articular cartilage (Fig. 30c, d). Some multinuclear cells and vessels are observed close to the inferior margin (Fig. 30e).

The morphometric quantification of tissue distribution inside the scaffold, excluding the solid biomaterial is:

ROI (%)	Cartilage	Bone	Empty Pores	Undifferentiated
Superior	72,11	1,44	10,36	16,09
Inferior	71,60	1,35	10,57	16,47
Periphery	65,84	3,01	8,15	23,00

Globally, there is a 69,52% of cartilage; 1,92% of bone and 17,35% of undifferentiated tissue content within total scaffold area. At the time of sacrifice, 9,87% are still empty pores and 1,35% is solid scaffold biomaterial.

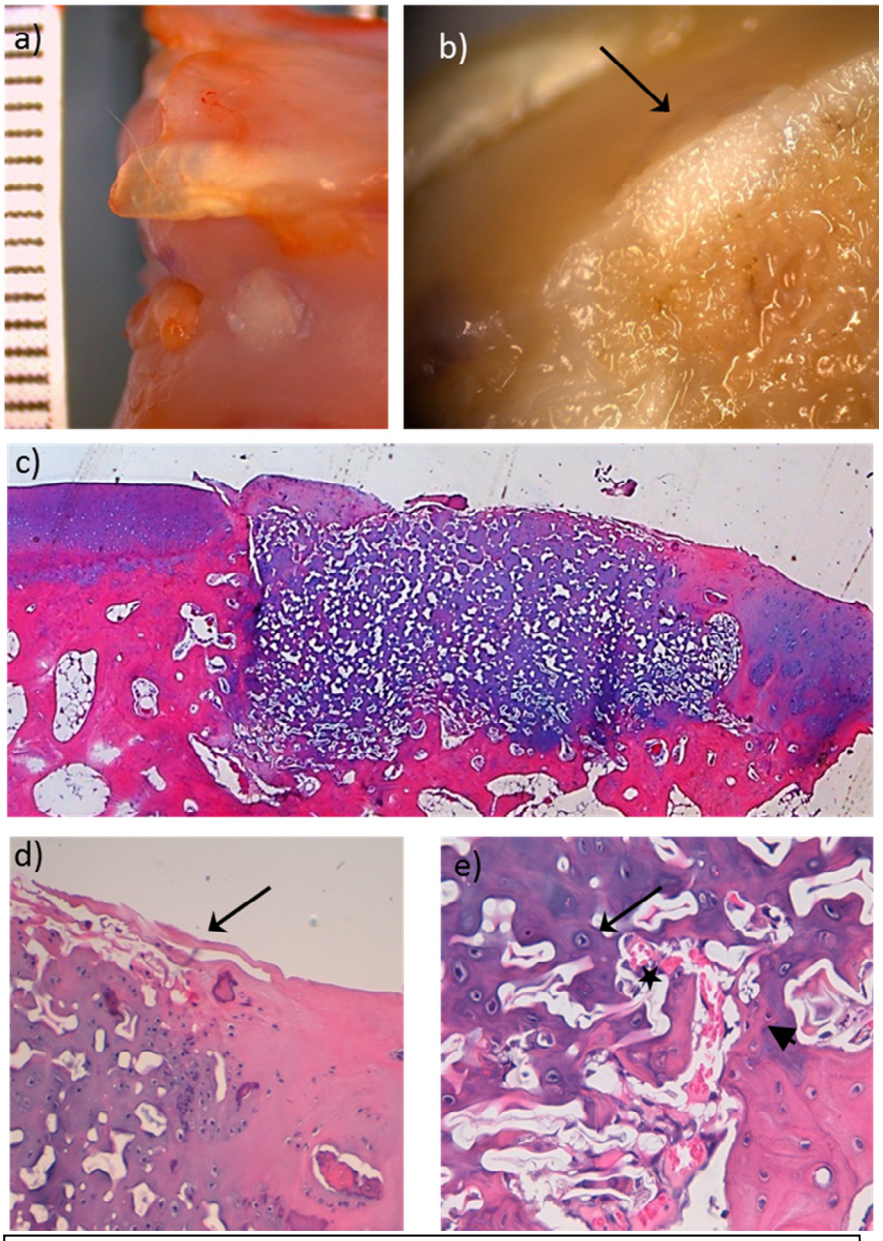

Fig. 30: Sample 48D. a) Macroscopic view after animal sacrifice. b) Sagittal cut of distal femur, following tissue decalcification, 4 weeks after sacrifice. Scaffold in place shown by arrow. c) Reconstruction by means of 2 images at 2,5x; panoramic view. d) 20x magnification of the right superior margin; excellent integration, surface fibrosis and lamination shown by arrow. e) 40x inferior border magnification; cartilage (arrow) and bone (arrowhead) integration. Vessel shown by star. All histological slides with H-E stain.

Sample 54I (Fig. 31)

On a macro view, cartilage injury site is completely occupied by disc and has sectors with no peripheral integration with native tissue (Fig. 31a, b). At the articular surface, superficial disc area is mostly white, while adjacent cartilage presents irregularities and reddish colors (Fig. 31a).

Histologically, we observe that the scaffold is aligned with surface, located within native cartilage tissue, in direct contact with joint cavity (Fig. 31c). There is a slight disruption given by fissures of the cartilage surface associated to a mild hypocellularity. Furthermore, there is a 1.500 μm long gap separating the 2 clearly uninjured fronts, one of which is bonded to scaffold by a fine fibrous band (Fig. 31c). Tidemark is present; scaffold does not protrude into deeper bone tissue (Fig. 31d).

Overall, repair tissue at joint surface morphometrically is: 93,81% of cartilage (HC+FC); 1,26% of bone and 4,92% of undifferentiated tissue. Histologically: Out of the 93,81% of quantified cartilage, 10% has hyaline cartilage appearance and 90% fibrous cartilage features; MCRS: 8.

The scaffold has a rectangular shape, located at 0 μm from the joint cavity (Fig. 31c), with a total area of 411.550 μm^2. The scaffold pores are occupied by cartilage and bone, as well as

undifferentiated tissue with an underdeveloped cell matrix (Fig. 31d, e). In order to discriminate cells, we have compared features with native surrounding tissue, enabling us to identify cartilage and bone structures. Tissue not complying with such characteristics has been classified as undifferentiated. Restricted bonding with host tissue occurs in about 40% of the inferior and lateral borders; however, no continuity is seen on right inferior and lateral margins (Fig. 31c, d). No vessels or multinucleated cells are found.

The morphometric quantification of tissue distribution inside the scaffold, excluding the solid biomaterial is:

ROI (%)	Cartilage	Bone	Empty Pores	Undifferentiated
Superior	12,69	27,22	41,94	18,15
Inferior	26,15	16,49	24,80	32,57
Periphery	43,52	7,97	8,49	40,03

Globally, there is a 30,07% of cartilage, 15,33% of bone and 29,20% of undifferentiated tissue content within total scaffold area, although 22,35% are still empty pores and 3,05% is solid scaffold biomaterial.

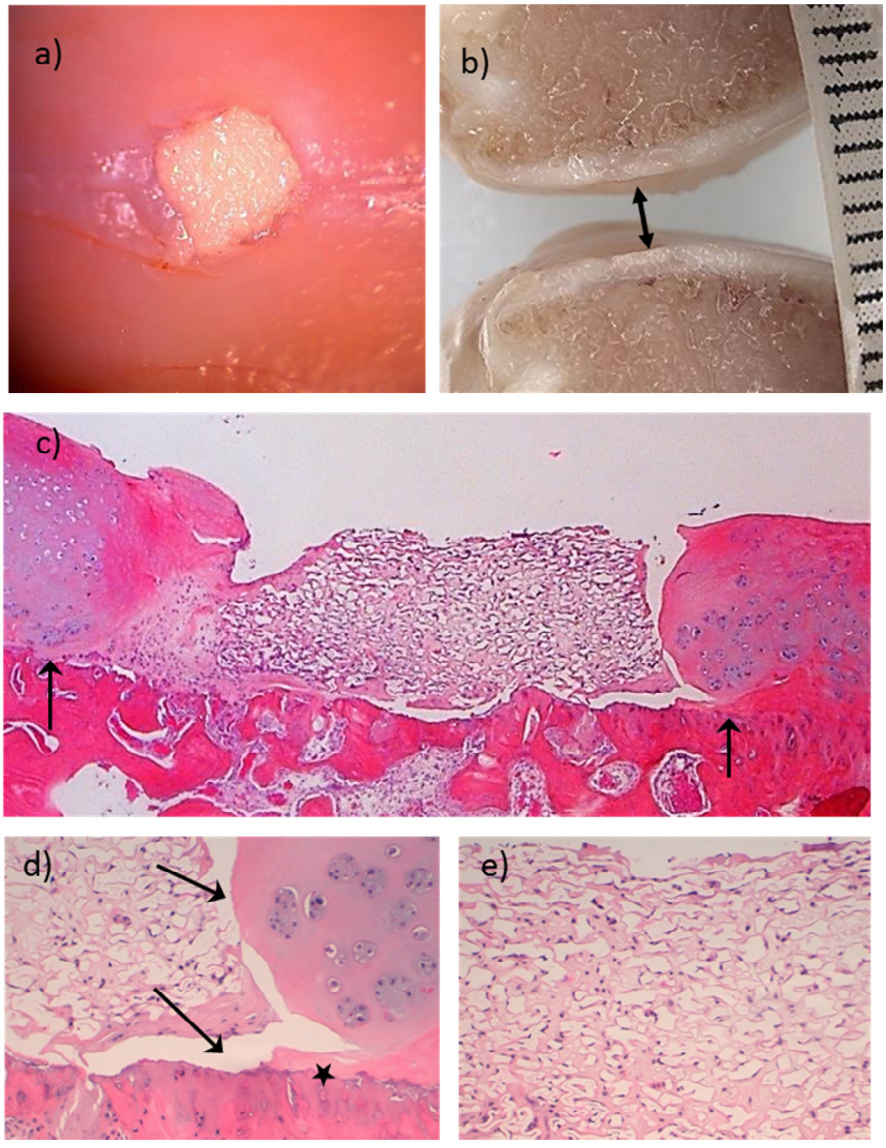

Fig. 31: Sample 54I. a) Macroscopic view after animal sacrifice. b) Sagittal cut of distal femur, following tissue decalcification 4 weeks after sacrifice. Scaffold in place shown by arrows. c) Reconstruction by means of 2 images at 2.5x; panoramic view. Tidemark is signaled by arrows. d) 20x magnification of right margin; no integration shown by arrows and some fibrosis present. Present Tidemark shown by star. e) 20x central superior margin magnification; undifferentiated scarce tissue is observed. All histological slides in H-E stain

3.1.4 **Group D** (7% cross-linker)

Trial group D comprehends five samples, two of which have been excluded, due to early rabbit loss (3 weeks). There is an equilibrium between superficial (n=1,5) and deep-seated (n=1,5) scaffold behavior that partially rebuilds the injury site.

At superficial joint site (Fig. 32a), cartilage, as well as fibrous tissue and bone are present in the repair tissue. Still, cartilage is preponderant, followed by bone and undifferentiated repair tissue. The repair of previously healthy hyaline cartilage has been poor, as seen on low repair scores. Different criteria applied by the modified cartilage repair score (MCRS) described earlier define the quality of repair tissue.

In the interior of scaffolds (Fig. 32b), bone tissue is the most abundant, nevertheless, an equilibrium between the tissues being studied can be interpreted. Scaffold framework is irregular, deformed, collapsed, and mostly unoccupied by cells.

Repair tissue at joint surface (Fig. 32a):

- Morphometric quantification: Cartilage (HC+FC): 57,30%; Bone: 22,93%; Undifferentiated tissue: 19,48%.
- Histological criteria: Out of 57,30% of the measured cartilage, 27% had hyaline cartilage appearance and

73% had fibrous characteristics MCRS group average: 10,0 (CI: 5 - 20).

Repair tissue inside the scaffolds (Fig. 32b):

- Morphometric quantification (respect to total scaffold area): Cartilage: 11,01%; Bone: 13,99%; Undifferentiated tissue: 8,95%; Empty pore: 44,25%, Solid scaffold: 21,80%.

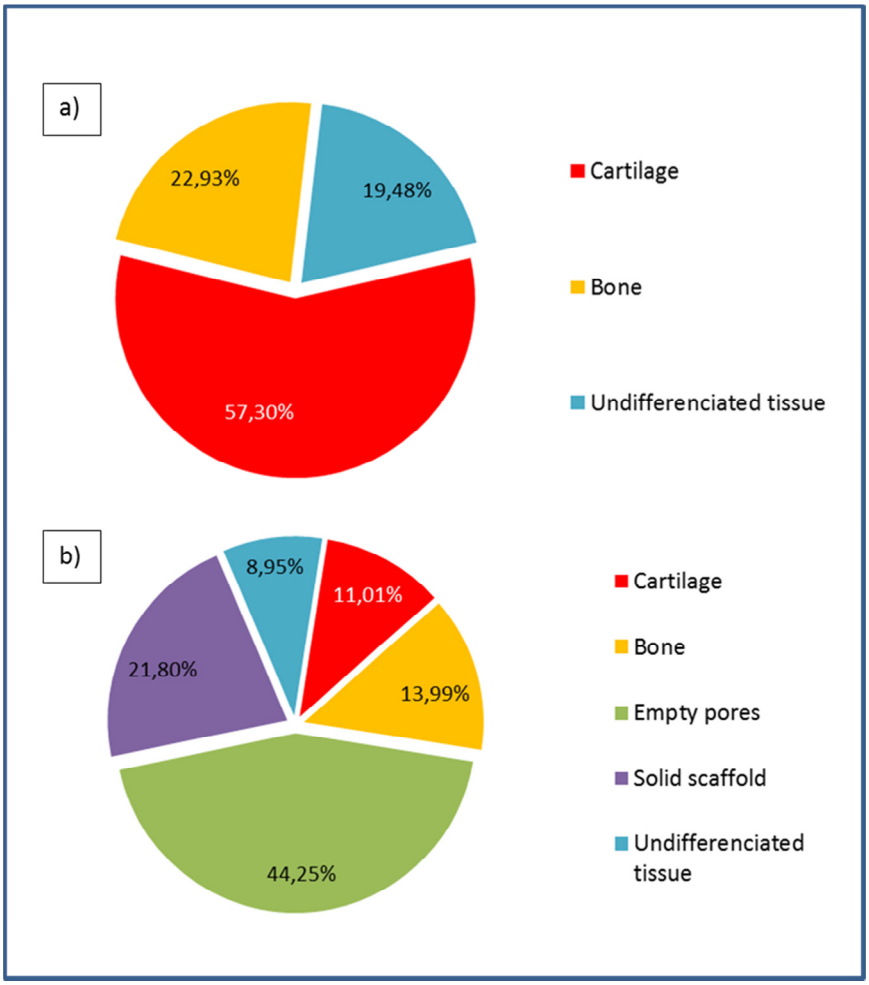

Fig. 32: Group D. Morphometric quantification of tissue distribution:
a) At joint surface. b) Inside the scaffolds respect to total scaffold area.

The following section contains case by case analysis of group D samples. Detailed description of morphological features is displayed:

Sample 58I (Fig. 33)

On a macro view of the distal femur, it can be observed that total fusion of the regenerated tissue on the implanted disc has occurred (Fig. 33a, b). However, there is a bumpy surface, given an uneven growth of repair tissue. Furthermore, at the articular surface, there is a whitish zone that protrudes into the joint area. The rest of the tissue growth at the injury site has similar characteristics to those of adjacent cartilage (Fig. 33a).

Histological study shows that repair tissue has a plug-like appearance with hyaline cartilage features on the surface (Fig. 33c). The repair tissue present from joint surface to the scaffold superior margin is of cartilage nature. Nontheless, it contains a circular 800 μm diameter bone area in the center. It is exposed in a sandwich disposition (Fig. 33c, d). There is also, a minor disruption of the structural integrity, set by fissures (Fig. 33c). The tidemark has not been repaired.

Overall, repair tissue at joint surface morphometrically is: 67,92% of cartilage (HC+FC); 28,72% of bone and 3,36% of undifferentiated tissue. Histologically: Out of the 67,92% of

quantified cartilage, 45% has hyaline cartilage appearance and 55% fibrous cartilage features; MCRS: 13.

The scaffold displays a collapsed rectangular shape, located at 1,500 μm from the joint cavity (Fig. 33c), having a total area of 1.602.219 μm^2. The scaffold pores are mostly unoccupied, especially in a central horizontal band, where fragile biomaterial walls have ruptured (Fig. 33c). In the scarce areas occupied, cell population is mainly undifferentiated, but some areas feature hyaline-like cells (Fig. 33d). In order to discriminate cells, we have compared characteristics with native surrounding tissue, enabling us to identify cartilage and bone structures. Tissue not complying with such characteristics has been classified as undifferentiated. There is partial scaffold integration with surrounding tissue (Fig. 33e). No fibrosis, multinuclear cells or new vessel growth can be identified.

The morphometric quantification of tissue distribution inside the scaffold, excluding the solid biomaterial is:

ROI (%)	Cartilage	Bone	Empty Pores	Undifferentiated
Superior	18,75	13,29	51,36	16,60
Inferior	2,81	8,82	83,29	5,08
Periphery	13,95	15,43	54,09	16,53

Globally, there is a 7,85% of cartilage, 8,84% of bone and 8,52% of undifferentiated tissue content within total scaffold area,

although 50,11% are still empty pores and 24,68% is solid scaffold biomaterial.

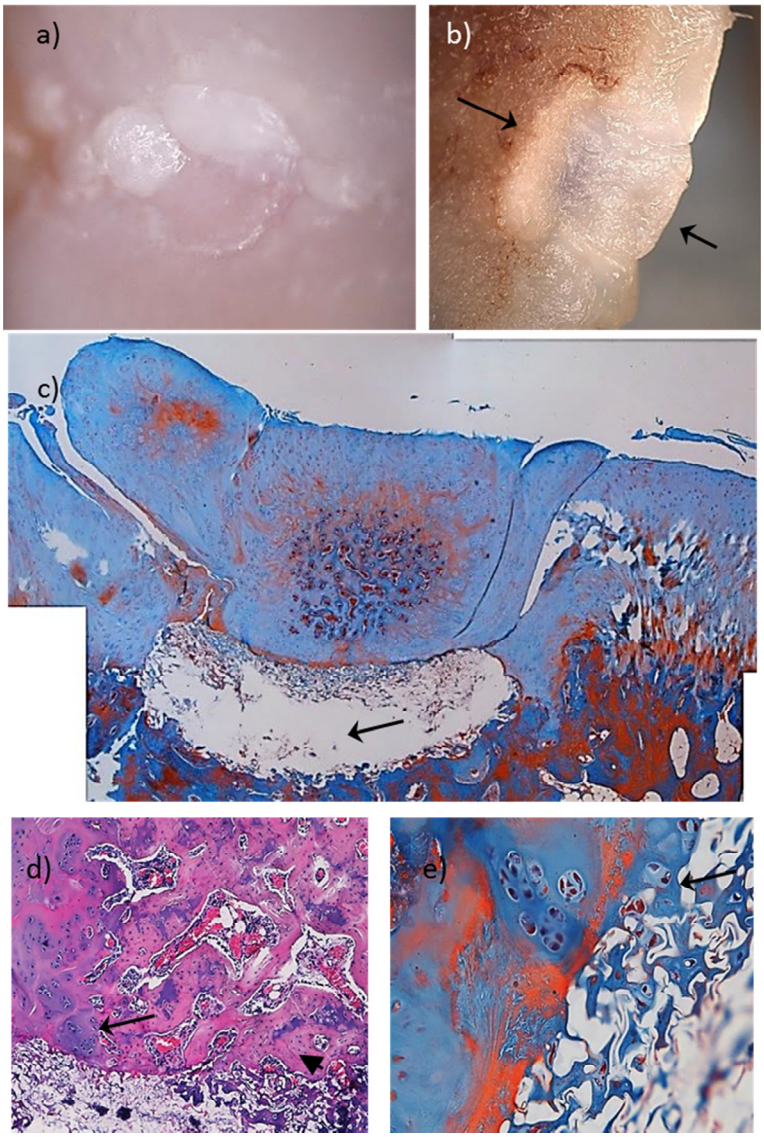

Fig. 33: Sample 58I. a) Macroscopic view after animal sacrifice. b) Sagittal cut of distal femur, following tissue decalcification, 4 weeks after sacrifice. Scaffold in place and repair tissue shown by arrows c) Reconstruction by means of 5 images at 2,5x; panoramic view. Pore disruption shown by arrow. MT stain. d) 10x magnification of central superior margin; bone (arrowhead) and cartilage (arrow) clusters. H-E stain. e) 40x magnification of superior margin. Integration of scaffold with adjacent tissues shown by arrow. MT stain.

Sample 59D (Fig. 34)

On a macro view, it can be observed that the disc is close to the surface, but most of the injury has been covered by repair tissue (Fig. 34a, b). Disc surface area is glassy, similar to adjacent cartilage. However, there is a peripheral uncovered zone of reddish color (Fig. 34a, b).

Upon histological study of the surface, the disc presents a 10º-20º inclination respect to joint surface. As a consequence, the right half of the disc is in direct contact with joint surface, while the left half is covered by abundant new repair tissue (Fig. 34b, c). The thickness of the repair tissue on the left half of the scaffold is 659 μm including cartilage and bone tissue. Cartilage on the left surface has hyaline cartilage appearance and is 219 μm thick. Directly under this HC there is an area of repair bone tissue of 440 μm thick x 1426 μm long; located between HC and the disc. On the articular surface of the right half of the scaffold, there is a predominant horizontal lamination. A 1.200 μm thin fibrous band (Fig. 34e) and a 400 μm area of uncovered scaffold are observed. In general, over half of the scaffold (left half) is covered by cartilage and bone (Fig. 34c). Tidemark has not been repaired.

Overall, repair tissue at joint surface morphometrically is: 49,36% of cartilage (HC+FC); 28,15% of bone and 22,46% of undifferentiated tissue. Histologically: Out of the 49,36% of

quantified cartilage, 30% has hyaline cartilage appearance and 70% fibrous cartilage features; MCRS: 11.

Since scaffold displays a tilted, elongated irregular arrangement, it is located between at 0 and 600 μm from the joint cavity (Fig. 34c), with a total area of 1.307.166 μm^2. The scaffold pores are partly filled, devising a vacant area in the superior third of the scaffold (Fig. 34c, e). Cell population is partially undifferentiated (Fig. 34d), however, chondral-like cells are present in areas close to native cartilage. We have compared characteristics with native surrounding tissue, enabling us to identify cartilage and bone structures. Tissue not complying with such characteristics has been classified as undifferentiated. Scaffold integration with surrounding bone and cartilage tissues is limited yet existent (Fig. 34d, e). Occasional vessels are present and scarce multinuclear cells are seen as well.

The morphometric quantification of tissue distribution inside the scaffold, excluding the solid biomaterial is:

ROI (%)	Cartilage	Bone	Empty Pores	Undifferentiated
Superior	4,22	20,92	69,29	5,57
Inferior	18,63	48,55	19,13	13,69
Periphery	42,82	28,84	23,83	4,51

Globally, there is a 18,87% of cartilage, 28,66% of bone and 7,05% of undifferentiated tissue content within total scaffold

area, despite the fact that 30,43% are still empty pores and 14,99% is solid scaffold biomaterial.

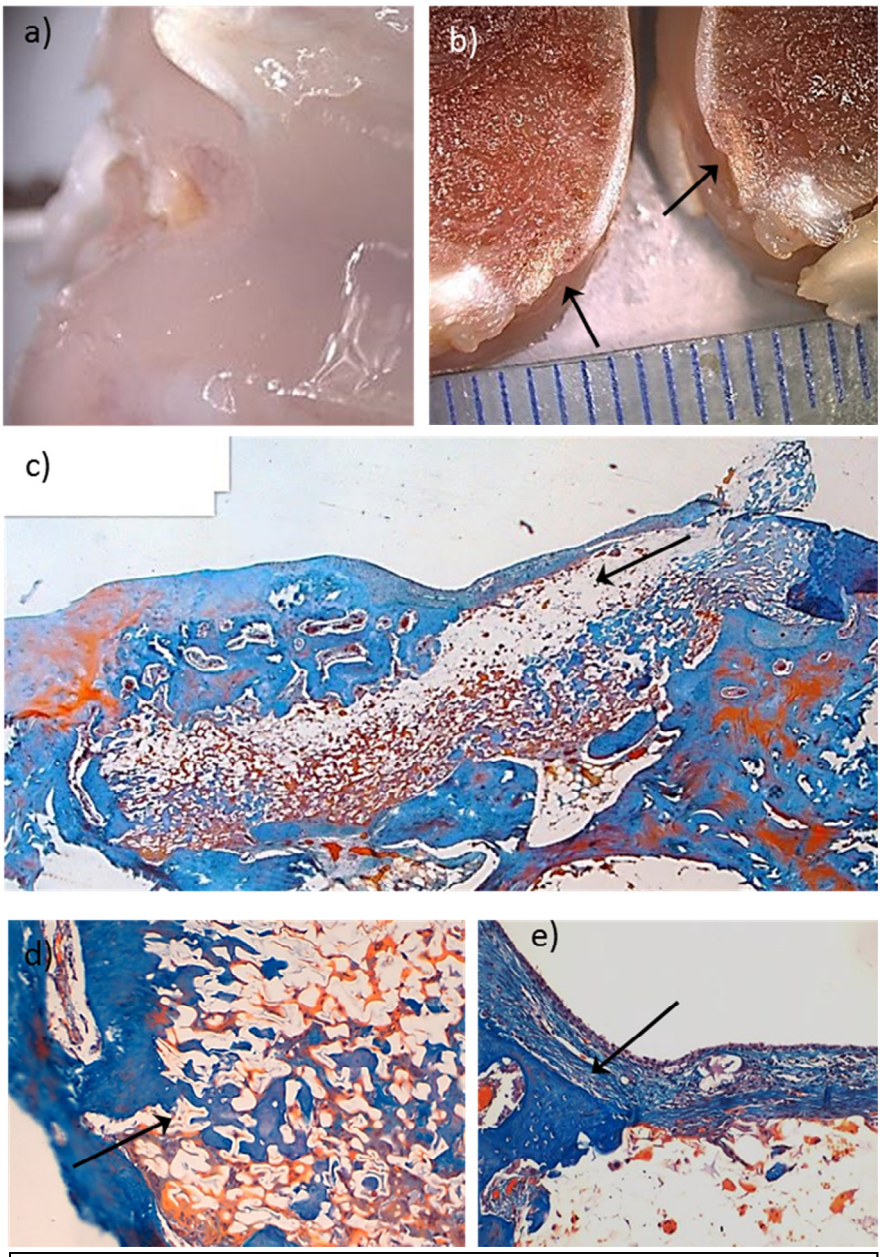

Fig. 34: Sample 59D. a) Macroscopic view after animal sacrifice. b) Sagittal cut of distal femur, following tissue decalcification, 4 weeks after sacrifice. Scaffold in place shown by arrows. c) Reconstruction by means of 4 images at 2,5x; panoramic view. Superior third of scaffold unoccupied shown by arrow. d) Left inferior border; 20x magnification. Scaffold integration with adjacent tissue shown by arrow. e) Superior central margin 20x magnification of transition from deep to superficial scaffold; fibrosis (arrow) and poor integration can be seen. All histological slides in MT stain.

Sample 53D (Fig. 35)

On a macro view of this sample, it can be observed that the injury site at articular surface is completely covered, in continuity with native cartilage, with a white matte appearance that predominates throughout the whole disc (Fig. 35a, b).

Histologically we can verify that the scaffold is aligned with surface, located within native cartilage tissue, in direct contact with joint cavity (Fig. 35c). At joint surface, a scarce repair cartilage can be seen, mainly near the injury borders (Fig. 35c, e); however, a 700 μm long, zone of fibrous expression can be seen at the superior margin (Fig. 35c). Different type of cartilage can be noted on picrosirius stain under polarized light when compared to HC (Fig. 35d). Type I collagen with typical birefringence is existent in surface repair tissue at superior margin of scaffold, indicating the presence of fibrocartilage. Adjacent native cartilage has grown and progressively covered 200 μm of the disc surface (Fig. 35c, e). On the articular surface, there is superficial horizontal lamination and severe hypocellularity on the repair tissue. Despite the absence of a tidemark, there is a partial bond with adjacent tissue (Fig. 35c, d).

Overall, repair tissue at joint surface morphometrically is: 54,60% of cartilage (HC+FC); 11,93% of bone and 32,62% of undifferentiated tissue. Histologically: Out of the 54,60% of

quantified cartilage, 5% has hyaline cartilage appearance and 95% fibrous cartilage features; MCRS: 8.

The scaffold presents a rectangular shape, located at 0 μm from the joint cavity (Fig. 35b, c), having a total area of 2.655.116 μm^2. The scaffold pores are mostly vacant, yet some cell growth is visible at the periphery (Fig. 35c, e), The scaffold is partially bonded to adjacent tissues and no obvious fibrous tissue is perceived around the scaffold (Fig. 35e).

The morphometric quantification of tissue distribution inside the scaffold, excluding the solid biomaterial is:

ROI (%)	Cartilage	Bone	Empty Pores	Undifferentiated
Superior	8,59	7,09	65,32	19,00
Inferior	1,31	3,97	83,81	10,91
Periphery	16,78	6,96	62,17	14,09

Globally, there is a 6,30% of cartilage, 4,48% of bone and 11,28% of undifferentiated tissue content within total scaffold area, despite the fact that 52,22% are still empty pores and 25,72% is solid scaffold biomaterial.

.

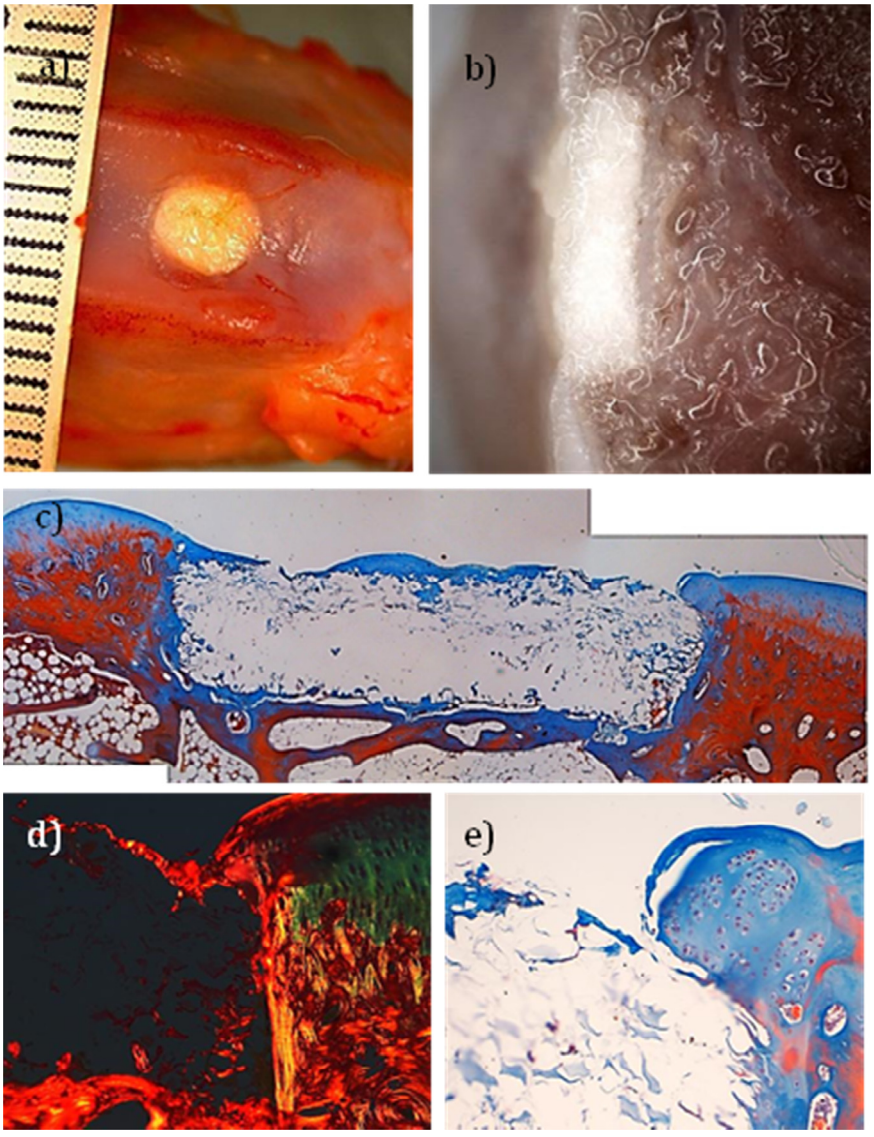

Fig. 35: Sample 53D. a) Macroscopic view after animal sacrifice. b) Sagittal cut of distal femur, following tissue decalcification, 4 weeks after sacrifice. Scaffold in place. Note the whitish appearance of the disc. c) Reconstruction by means of 3 images at 2,5x; panoramic view, MT stain. d) Polarized light, picrosirius stain. Right border 10x magnification; Type I collagen with typical birefringence present in surface repair tissue at superior margin of scaffold. e) 20x magnification of right superior border; proliferating cartilage over the scaffold and poor scaffold integration can be distinguished. MT stain.

Sample 49I* (Fig. 36)

**Sample deceased at 3 weeks, therefore not considered for group performance*.

On a macro view of the distal femur, the disc is revealed in a deeper layer when compared to the native surface (Fig. 36a, b). At the surface of the disc, there is continuity of a marginal repair tissue band with host tissue (Fig. 36c). Surface of the disc at joint site is pale and glossy (Fig. 36a).

Histological study reveals that there is a 1.500 μm gap in the surface, between the two superficial cartilage ends (Fig. 36c), partly covered by a 0 – 200 μm thick fibrous band of repair tissue (Fig. 36c). There is no integration with host tissue, and scaffold is surrounded by immature hypercellular tissue (Fig. 36d). Tidemark is absent. MCRS: Not quantified.

The scaffold presents a bent rectangular shape, located at 0 - 100 μm from the joint cavity (Fig. 36c), having a total area of 2.358.655 μm^2. The scaffold pores are mostly empty, yet scarce peripheral cell growth is perceived (Fig. 36d, e). There are some multinuclear cells and new forming vessels (Fig. 36e).

Altogether, there is selected tissue growth only inside the periphery of scaffold (Fig. 36c, d, e), with immature cartilage tissue attempting to cover the surface (Fig. 36c).

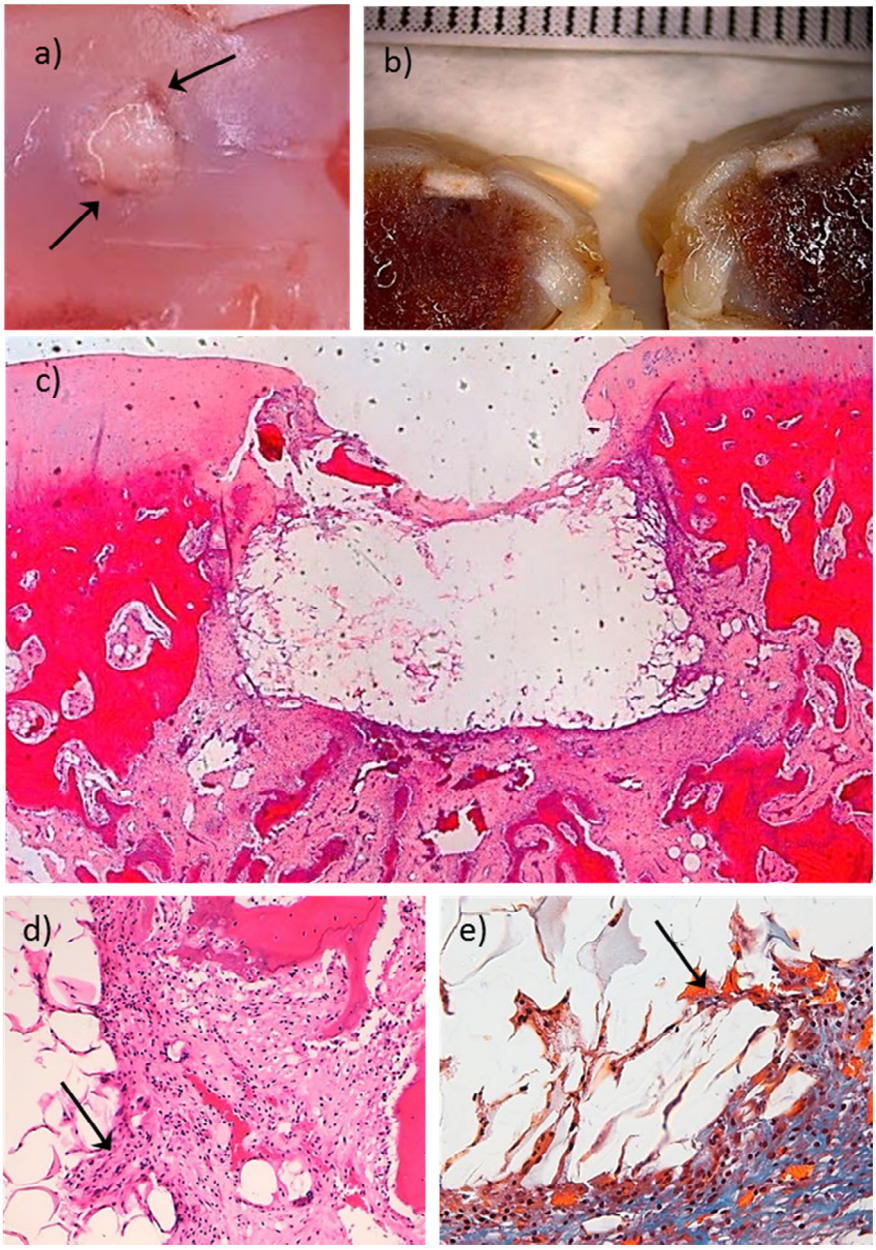

Fig. 36: Sample 49I. a) Macroscopic view after animal decease at 3 weeks. No integration with surrounding adjacent tissue is shown by arrows. b) Sagittal cut of distal femur, following tissue decalcification, 4 weeks after sacrifice. Scaffold in place. Note the whitish appearance of the disc. c) Reconstruction by means of 4 images at 2,5x; panoramic view, H-E stain. d) 20x magnification of right margin; undifferentiated tissue starting to integrate shown by arrow. H-E stain. e) 40x magnification of inferior border; new vessel growth shown by arrow. MT stain.

Sample 49D* (Fig. 37)

**Sample deceased at 3 weeks, therefore not considered for group performance*.

On a macro view of the femur, the disc is also observed in a slight deeper layer when compared to the surface (Fig. 37a, b). There is a bordering repair tissue band of pinkish color partially covering the disc (Fig. 37a), while surface of bare scaffold is whitish and matte.

Histologically, there is a 1.000 μm gap in the surface (Fig. 37c), partially covered by a 0 – 70 μm thick fibrous band of repair tissue. In continuity with this fibrous band, there is apparent hyaline cartilage growth close to the rim (Fig. 37d), that is 1.162 μm long x 286 μm thick, yet its histological features are those of immature cartilage. There is also a slight continuity with adjacent tissue (Fig. 37d), mainly in the periphery. Tidemark is absent. MCRS: Not quantified.

The scaffold presents bent rectangular shape, located at 250 μm from the joint cavity (Fig. 37c), having a total area of 1.427.596 μm^2. The scaffold pores are mostly empty, and scarce peripheral cell growth is seen (Fig. 37c, d). No multinuclear cells nor vessels were found. Densely packed areas of undifferentiated cells are found in 25% of the base perimeter (Fig. 37c), filling up remaining spaces in trabecular bone tissue.

Overall, there is certain tissue growth in the periphery of scaffold, with immature cartilage tissue attempting to cover the surface (Fig. 37c, d).

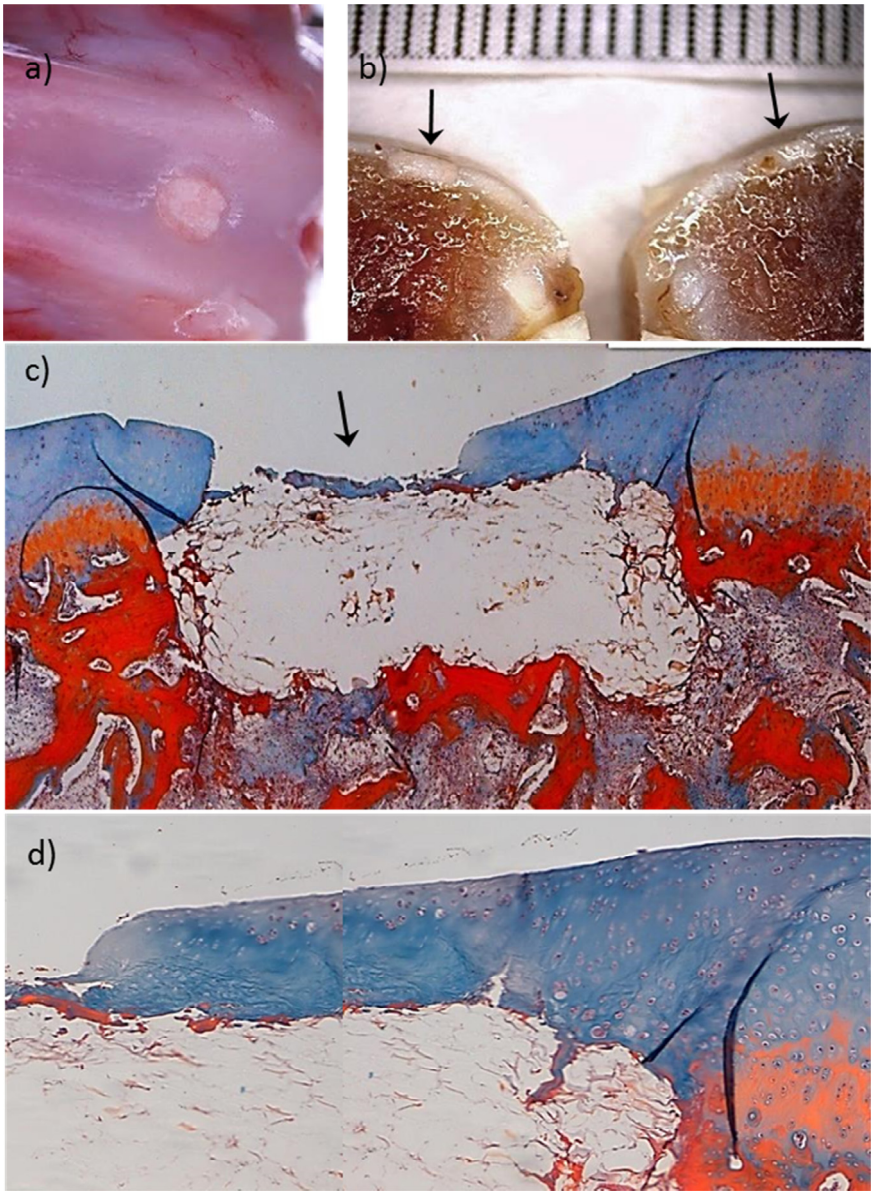

Fig. 37: Sample 49D. a) Macroscopic view after animal decease at 3 weeks. b) Sagittal cut of distal femur, following tissue decalcification 4 weeks after sacrifice. Scaffold in place shown by arrows. Note the whitish appearance of the disc. c) Reconstruction by means of 4 images at 2.5x; panoramic view. Fibrosis shown by arrow. d) 10x magnification of right superior margin; proliferating cartilage strip with immature hyaline like features. All histological slides in MT stain.

3.1.5 Control Groups

Control group analyzes seven samples, divided into two subgroups. Group E has five samples (n=5), which have been treated with the same procedural standards as study groups, but no scaffold has been implanted. Group F contains five virgin, native, untouched knees (n=5). Finally, one control has the injury outline, but no articular cartilage was extracted, therefore, will not be classified in any of the groups (n=1).

3.1.5.1 Control Group E

In Group E, cartilage, as well as fibrous tissue and subchondral bone are present in the repair tissue. Fibrocartilage scar tissue is preponderant, followed by bone repair tissue. The repair of previously healthy cartilage has been partially reconstructed, as seen on intermediate repair scores. Different criteria applied by the modified cartilage repair score (MCRS) define the quality of repair tissue. MCRS group average: 15,0 (CI: 11 - 18). On the repair cartilage tissue, 50% has hyaline cartilage appearance and 50% fibrous cartilage features.

The following section contains case by case analysis of group E samples. Detailed description of morphological features is displayed:

Sample 21D(Fig. 38)

On a macro view of the distal femur, the circular injury site is completely covered, however it is clearly distinct from the native surface since it is mostly white and glossy (Fig. 38a). No fissures or layers are identified. Also, a good peripheral integration with native tissue can be seen (Fig. 38a, b).

Histological analysis reveals that there is superficial horizontal lamination in the repair tissue (Fig. 38c), with a moderate hypercellularity. Repair tissue has cartilage appearance, both hyaline (close to subchondral bone) and fibrous, which appears to cover the injury site (Fig. 38d, e). Thickness of the repair tissue is: 360 μm (89% of native articular cartilage); it is completely bonded to host tissue, laterally with native articular cartilage and inferiorly with subchondral bone (Fig. 38c, d). Tidemark is partially present (Fig. 38c). No vessels or multinucleated cells are seen in repair tissue.

MCRS: 17; Hyaline cartilage: 60%, fibrous cartilage: 40%.

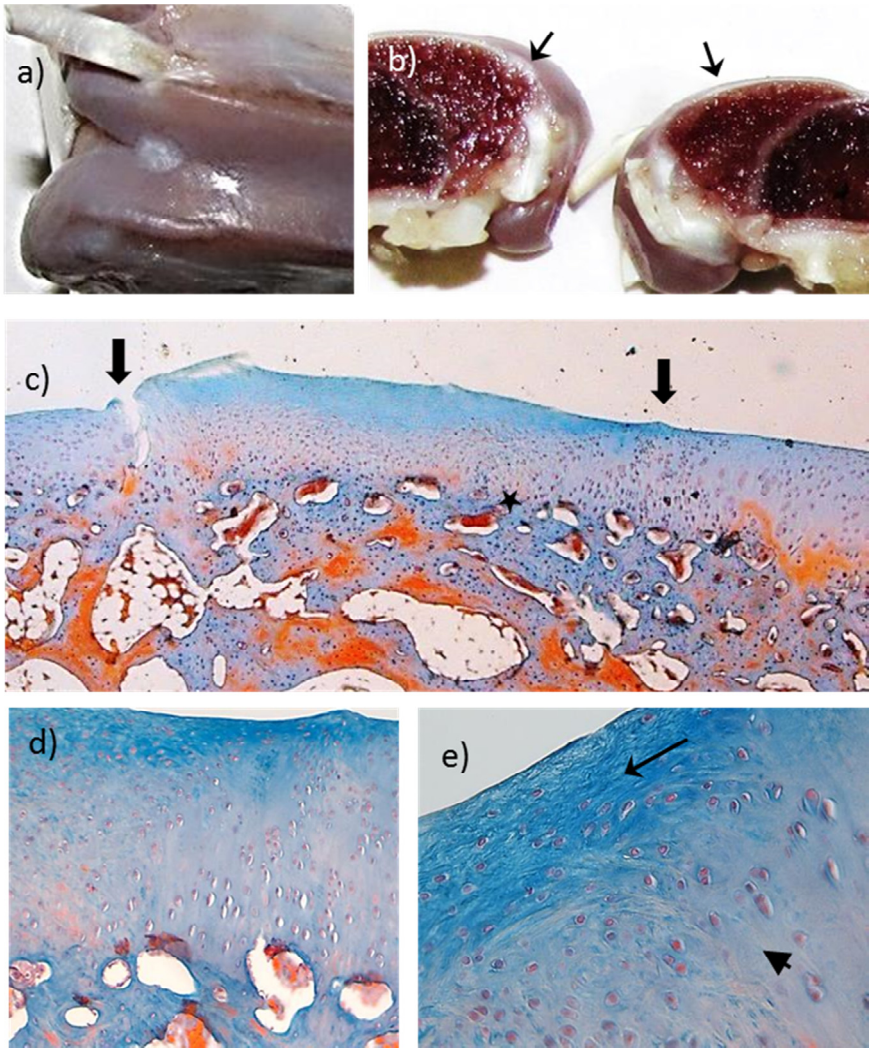

Fig. 38: Sample 21D. a) Macroscopic view after animal sacrifice. Note the whitish appearance of the disc. b) Sagittal cut of distal femur, following tissue decalcification, 4 weeks after sacrifice. Injury site shown by arrows. c) Image at 2,5x; panoramic view. Arrows indicate injury site, star shows the presence of tidemark. d) 20x magnification of right border. Color and structure of repair cartilage similar to native cartilage is noted. e) 40x magnification of surface; fibrous (arrow) and hyaline cartilage (arrowhead) can be observed. All histological slides in MT stain.

Sample 47I (Fig. 39)

On a macro view, the round injury site is completely covered by repair tissue, but easily recognizable from the native cartilage, since its surface area is rough and protrudes into joint cavity, with a glossy and pale appearance (Fig. 39a). Repair tissue has a peripheral integration with native tissue (Fig. 39a, b), and no fissures are observed.

Histologically, there is superficial horizontal lamination and a moderate hypercellularity within repair tissue (Fig. 39c). Moreover, fibrous tissue covers superficial injury site. In a deeper layer there seems to be clusters of hyaline cartilage and fibrous bands (Fig. 39d). A wide vertical band of 1.290 μm long of mixed fibrous and hyaline tissue in contact with superficial repair cartilage is identified (Fig. 39c, d). It penetrates 1.200 μm beyond the tidemark into subchondral bone. The repair tissue thickness varies from 1.100 to 2.600 μm, including this mixed cartilage tissue band. It is completely bonded to host articular cartilage as well as subchondral bone tissue (Fig. 39c). Tidemark has not been reconstructed. No vessels or multinucleated cells are observed in repair cartilage tissue.

MCRS: 14; Hyaline cartilage: 40%, fibrous cartilage: 60%.

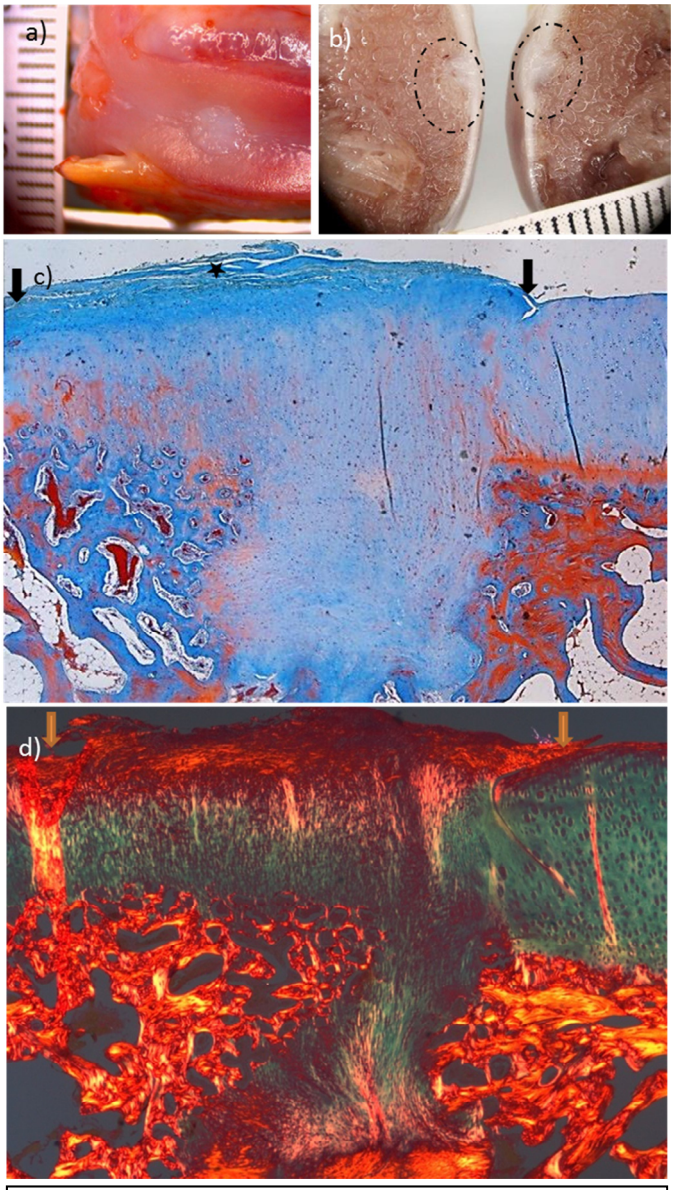

Fig. 39: Sample 47I. a) Macroscopic view after animal sacrifice. b) Sagittal cut of distal femur, following tissue decalcification, 4 weeks after sacrifice. Injury site shown by dotted ovals. c) Reconstruction by means of 4 images at 2,5x; panoramic view, MT stain. Note hyaline-like features yet unorganized column structure of repair cartilage compared with native cartilage. Superficial horizontal lamination is marked by star. d) Polarized light, picrosirius stain; type I (birefringent red-orange) and type II (Blue-greenish) collagen can be seen in repair tissue. Arrows indicate injury site.

Sample 53I (Fig. 40)

On a macro view, the rounded injury site is fully covered. Surface area is smooth and similar to host tissue, although there is a bordering white lump in the distal margin (Fig. 40a). There is apparent continuity with native tissue, although the borders of the injury are recognizable (Fig. 40a, b).

Histologically, slight superficial horizontal lamination is noted (Fig. 40c). In the surface, fibrous tissue covers injury site, while in a profounder layer, cartilage with immature hyaline cartilage features is observed (Fig. 40d). The repair tissue thickness is 400 μm (125% of native AC). It is partially bonded to host tissue, since it is completely bonded on the left and inferior borders, yet partially bonded with fibrous appearance on the right margin (Fig. 40c, d). Abundant vacuoles with diameters ranging from 5 μm to 33 μm are seen in new fibrocartilage grown tissue on the right sideline (Fig. 40c, e). Tidemark is partly present (Fig. 40c). No vessels or multinucleated cells are identified in cartilage tissue.

MCRS: 18; Hyaline Cartilage: 80%, fibrous cartilage: 20%.

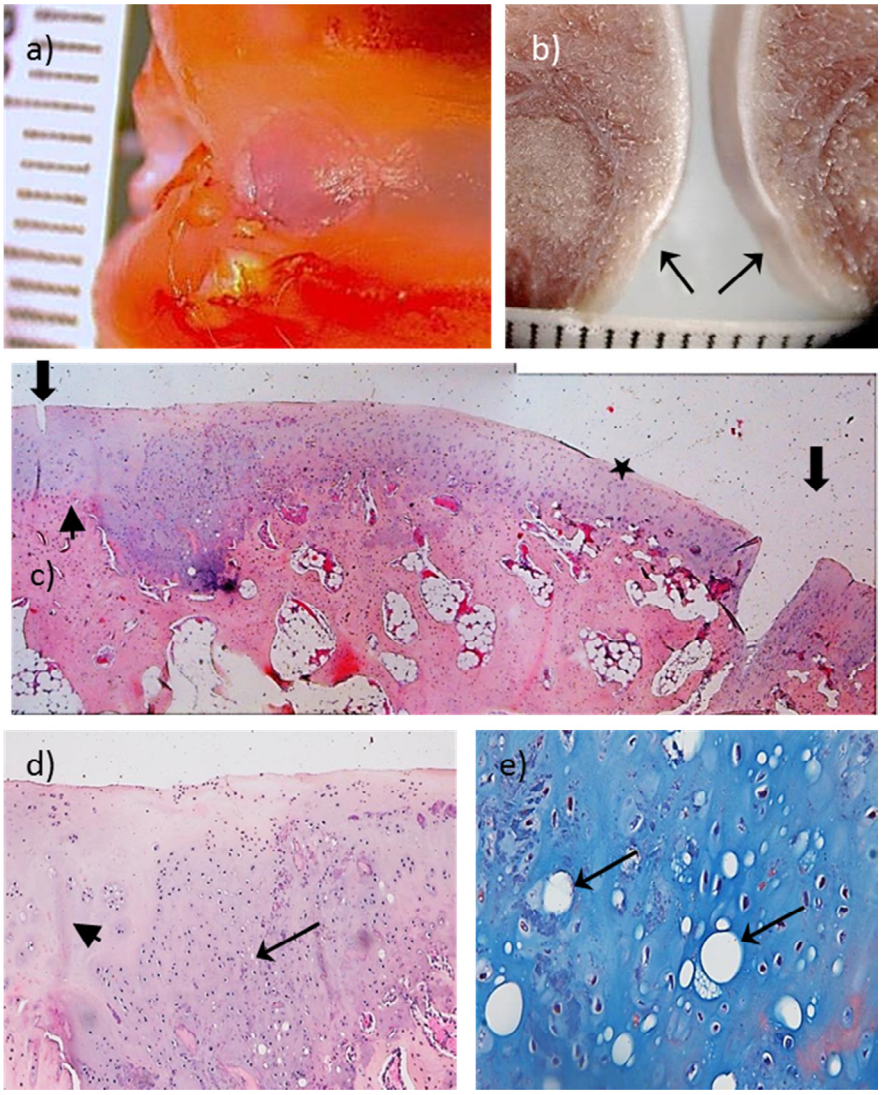

Fig. 40: Sample 53I. a) Macroscopic view after animal sacrifice. b) Sagittal cut of distal femur, following tissue decalcification, 4 weeks after sacrifice. Injury site shown by arrows. c) Reconstruction by means of 2 images at 2,5x; panoramic view, H-E stain. Arrows indicate injury site. Horizontal lamination marked by star, tidemark shown by arrowhead. d) 10x magnification of superior left border; fibrous cartilage (arrow) characterized by hypercellularity and hyaline cartilage (arrowhead).with a mature ECM, H-E stain. e) 40x magnification of right superior border. MT stain; presence of vacuoles are shown by arrows.

Sample 59I (Fig. 41)

On a macro view it can be observed that the circular injury site is not fully covered, since a small central fissure is noticeable (Fig. 41a, b). Surface area is irregular, chapped, with central whitening and an external pinkish color. Peripheral integration occurs in most of the disc, but not completely (Fig. 41a).

Histological study reveals the presence of cysts and fissures on the repair tissue (Fig. 41c). Severe hypercellularity is also observed (Fig. 41d). In the repair tissue, superficial as well as profound fibrocartilage tissue can be found (Fig. 41d, e). The repair cartilage thickness is 180 μm (77,9% of native AC). The continuity of repair with host tissue is high, although incomplete (Fig. 41c). Tidemark is mostly present (Fig. 41c). No vessels or multinucleated cells are seen in repair cartilage tissue.

MCRS: 11; Hyaline cartilage: 20%, fibrous cartilage: 80%.

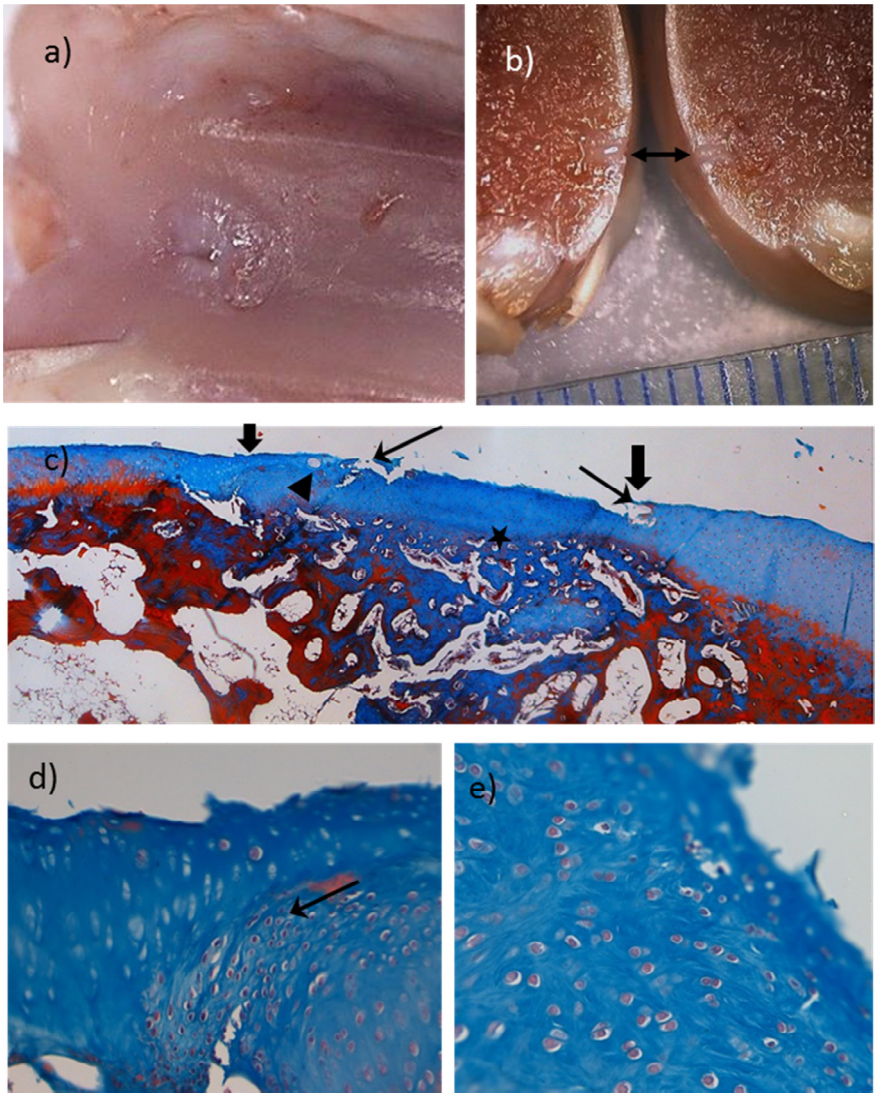

Fig. 41: Sample 59I. a) Macroscopic view after animal sacrifice. b) Sagittal cut of distal femur, following tissue decalcification, 4 weeks after sacrifice. Injury site shown by arrows. c) Reconstruction by means of 2 images at 2,5x; panoramic view. Thick arrows indicate injury site, thin arrows indicate fissures. Tidemark is marked by star. d) 20x magnification of left superior margin; transition zone of native and fibrous cartilage (shown by arrow). e) 40x magnification of surface. Fibrous cartilage can be observed. No organized column pattern can be distinguished. All histological slides in MT stain.

Sample 60D* (Fig. 44)

** Control following a unique pattern of cartilage injury, where outline of the injury was performed, but no AC was extracted, thus not comparable with other samples.*

On a macro view of the distal femur, the circular injury site is completely covered by tissue (Fig. 44a, b); however, there is a marginal whitish 1 mm rim. At the surface, the eccentric pinkish area contained within the injury site has a normal hyaline cartilage presence (Fig. 44a). Surface area is mainly smooth and glossy. There is peripheral integration with native tissue (Fig. 44a, b).

Histologically, there is severe disruption and disintegration of the normal architecture at the articular surface. The central area is occupied by a 370 μm thick cartilage band that has features similar to normal cartilage, despite a tear produced by histological process. In addition, a tidemark is present, followed by subchondral bone in deeper layers (Fig. 44c). At both sides of the injury, a fibrous repair tissue is observed, from the surface, up to 600 μm deep (Fig. 44d, e). It is most abundant at the right margin and it is only partially bonded to adjacent host tissues.

No vessels or multinucleated cells are comprehended in cartilage tissue.

MCRS: 8; Hyaline cartilage: 30%, fibrous cartilage 70%.

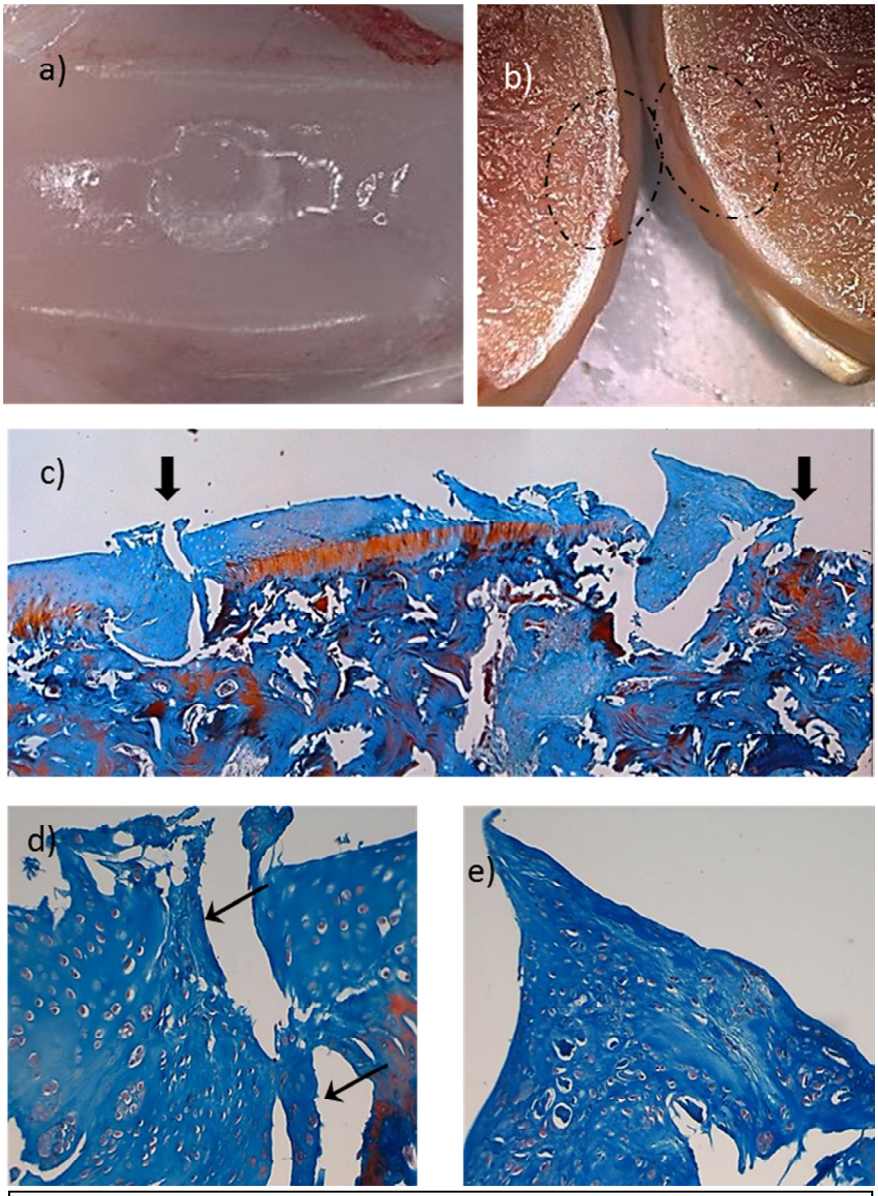

Fig. 44: Sample 60D. a) Macroscopic view after animal sacrifice. b) Sagittal cut of distal femur, following tissue decalcification, 4 weeks after sacrifice. Injury site enclosed by dotted ovals. c) Reconstruction by means of 2 images at 2,5x; panoramic view. Arrows indicate injury site. d) 20x magnification of left margin; new fibrocartilage is observed at injury site, shown by arrows. e) 20x magnification of right margin; fibrocartilage growth is apparent in a more abundant proportion. All histological slides in MT stain.

3.1.5.2 Control Group F

In group F, there are five samples (n=5). Two representative samples will be described in detail. Normal, healthy untouched articular cartilage reveals certain anatomic structures that were partially mimicked by trial groups as well as control group E. MCRS group average: 26,0 (CI: 26); Hyaline Cartilage: 100%.

The following section contains case by case analysis of two samples from group F samples. Detailed description of morphological features is displayed. Finally, the last sample is a control following a unique pattern of cartilage injury, not comparable with others and therefore not included in either E or F groups.

Sample 45I (Fig. 42)

On a macro view, surface area is smooth and homogeneous, with a glossy and pinkish aspect (Fig. 42a). Following the longitudinal cut of the distal femur (Fig. 42b), the homogeneity of the articular surface can be noted, as well as the cartilage-bone interface.

Histologically, normal articular hyaline cartilage features take place (Fig. 42c); superficial fibers (not noticeable with MT stain) run in parallel to joint surface, bend at one third of the cartilage thickness, and continue perpendicularly until the tidemark is reached. This description of fibers is indirectly observed by morphology and alignment of cells (Fig. 42d, e). Thus, on the surface, cells are flat and assume a horizontal disposition (Fig. 42d). In deeper layers they are rounded and have a vertical alignment (Fig. 42e). Articular cartilage thickness varies from 200 μm to 670 μm depending on anatomic location on the samples; tidemark is present all throughout the sample (Fig. 42e). This continuous line is parallel to the articular surface, revealing the transition from non-calcified deep zone, to calcified zone. No vessels or multinucleated cells are present in cartilage tissue; however vessels are present in subchondral bone.

MCRS: 26; Hyaline cartilage: 100%.

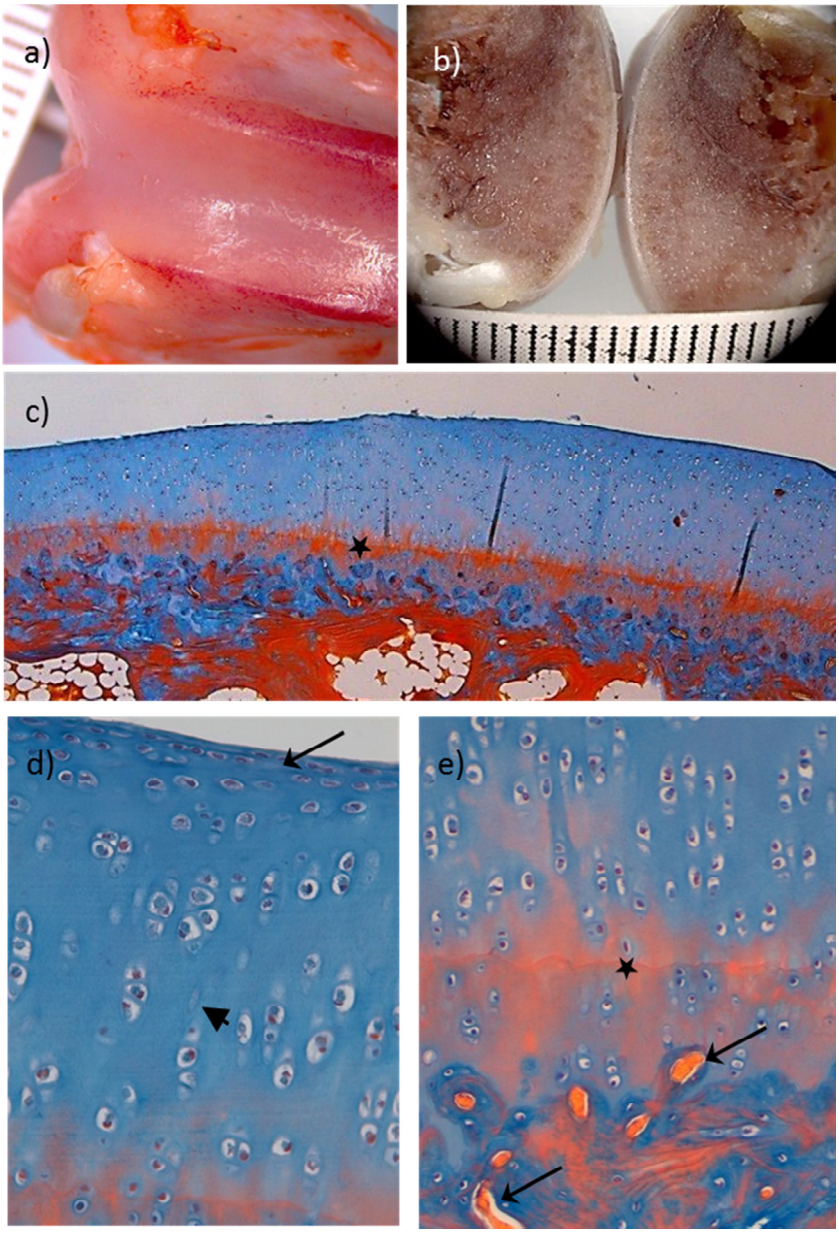

Fig. 42: Sample 45I. a) Macroscopic view after animal sacrifice. b) Sagittal cut of distal femur, following tissue decalcification, 4 weeks after sacrifice. c) Reconstruction by means of 2 images at 2,5x; panoramic view. Tidemark marked by star. d) 40x magnification of superior margin; hyaline cartilage features are displayed. Superficial chondrocytes are flat and parallel to the surface (arrow) and form perpendicular columns (arrowhead) in deeper layers. e) 40x magnification of inferior margin; Tidemark (star) and subchondral bone are observed. Note the presence of capillaries at subchondral bone, shown by arrows. All histological slides in MT stain.

Sample 46I (Fig. 43)

On a macro view of the distal femur, surface area is smooth and homogeneous, with a glossy and pinkish aspect, similar to the previous sample (Fig. 43a, b).

Histologically, normal articular hyaline cartilage features take place, with typical structure and alignment as described in the previous sample. Cartilage tissue thickness varies depending on anatomic location and in this sample knee varies from 250 μm to 500 μm. The tidemark is present (Fig. 43c). The limit between cartilage and subchondral bone is certainly recognized with by means of picrosirious stain viewed under polarized light microscopy (Fig. 43d). Furthermore it displays a different color spectrum in hyaline cartilage, containing type II collagen, than that of type I collagen, contained in bone tissue. No vessels or multinucleated cells are observed in cartilage tissue.

MCRS: 26; Hyaline Cartilage: 100%.

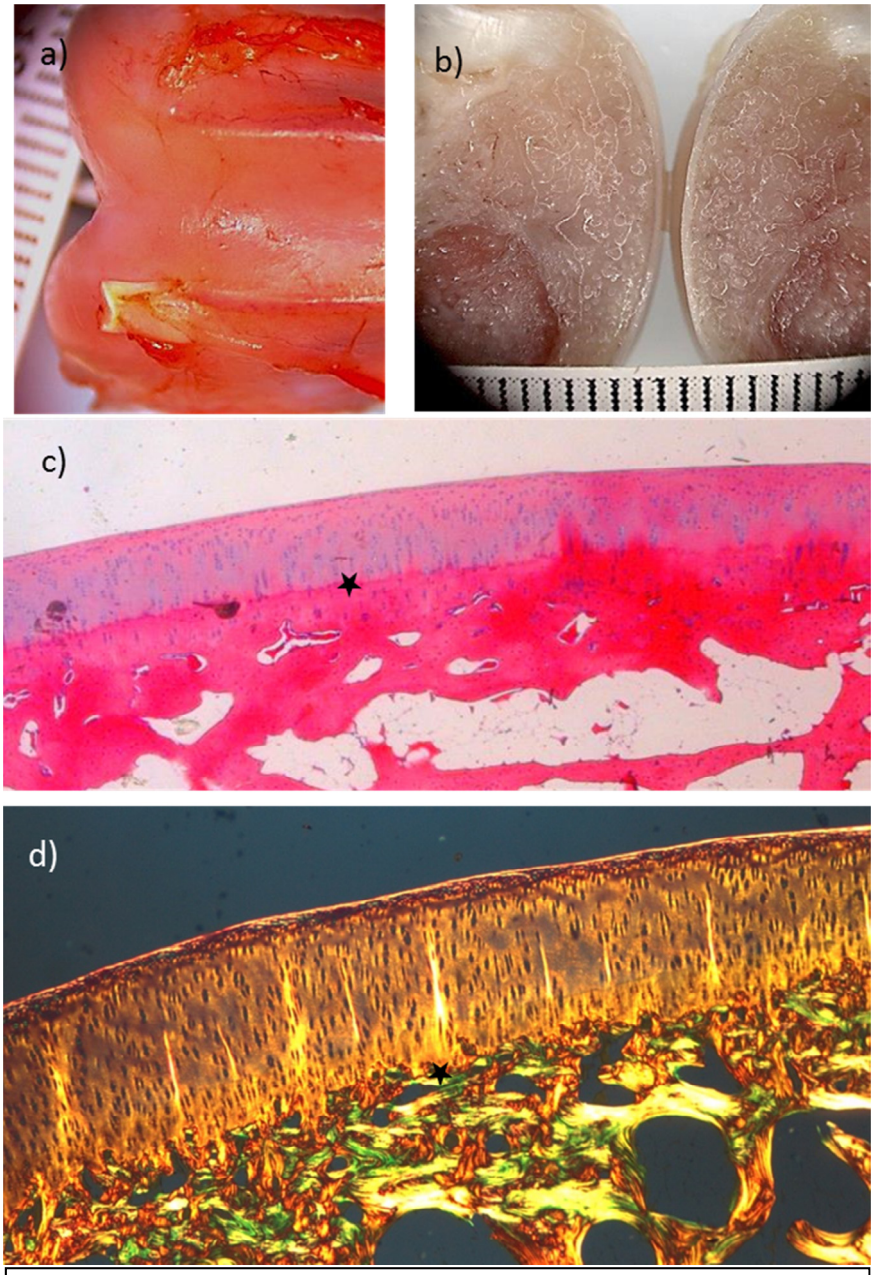

Fig. 43: Sample 46I. a) Macroscopic view after animal sacrifice. b) Sagittal cut of distal femur, following tissue decalcification, 4 weeks after sacrifice. c) Image at 2,5x close-up; panoramic view, H-E stain. Deep perpendicular column structure is noticed. Tidemark is marked by star. d) Pricrosirius stain, polarized light microscopy; 10x magnification. Hyaline cartilage containing type II collagen displays a different color spectrum from type I collagen, which is contained in bone tissue. Tidemark marked by star.

3.2 Statistical Scrutiny

After closely analyzing all of our results, based on the data supplied by the repair tissue score and the morphometric scrutiny of all samples, several tendencies were revealed.

A separate exploration has been made of the joint surface repair tissue and the tissue grown within de scaffold itself. Data has been classified by trial group, type of tissue and spatial location. Similarly, discrimination and analysis was made by tissue growth within scaffolds.

All statistical analyses were performed by comparing mean results of trial groups (A, B, C, D).

3.2.1 Joint surface

Joint surface repair tissue was measured under two different sets of criteria: the histological criteria (based on the MCRS) and the morphometric quantification at selected ROI.

Modified Cartilage Repair Score (MCRS)

By means of the repair score employed, there is an inverse relationship between the stiffness of the scaffold and the mean value score representing general group behavior (Fig. 45). There is a slight tendency to decrease mean MCRS values with increased stiffness of scaffold (R=-0,799) (Fig. 48). Still for point values, a large dispersion of data is observed, particularly on group C. In other words, there is a tendency to find better repair tissue at joint surface (higher MCRS) with less stiff scaffolds. No statistically significant difference was found (p=0,460).

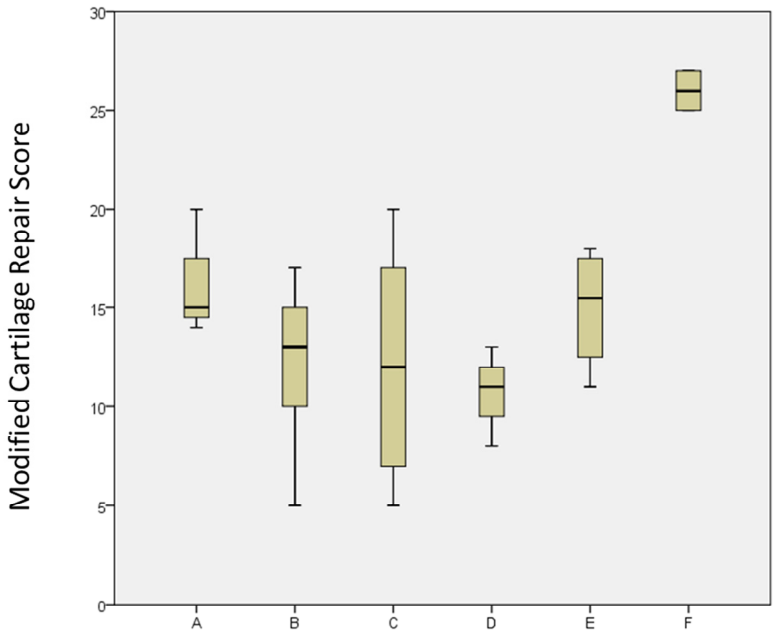

Fig. 45: Modified Cartilage Repair Score (MCRS) by group. Group A=1% cross-linker, Group B= 2% cross-linker, Group C= 5% cross-linker, Group D: 7% cross-linker, Group E= Control, Group F= Healthy control).

Hyaline Cartilage Content

Hyaline cartilage percentage is one of the criteria used by MCRS. It evaluates histological appearance of hyaline cartilage in repair tissue, at the joint surface in contrast to fibrocartilage. There is also an inverse relationship between the stiffness of the scaffold and the mean value score representing general group content of HC (Fig. 46). There is a slight tendency to decrease mean HC percentage values with increased stiffness of scaffold (R=-0,995) (Fig. 48). Still for point values, a large dispersion of data is observed, particularly on group C. In other words, there is a tendency to find more hyaline cartilage content at joint surface with less stiff scaffolds. No statistically significant difference was found (p=0,238).

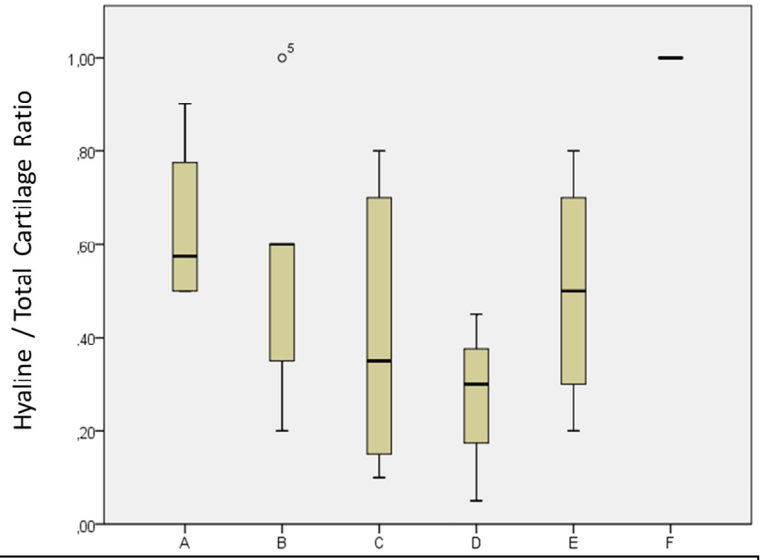

Fig. 46: Hyaline cartilage content of repair tissue by group with respect to total cartilage. Group A=1% cross-linker, Group B= 2% cross-linker, Group C= 5% cross-linker, Group D: 7% cross-linker, Group E= Control, Group F= Healthy control).

Thickness of repair tissue

Thickness of repair tissue expressed in percent when compared to native adjacent cartilage is also one of the criteria used by MCRS. It evaluates histological measure of repair tissue with respect to uninjured cartilage. An inverse relation between the stiffness of the scaffold and the mean value representing general group behavior is observed (Fig. 47). There is a tendency to decrease mean values of repair tissue thickness with increased stiffness of scaffold (R=-0,913) (Fig. 48). Still for point values, a large dispersion of data is observed. In other words, there is a tendency to find thicker repair tissue at joint surface with less stiff scaffolds. No statistically significant difference was found (p=0,093).

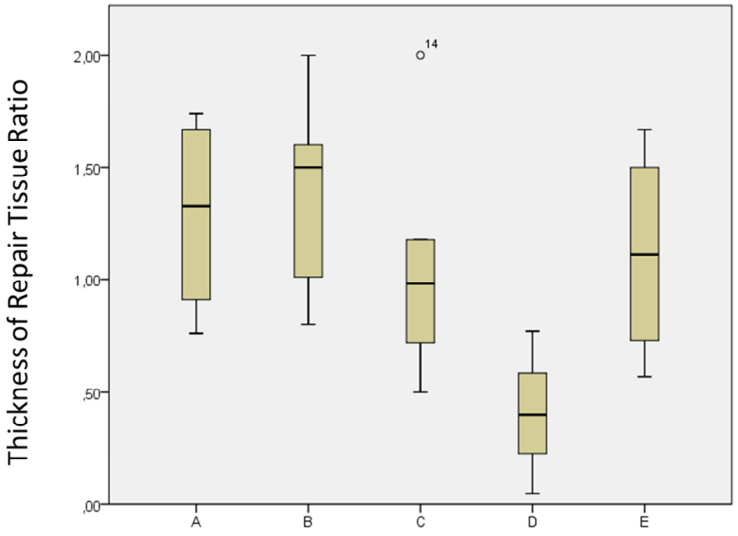

Fig. 47: Thickness of repair tissue with respect to native cartilage by group. Group A=1% cross-linker, Group B= 2% cross-linker, Group C= 5% cross-linker, Group D: 7% cross-linker, Group E= Control).

Tendency of Histologic Criteria (Fig. 48)

As revealed in the three histologic criteria of the repair tissue at joint surface described above, (MCRS, Hyaline cartilage content and thickness of repair tissue), there is a general tendency to decrease repair tissue content and quality, with increasing cross-linker concentration.

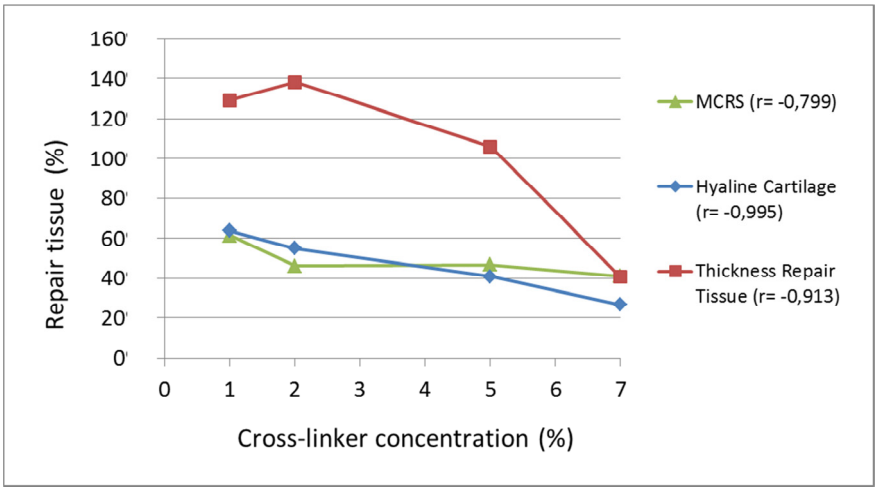

Fig. 48: Joint Surface repair tissue distribution by group. No statistically significant differences were observed. Tendency (r) is shown for each cross-linker concentration. Group A=1% cross-linker, Group B= 2% cross-linker, Group C= 5% cross-linker, Group D: 7% cross-linker, Group E= Control, Group F= Healthy control). Typical error is shown on table 6.

		N	Median	Typical Error	CI 95%	
					Inferior limit	Superior limit
MCRS	A	4	61,5	5,2	45,0	78,1
	B	5	46,2	8,1	23,8	68,6
	C	6	46,8	9,8	21,6	72,0
	D	3	41,0	5,6	17,0	65,1
Hyaline Cartilage	A	4	63,8	9,4	33,7	93,8
	B	5	55,0	13,6	17,2	92,8
	C	6	40,8	12,3	9,3	72,4
	D	3	26,7	11,7	-23,5	76,9
Thickness Repair Tissue	A	4	129,0	23,0	55,9	202,1
	B	5	138,2	21,5	78,6	197,8
	C	6	106,0	21,2	51,5	160,5
	D	3	40,7	20,8	-48,8	130,1

Table 6: Typical error for Joint Surface repair tissue distribution by group.

Repair Tissue Content

Repair tissue content on joint injured surface was mainly cartilage in all groups studied (Fig. 49). A decreasing tendency in cartilage content can be detected with increasing stiffness of implanted scaffolds (higher cross-linker concentration) (r= -0,555). Also, upon less cartilage production, an increase in undifferentiated tissue is seen. Although a tendency is clearly observed, these changes were not statistically significant (Table 7). Picrosirius stains and immunohistochemistry illustrate as well, that more fibrous content seems to be present with increasing stiffness of scaffolds.

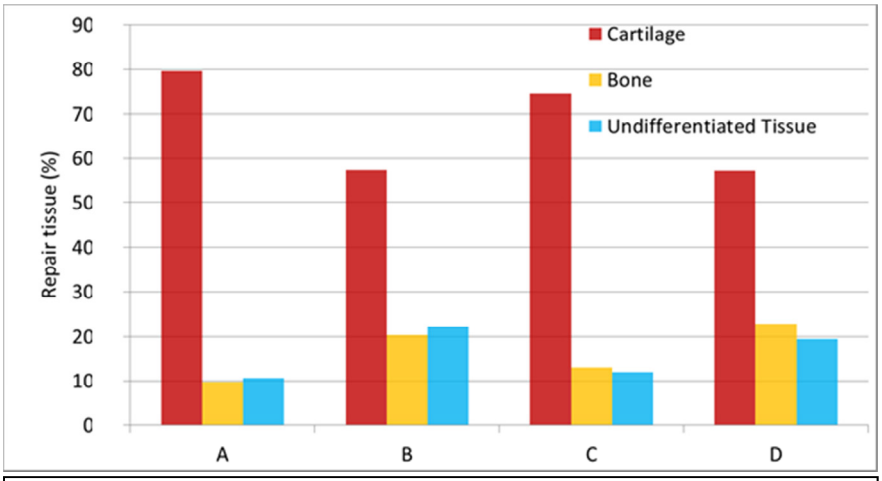

Fig. 49: Joint Surface repair tissue distribution by group. No statistically significant differences were observed. Group A=1% cross-linker, Group B= 2% cross-linker, Group C= 5% cross-linker, Group D: 7% cross-linker).

Repair Tissue	p value
Cartilage	0,29
Bone	0,29
Undifferentiated	0,46

		N	Median	Typical Error	CI 95%	
					Inferior limit	Superior limit
Cartilage	A	4	79,6	3,1	69,6	89,6
	B	5	57,4	13,6	19,6	95,1
	C	6	74,5	8,0	53,8	95,1
	D	3	57,3	5,5	33,5	81,1
Bone	A	4	9,7	5,4	-7,3	26,8
	B	5	20,4	7,0	0,8	39,9
	C	6	13,0	5,3	-0,6	26,6
	D	3	22,9	5,5	-0,7	46,6
Undifferentiated	A	4	10,6	2,9	1,4	19,9
	B	5	22,3	8,6	-1,7	46,2
	C	6	11,9	4,9	-0,7	24,6
	D	3	19,5	8,6	-17,4	56,4

Table 7: Statistical analysis of repair tissue at joint surface.

3.2.2 Inside the scaffolds

A general pattern of scaffold behavior is perceived, where empty scaffold pore decreases in relation to the increasing porosity, in groups A, B and C (Table 8). In group D however, stiffness of the scaffolds increase to a critical point (>5% cross-linker) where mechanical properties are lost, thus the scaffold pore walls are partially shattered and the resultant decrease in porosity is correlated with the augmented area of empty scaffold pore (Table 8). Such mechanical behavior can be appreciated on roughly all areas of interest.

Group	Porosity (%)	Empty Pores (%)	Solid scaffold (%)
A	82	46,0	10,1
B	84	44,8	7,9
C	88	29,1	4,0
D	67	44,2	21,8

Table 8: Correlation between porosity of each group and the percentage of empty pores.

Superior area

Comparing trial groups by superior area of interest, the amount of tissue growth increases with the cross-linker concentration from group A to C (Fig. 50), but then it sharply decreases with the highest cross-linker concentration in group D. However, no statistically significant differences were found in any repair tissue (Table 9):

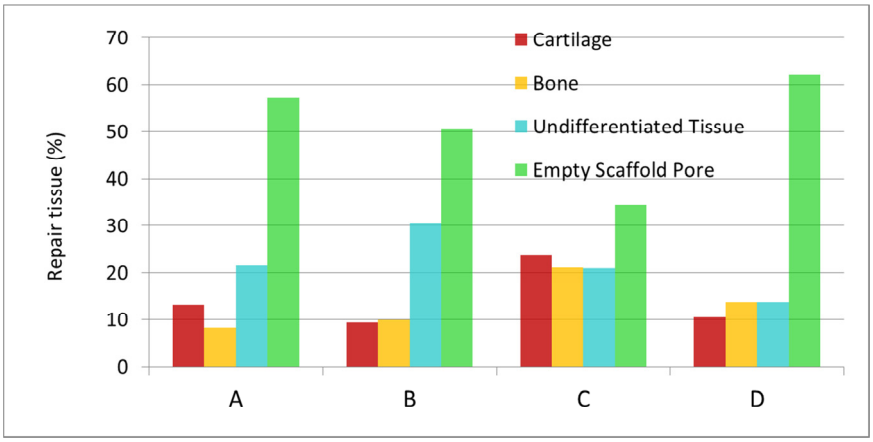

Fig. 50: Superior area tissue distribution by group. No statistically significant differences were observed. Group A=1% cross-linker, Group B= 2% cross-linker, Group C= 5% cross-linker, Group D: 7% cross-linker).

Repair Tissue	p value
Cartilage	0,57
Bone	0,47
Undifferentiated	0,45
Empty Pores	0,15

Table 9: Statistical analysis of repair tissue inside the scaffold: Superior area.

		N	Median	Typical Error	CI 95%	
					Inferior limit	Superior limit
Cartilage	A	4	13,2	10,6	-20,5	46,9
	B	5	9,4	5,7	-6,5	25,2
	C	6	23,7	10,6	-3,6	50,9
	D	3	10,5	4,3	-8,0	29,0
Bone	A	4	8,2	4,4	-5,8	22,2
	B	5	9,9	7,0	-9,6	29,3
	C	6	21,1	6,3	4,9	37,3
	D	3	13,8	4,0	-3,4	31,0
Undifferentiated	A	4	57,1	11,0	22,0	92,2
	B	5	50,4	7,9	28,4	72,4
	C	6	34,4	7,6	14,7	54,0
	D	3	62,0	5,4	38,6	85,4
Empty Scaffold Pore	A	4	21,5	5,0	5,5	37,4
	B	5	30,3	8,5	6,7	53,9
	C	6	20,9	4,6	9,1	32,7
	D	3	13,7	4,1	-4,1	31,5

Table 9 (Continued): Statistical analysis of repair tissue inside the scaffold: Superior area.

Inferior area

Tissue growth inside the inferior area of scaffolds displays a similar pattern than that ocurring at the superior area. Hence, comparing trial groups by inferior area of interest, there is also more tissue growth in group C than on other groups (Fig. 51); consequently, having the lowest porcentage of empty pores (29,1%). As in the superior area, no statistically significant differences were found in any repair tissue (Table 10).

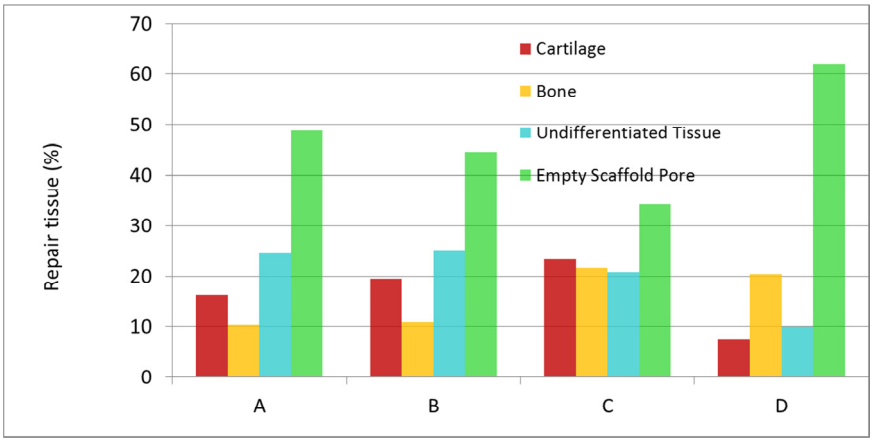

Fig. 51: Inferior area tissue distribution by group. No statistically significant differences were observed. Group A=1% cross-linker, Group B= 2% cross-linker, Group C= 5% cross-linker, Group D: 7% cross-linker).

Repair Tissue	p value
Cartilage	0,51
Bone	0,53
Undifferentiated	0,50
Empty Pores	0,54

Table 10: Statistical analysis of repair tissue inside the scaffolds: Inferior area.

		N	Median	Typical Error	CI 95%	
					Inferior limit	Superior limit
Cartilage	A	4	16,3	14,6	-30,2	62,7
	B	5	19,5	13,0	-16,6	55,5
	C	6	23,3	10,2	-3,0	49,6
	D	3	7,6	5,5	-16,3	31,4
Bone	A	4	10,4	4,9	-5,2	25,9
	B	5	10,8	5,3	-3,9	25,6
	C	6	21,6	5,3	8,0	35,3
	D	3	20,4	14,1	-40,3	81,2
Undifferentiated	A	4	48,9	9,6	18,4	79,3
	B	5	44,6	9,0	19,7	69,5
	C	6	34,3	7,6	14,6	53,9
	D	3	62,1	21,5	-30,3	154,5
Empty Scaffold Pore	A	4	24,5	7,6	0,3	48,8
	B	5	25,1	11,9	-8,0	58,2
	C	6	20,8	4,4	9,6	32,1
	D	3	9,9	2,5	-1,0	20,8

Table 10 (Continued): Statistical analysis of repair tissue inside the scaffolds: Inferior area.

Peripheral area

Comparing trial groups by peripheral area of interest, in agreement with the tendancy of superior and inferior areas, there is more tissue growth in group C than on other groups (Fig. 52), having the later, the lowest porcentage of empty pores (29,1%). Furthermore, at the periphery, cartilage tissue growth is more abundant in all groups but B, when compared to cartilage tissue growth in other sections of the scaffold i.e. superior and inferior. Overall, No statistically significant differences were found in any repair tissue (Table 11):

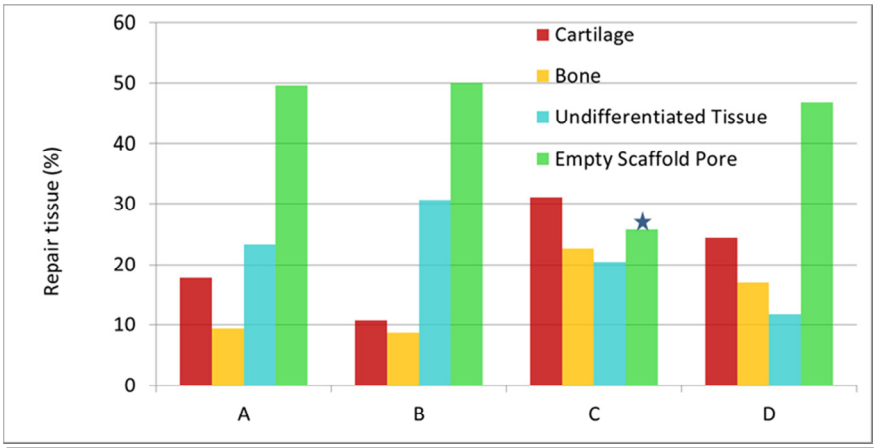

Fig. 52: Peripheral area tissue distribution by group. No statistically significant differences were observed. On non-parametric analysis, empty scaffold pore was statistically increased in group B compared to group C (p=0,045). Group A=1% cross-linker, Group B= 2% cross-linker, Group C= 5% cross-linker, Group D: 7% cross-linker).

Repair Tissue		p value			
Cartilage		0,35			
Bone		0,25			
Undifferentiated		0,28			
Empty Pores		0,16			
		N	Median	Typical Error	CI 95% Inferior limit	CI 95% Superior limit
Cartilage	A	4	17,8	15,1	-30,3	65,8
	B	5	10,8	5,5	-4,6	26,1
	C	6	31,0	10,2	4,7	57,3
	D	3	24,5	9,2	-15,0	64,0
Bone	A	4	9,4	4,7	-5,6	24,3
	B	5	8,7	4,9	-4,9	22,2
	C	6	22,7	7,3	3,8	41,5
	D	3	17,1	6,4	-10,3	44,5
Undifferentiated	A	4	49,6	10,7	15,4	83,8
	B	5	50,0	6,5	32,1	67,9
	C	6	25,9	6,8	8,3	43,5
	D	3	46,7	11,7	-3,5	96,9
Empty Scaffold Pore	A	4	23,3	6,0	4,2	42,4
	B	5	30,6	9,6	3,9	57,2
	C	6	20,4	5,0	7,7	33,1
	D	3	11,7	3,7	-4,1	27,5

Table 11: Statistical analysis of repair tissue inside the scaffolds: Peripheral area.

Conversely, on non-parametric analysis, comparing two independent variables, a statistical significant difference was found between the amount of empty pores in group B and the amount of empty pores in group C (p=0,045).

Cartilage tissue

Morphometrically quantified cartilage tissue compared the different ROIs studied inside the scaffolds and the various cross-linker concentration groups. Cartilage is seen mostly at periphery of scaffolds, except in group B, where most of the cartilage concentration is on the inferior fragment (Fig. 53). There is a higher content of cartilage in all areas of group C compared with other groups. No statistically significant differences were found (Table 11).

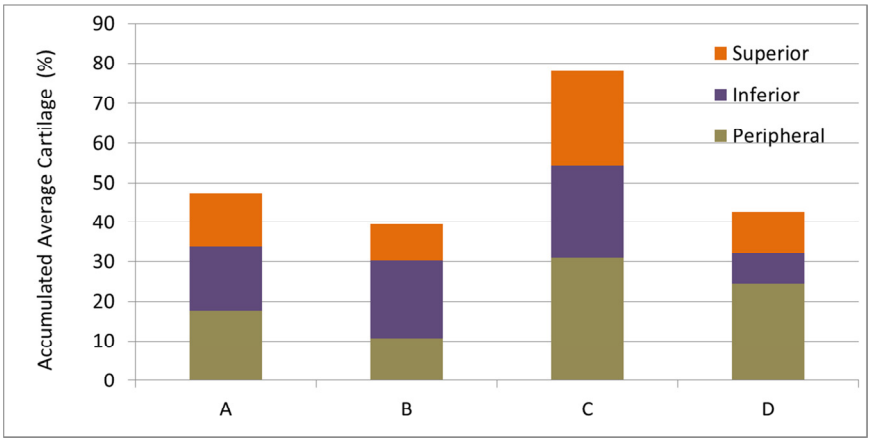

Fig. 53: Cartilage tissue inside the scaffolds. No statistically significant differences were observed. Group A=1% cross-linker, Group B= 2% cross-linker, Group C= 5% cross-linker, Group D: 7% cross-linker).

Relative cartilage	p value
Superior area	0,57
Inferior area	0,51
Peripheral area	0,35

Table 11: Statistical analysis of cartilage tissue content inside the scaffolds.

Bone tissue

In contrast to cartilage content, bone tissue is observed mainly at inferior and peripheral sections of scaffolds (Fig. 54). The highest content of bone is in groups C and D. Like cartilage, no statistically significant differences were found (Table 12).

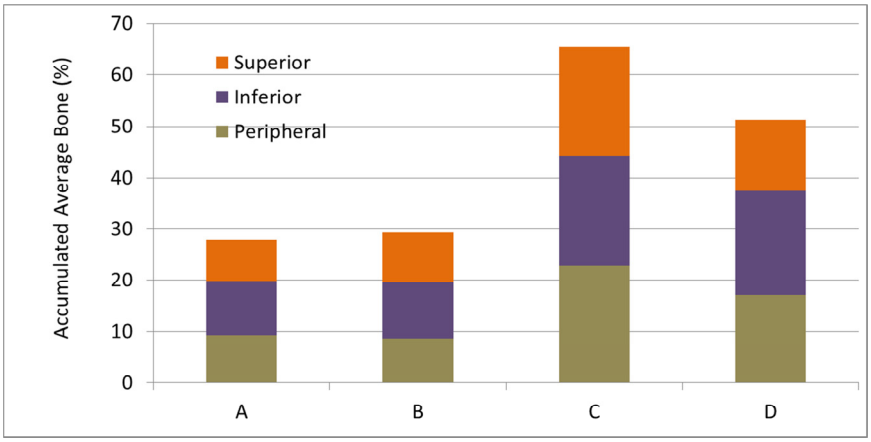

Fig. 54: Bone tissue inside the scaffolds. No statistically significant differences were observed. Group A=1% cross-linker, Group B= 2% cross-linker, Group C= 5% cross-linker, Group D: 7% cross-linker).

Relative Bone	p value
Superior area	0,47
Inferior area	0,53
Peripheral area	0,25

Table 12: Statistical analysis of bone tissue content inside the scaffolds.

Undifferentiated tissue

Undifferentiated tissue content has a different pattern than that observed in either cartilage or bone tissue. Undifferentiated tissue is seen comparatively homogeneously distributed throughout all the scaffolds in all groups (Fig. 55). However, groups A and B have a higher content of undifferentiated tissue compared with other groups. Once again, no statistically significant differences were found when undifferentiated tissue content was analyzed (Table 13).

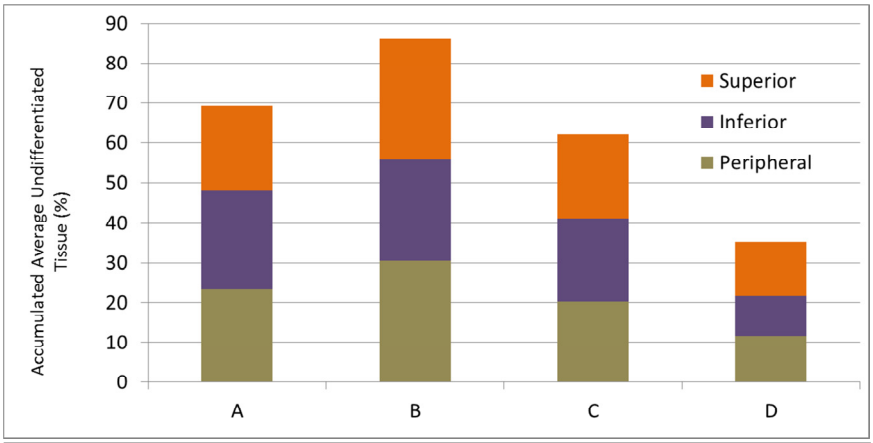

Fig. 55: Undifferentiated tissue inside the scaffolds. No statistically significant differences were observed. Group A=1% cross-linker, Group B= 2% cross-linker, Group C= 5% cross-linker, Group D: 7% cross-linker).

Relative Undifferentiated tissue	p value
Superior area	0,45
Inferior area	0,50
Peripheral area	0,28

Table 13: Statistical analysis of undifferentiated tissue content inside the scaffolds.

The empty scaffold pores represent the area inside the scaffold not occupied by any tissue or solid biomaterial. There is a slightly higher extent of empty pores perceived in the superior areas of scaffolds, although there is a roughly similar distribution of empty scaffold pores throughout all scaffold areas (Fig. 56). The highest content of empty pores (lowest percentage of tissue) is noted on group D, while group C has the least (higher percentage of tissue). As found with the other tissues, no statistically significant differences were found (Table 14).

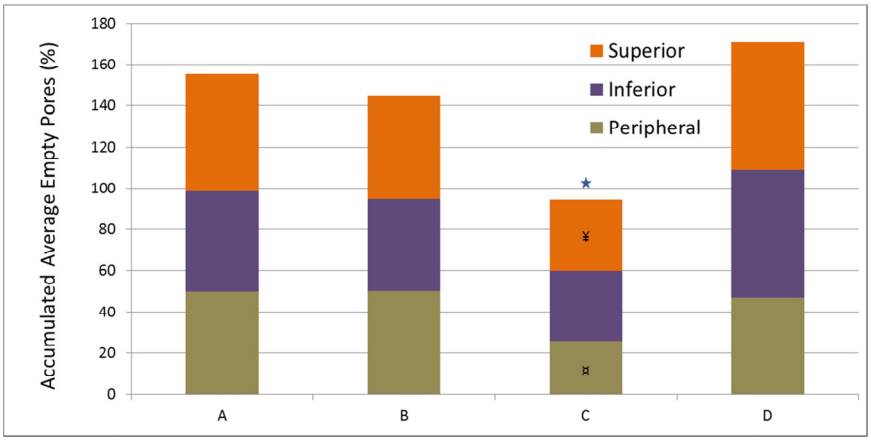

Fig. 56: Empty scaffold pores. No statistically significant differences were observed. ¥ On non-parametric analysis, empty scaffold pore was statistically decreased in the superior area of group C compared to group D (p=0,039). ¤ Empty scaffold pore was statistically decreased in the peripheral area of group C compared to group B (p=0,045). Group A=1% cross-linker, Group B= 2% cross-linker, Group C= 5% cross-linker, Group D: 7% cross-linker).

Relative Empty Scaffold Pores	p value
Superior area	0,15
Inferior area	0,54
Peripheral area	0,16

Table 14: Statistical analysis of empty pores inside the scaffolds.

Conversely, on non-parametric analysis, comparing two independent variables, statistically significant difference was found between the amount of empty pore relative to superior area in group C and D. (p=0,039). Likewise, statistically significant difference was found between the amount of empty pore relative to peripheral area in group B and C. (p=0,045).

Correlations

We have studied the correlations between repair tissue variables measured at joint surface and those measured inside scaffolds (Table 15). Out of all correlations made, we point out the statistically significant negative correlation existing between the repair tissue area at joint surface and the amount of cartilage inside the scaffolds for all groups (Pearson=-0,514; p= 0,029). Similarly, a statistically significant negative correlation between repair bone tissue at joint surface and cartilage inside the scaffolds (Pearson=-0,476; p= 0,046). In other words, there is an inverse association between the amount of cartilage found inside the scaffolds and the repair tissue area at joint surface, particularly bone.

		Repair tissue area	Repair cartilage	Repair bone	Repair undifferentiated tissue	Cartilage inside the scaffold	Bone inside the scaffold	Undifferentiated tissue inside the scaffold
Repair tissue area	Pearson	1	0,122	0,172	-0,336	-,514*	0,086	-0,143
	p		0,629	0,495	0,172	0,029	0,734	0,571
Repair cartilage	Pearson	0,122	1	-,780**	-,816**	0,304	-0,189	-0,141
	p	0,629		0	0	0,221	0,454	0,578
Repair bone	Pearson	0,172	-,780**	1	0,275	-,476*	0,331	0,176
	p	0,495	0		0,27	0,046	0,179	0,484
Repair undifferentiated tissue	Pearson	-0,336	-,816**	0,275	1	-0,033	-0,015	0,052
	p	0,172	0	0,27		0,895	0,952	0,837
Cartilage inside the scaffold	Pearson	-,514*	0,304	-,476*	-0,033	1	-0,371	-0,175
	p	0,029	0,221	0,046	0,895		0,13	0,487
Bone inside the scaffold	Pearson	0,086	-0,189	0,331	-0,015	-0,371	1	-0,109
	p	0,734	0,454	0,179	0,952	0,13		0,667
Undifferentiated tissue inside the	Pearson	-0,143	-0,141	0,176	0,052	-0,175	-0,109	1
	p	0,571	0,578	0,484	0,837	0,487	0,667	
*. Correlation is significant, 0,05 (bilateral).								
**. Correlation is significant 0,01 (bilateral).								

Table 15: Correlation between repair tissues at joint surface and inside scaffolds.

4. Discussion

The results of our study indicate that cells derived from subchondral bone marrow in adult rabbit knees after a 12-week healing period, are not only incorporated into porous (PEA-co-PHEA) scaffolds, but also develop into cartilage or bone tissue cells. Similarly, Lebourg *et al.*[206] found that the repair of chondral lesions with polycaprolactone (PCL) and PCL/HA scaffolds succeeded in forming hyaline cartilage with good properties, 12 weeks after injury in a rabbit model. Likewise, an *in vivo* study in rodents published by He *et al.*[207], revealed an increased cartilage-like tissue growth 12 weeks after scaffold implantation. However, to our knowledge there is no other experimental study published that follows the same protocol and biomaterials used in our study. Although findings are on the same line, results are not directly comparable.

Furthermore, 12 weeks after scaffold implantation, despite new cartilage growth, an important proportion of cell population scrutinized in our experimental study still remains undifferentiated, which ratifies previous observations by our research group where scaffold occupation and remodeling can take place up to one year post implantation[147].

The nature and stiffness of scaffolds was not a factor in this weight-bearing *in vivo* model, based on the failure to detect statistically significant differences in the tissue regeneration parameters studied, although the scaffolds themselves performed differently in terms of porosity and structural

integrity as described by Bozzini *et al.*[208]. Under our current statistical results we were not able to fully establish a valid statistically significant correlation between the stiffness of scaffolds and articular cartilage regeneration; hence (PEA-co-PHEA) stiffness variations achieved with different cross-linker concentrations may not be accredited as a parameter that enhances AC regeneration.

The shape of (PEA-co-PHEA) implants with 7% cross-linker changed 12 weeks after implantation, whereas the shape of implants with 1%, 2%, and 5% cross-linker did not, because of the difference in the chemical cross-linker concentration and mechanical properties of the implants. Implant stiffness can affect the structural integrity of the scaffold, making it more fragile after a critical cross-linker value. In our experimentations, 7% cross-linker scaffolds (group D), having a much higher stiffness, were not able to maintain their structural integrity as the other scaffolds did. In addition, while it is accurate to state that the amount of samples in 7% cross-linker group is low, due to early rabbit loss, there is a tendency to find deformed and collapsed scaffolds in this group.

Results of this study also indicate an inverse correlation between the stiffness of the scaffold and the corresponding cartilage repair score. In fact, articular cartilage regeneration and new tissue growth within scaffolds, increased with less stiff scaffolds, as seen not only on scaffold integration with

surrounding tissue at different implant zones, but also at joint surface. These findings agree with those described by Vickers *et al.*[209], where collagen-GAG scaffolds were chemically cross-linked to achieve a range of cross-link densities. Scaffolds with low cross-link densities experienced cell-mediated contraction, increased cell number densities and showed a greater degree of chondrogenesis. Further in Vickers's deductions, scaffolds would have an initial pore diameter large enough to facilitate cell seeding along with a mechanical stiffness low enough to allow for cell-mediated contraction to yield a reduced pore volume to favor chondrogenesis.

Our outcomes illustrate that while the 1% cross-linker scaffolds (group A) have more proportion of total cartilage repair tissue at superficial joint site, the 5% cross-linker (group C) had a higher cell scaffold occupation in addition to a similar joint repair ratio. This suggests that a 5% cross-linker concentration might also yield upright results, although group data dispersion was considerable. Moreover, our results point that an increase in cross-linker concentration after such critical value, decreases cell population, as witnessed on the 7% cross-linker group (D), and therefore the regeneration potential of the scaffold. In contrast to results obtained by Tayton *et al.*[210], in our study, varying polymer concentrations, yielded superior mechanical properties in scaffolds, however, after a given threshold, such concentration diminishes its regeneration potential. Interestingly, a common pattern of central inoccupation was

noted inside the scaffolds of the 2% cross-linker scaffolds (group B). This may, however be attributed to the cell repopulation process, which begins in the periphery and inferior margins of scaffold by bonding to adjacent host tissues and advances centripetally until injury defect is sealed, as witnessed in most of our trials. This effect possibly also takes place in a three dimensional scaffold microenvironment, where the outer layers are colonized first by migrating cells and progressively reach the core or center of the scaffold.

Controls of our investigation (group E), submitted to similar procedural treatment than trial groups, have not achieved total cartilage repair when compared to virgin cartilage controls (group F). This stands in accordance with the extensively described phenomenon of fibrocartilage growth tissue at cartilage injury sites, published in the literature[211-213]. Moreover, as based on conclusions from Waldman *et al.*[214], the mechanical effect of the scaffold itself, could have stimulated cell colonization through conducted forces to subchondral bone at injury site. The cartilage repair scores of our control group (E) were similar to trial groups, yet inferior to the scores achieved by the 1% cross-linker group in our series.

As described by Thampi *et al.*[215], an active tissue remodeling response to scaffolds can be acknowledged, with complete cellular invasion, connective tissue encapsulation, fibrovascular tissue formation, and collagen deposition. Such remark

however, could not be correlated with cross-linker concentration in our conducting tests. It is conceivable that the scaffolds caused general inflammatory and even immune responses as it migrates to deeper tissue localizations, resulting in a fibrous tissue around certain implants. Nevertheless, the inflammatory reaction of synthetic scaffolds on the surrounding tissue *in vivo* has not been sufficiently discussed. It is likely that the fibrotic response in our observations would have resolved itself as the scaffolds degrade in time. However, as proposed by Yoon *et al.*[216], inflammatory response could be reduced by impregnating demineralized bone particles into the scaffolds. They suggest that this would contribute to reduce the fibrous tissue encapsulation and foreign body giant cell response that commonly occurs at the interface of implanted scaffolds.

We observed an inverse correlation, an thus less cartilage tissue inside the scaffolds when a superficial larger area was restored by repair tissue. Similarly, less cartilage inside the scaffold is observed when more subchondral bone at articular surface is restored. Moreover, on repaired superficial tissue, as well as inside the scaffolds of our trial groups, a high tissue turnover can be inferred by the presence of new vessel growth and giant multinuclear cells. Bone content clarifies the spread distribution of new vessel growth throughout the scaffold; although we want to point out that vessels were always surrounded by undifferentiated, fibrous or bone tissue, but

never by hyaline cartilage. Permeable surface gap, on the other hand, could stimulate giant multinuclear cells for tissue repair, however this phenomenon was not perceived consistently in all trial samples, therefore deeper investigation in this matter should be addressed. The above mentioned results closely correlate with findings from Chang *et al.*[217], where as early as week 4, poly(lactide-co-glycolide) scaffolds seeded with endothelial progenitor cells, showed a higher degree of osteochondral angiogenesis in repaired tissues. Further, at week 12, the repair tissues showed enhanced hyaline cartilage regeneration with a normal columnar chondrocyte arrangement, greater GAG and type II collagen content. Moreover, they found that the endothelial progenitor cell-poly(lactide-co-glycolide) scaffold group showed organized osteochondral integration, the formation of vessel-rich tubercular bone and significantly higher bone volume per tissue volume and trabecular thickness in a rabbit model. In agreement with our results, active cartilage progression can be observed as early as 3 weeks, as seen on our early rabbit loss samples, in accordance with Chang's and Lebourg's findings[206,217].

Tissue Engineering and Cartilage Regeneration

Tissue Engineering (TE) is a rapidly expanding field of applied biology and biomedical engineering that aims to create tissues and organs for transplantation[69]. A fascinating aspect of this

field is the fundamental need to integrate the understanding of several areas of knowledge in order to create functional tissues. The process uncovers the delightful complexity of living tissues, and the joy of creation.

Cartilage tissue engineering has emerged as a strategy to regenerate new cartilage tissue, since natural cartilage repair is limited, due to the fact that it has no blood supply and thus chondrocyte metabolism is low. The results of current joint-preserving treatment protocols such as debridement, mosaicplasty, perichondrium transplantation and autologous chondrocyte implantation vary largely and the average long-term result is unsatisfactory[218-221].

Diverse strategies have been explored to arrange for a structure that combines both mechanical and biological environments suitable for appropriate cartilage regeneration. Among those, several biomaterials have been investigated, in order to provide the cells with a comfortable environment which stimulates cells to synthesize cartilage matrix, and to temporarily replace the function of the native matrix until new cartilage has formed. This biomaterial framework or scaffold is one key element in cartilage TE. Natural polymers including hyaluronan and chitosan have been investigated. Many of these polymers come in hydrogel forms, which make them suitable for studies in which mechanical loading is performed[222-224]. Since the scope of our experimental study was not to measure

mechanical loading, we favored a different type of scaffold composition. However, prior investigations at our collaborators' tissue engineering laboratory obtained enhanced chondrogenesis by the combination of chitosan porous supports with a double micro- and macro-pore structure and cell culture in a stirring bioreactor[225]. Furthermore, it was demonstrated how mechanical loading influenced cell morphology and extracellular matrix composition. Under dynamic conditions, chondrocytes kept their characteristic phenotype and tended to form cell aggregates surrounded by a layer of the main components of the hyaline cartilage extracellular matrix, type II collagen, and aggrecan.

Regarding synthetic scaffolds, the most widely used in cartilage tissue engineering are the poly-α-hydroxy esters, especially polylactic acid (PLA) and polyglycolic acid (PGA), because of their biodegradability and US Food and Drug Administration (FDA) approval for clinical use. Synthetic scaffolds, including copolymers of PEA have better mechanical strength than hydrogels, which makes it easier to fix them in a defect and improves their load-bearing properties. Besides, they are easier to manipulate and adjust, according to mechanical and biological characteristics being sought. Tayton *et al.*[210] demonstrated that by varying polymer concentrations, not only superior mechanical shear strength was achieved, but also osteoinductive and osteogenic capacity was observed. This stands in accordance with our present *in vivo* experiment,

where mechanical and biological properties of scaffolds are enhanced by varying component concentration.

Considering this vast amount of biomaterials suitable for cartilage tissue engineering, our research group has focused on a poly-ethylene copolymer at a concentration that confers it an optimal hydrophilic/hydrophobic balance for cell proliferation[145]. Moreover, degradable and non-degradable units show improved ECM distribution compared to completely non-degradable scaffolds. Solchaga *et al.*[226] showed that scaffolds with slower degradation rates yielded cartilage of greater thickness in an osteochondral defect model, but cracks and fissures were evident on the cartilage surface. Such observations are consistent with our results, in the sense that different biomaterial properties yield various amounts of repair cartilage tissue.

Furthermore, while Forriol[9] and Rodrigues *et al.*[227], among other authors, have pre-seeded cells and achieved favorable results, Munirah *et al*.[228], for example, have also confirmed the presence of lacunae and cartilage-isolated cells embedded within basophilic ground substance, 4 weeks after implanting subcutaneously chondrocyte-seeded fibrin/PLGA hybrid scaffolds at the dorsum of nude mice. In our study, no pre-seeded scaffolds were used, given that comparable results of non-seeded scaffolds when compared with pre-seeded ones,

have been reported under same copolymer concentrations of PEA[146].

It is known that mesenchymal cells that migrate and occupy cartilage injury site can acquire a chondrocyte phenotype[218]. Based on such premise, in the present study, scaffolds were positioned in an animal model cartilage injury. Occupying cells would be mechanically stimulated by compression forces, among other factors within the joint, stimulating the ECM production and therefore a repair cartilage. Such approach is also confirmed by the work of Waldman *et al*.[214] previously mentioned. He demonstrated through an *in vitro* model, that stimulation by multi-axial forces can improve the quality of the new formed tissue. Moreover, as stated by Iwamoto *et al.*[229], the regenerative capacity of AC, likely possesses and potentially uses intrinsic stem cell source in the superficial layer, Ranvier's groove, the intra-articular tissues such as synovium and fat pad, as well as marrow from the subchondral bone.

On the other hand, Rodrigues, *et al*.[227] demonstrated that amniotic fluid-derived stem cells (AFSCs) could differentiate into either osteogenic or chondrogenic cells after implanting on agarose bilayered scaffolds. This result may be useful for potential applications in regeneration strategies for damaged or diseased joints.

While joint biomechanics depends highly on articular cartilage elastic properties, growth potential of repair cartilage is tightly related to scaffold stiffness and porosity[230]. These properties influence cell migration and diffusion of oxygen, nutrients, waste products and signaling molecules. For instance, Genes *et al.*[231] observed that increasing substrate stiffness influences chondrocyte morphology, which changed from a rounded shape on weaker substrates to a predominantly flat morphology on stiffer substrates. In contrast, our study finds a relationship related with chondrocyte tissue quantification, rather than chondrocyte morphology. However, the amount of undifferentiated tissue present in our 12 week rabbit model could play an important role in chondrocyte morphology if considered over an extended period of time.

Further, the load on cartilage is a stress and not a strain, hence the strain applied to the cells at first is a function of the scaffold stiffness, and then a combination of scaffold and ECM properties as the tissue is produced. For example, as researched by Ng *et al.*[232], high agarose concentrations (3%) produce initially stiffer tissue constructs, but long-term tissue properties become significantly inferior to those with 2% agarose. Similarly, our study reveals higher biomaterial stiffness with increasing cross-linker concentration.

One strategy that has been used for tissue engineering scaffolds where higher mechanical stiffness is needed, is to vary the

amount of cross-linker concentration. Results of Qiu *et al.*[233] study suggest that the 3D porous genipin cross-linked porcine acellular dermal matrix may enhance its mechanical properties and improve its resistance to enzymatic degradation by modifying cross-linker concentration. The present study, in an effort to determine the optimal stiffness for cartilage regeneration using a (PEA-co-PHEA) scaffold, developed a protocol with different amounts of cross-linker concentration, yielding scaffolds with diverse stiffnesses and porosities.

The repair process in the presence of a microfracture is expected to course like spontaneous healing, due to the migration of stem cells during bleeding of the subchondral plate. The implantation of a scaffold without cells was based on the expectation that, inside the macroporous structure, a clot would be formed, providing a migration path for mesenchymal stem cells to invade the interface and the scaffold, and then differentiate into chondrocytes. In our results, scaffolds were occupied by new cells as early as 3 weeks, as evidenced in our early rabbit loss samples, despite the fact that the regeneration potential for older rabbits (20 week old) is less than in younger experimental animals.

Bias and Limitations

At this point, it is appropriate to highlight the fact that all our trial samples and therefore all of the values analyzed are

conditioned to the 5 μm slice fragment that has been selected for histological processing. This slice is performed at different longitudinal segments of a three dimensional sample. Bidimensional analysis of a 3D structure may introduce inaccuracies. Innovative digital strategies can diminish biased results. Also, the implantation procedure may be a subject of bias, attributable to intangible variations. These can be lessened by having a trocar adjustable to the size of rabbits, avoiding milimetric precision on freehand or increasing the size of experimentation animals (goats or horses). Likewise, by performing procedures by only one surgeon, evading variability to some extent.

Assuming no variability during the implantation procedure, in our study there is a tendency of scaffolds, independent of the biomaterials´ stiffness, to submerge beneath the cartilage´s tidemark. Such findings are in agreement with those of Lebourg *et al.*[206] whose findings report implants in the interior of subchondral bone, with the repair tissue forming over the top of the scaffold. Nevertheless, over a third of the samples in our research were still rooted superficially, in contact with the joint cavity. While the thickness at anatomical site of injured AC may influence scaffold behavior, this deep or superficial attachment of scaffolds may also be a result of mechanical solicitation of augmented load demands conditional to rabbit active motion during the post-operative period. Consequently, biomaterial´s resistance in response to such load requirements is also

amplified. However, we did not find a statistical correlation between the depth of scaffold attachment and scaffold stiffness.

On deep-seated scaffold samples, at repair sites (where repair cartilage is built), occasional ectopic repair bone tissue is observed, forming a "sandwich-like" structure (Sample 58I). Cartilage-bone-cartilage tissue is the result of a reconstructed injury. This phenomenon is perhaps not related to scaffold nature itself, but rather linked to small in-depth location patterns of scaffold attachment that require supplementary tissue to fill larger areas. Additionally, morphometric measuring protocol may also introduce confusion in the sense that allocated ROI for repair tissue also contains profound tissue in relation to the tidemark.

Furthermore, bone content in repair tissue of superficial-seated scaffolds, particularly in sample 54I, is apparently not bone tissue *per se*. Surrounding tissue has cartilage features and tidemarks are usually present. While it may possibly be ectopic bone tissue growth, which we interpret to be unlikely, this outcome might be due to the limitations of the morphometric software. First of all, such software assigns labels to dyed tissue and biomaterial in designated ROIs. At that point, the software classifies matching color spectrum. This introduces the possibility of cross labeling and consequently assuming a false positive presence of a given tissue. Additionally, we associated Alcian blue stained images magnified larger than 4x, and

scrutinized by morphometric software with increased intraobserver variability.

Another relevant issue to discuss is scaffold stability at implanted position. This has been object of concern on recent reviews. In our study, the same procedure was completed during the surgical phase, where several flexo-extension cycles were performed and scaffold was confirmed to remain in place. However, due to unstable implantation, two samples were lost. These were excluded from scrutiny since scaffold was not present after processed. To avoid this situation, some authors have recommended different strategies for example sutures; even in humans, arthroscopic fixation techniques have been presented[234,235]. Other authors like Knecht *et al.*[236] compare diverse scaffolds stabilized with two different methods; he concludes that PGA scaffolds are the most stable, independent of the fixation mechanism used. Drobnic *et al.*[237], on the other hand, tests the stability of collagen implants, concluding that it is not viable to ignore a fixation mechanism, attributing the best results to fibrin sealants. In our experience, not only the anatomical site at rabbit knee joint contributed to the stability of implants, but also the diameter between cartilage injury and implanted disc has maintained scaffolds in place by means of a press-fit mechanism.

In spite of a small number of technical limitations, we consider that our experimental study has still managed to generate

important deductions that contribute to the optimization of strategies for tissue engineering of functional articular cartilage. Although the usage of morphometry in present times is not as common, it can still be utilized as a relatively quicker, inexpensive, objective, and reproducible method for analysis and quantification of tissues.

The use of technological advancements and software based on mathematical algorithms may provide a valuable insight that can not only complement, but also enhance the interpretation of experimental results.

Finally, in our opinion, agreeing with *Kock et al.*[238], collagen content is still far below native. Future research should particularly focus on approaches to increase type II collagen content, which is essential for proper mechanical functioning of the tissue. Also, it is essential that the depth-dependent matrix organization, especially the arcade-like collagen architecture, is reproduced to some extent. In this matter, multi-layered scaffolding might greatly contribute.

5. Conclusions

Our experimental research has enabled us to evaluate articular cartilage repair tissue at 12 weeks of the healing process, under biological conditions similar to those of the human. We therefore conclude:

1. Tissue engineered P(EA-co-HEA) scaffolds induce cartilage regeneration on the injured articular surface, holding a non-statistically significant inverse correlation with the stiffness of the biomaterial.
2. At articular surface, scaffolds manufactured with 1% cross-linker concentration (group A) yield the best results, with a modified cartilage repair score of 16, closest to that of native uninjured cartilage. Similarly, group A scaffolds achieved a higher percentage of hyaline cartilage content and together with group B scaffolds, a greater thickness of repaired tissue.
3. At articular surface, the poorest response was obtained by scaffolds with 7% cross-linker concentration (group D), with a modified cartilage repair score of 10, and less production of hyaline cartilage as well as repair tissue thickness.
4. Inside the biomaterial, at superior and inferior sections of the scaffolds, 5% cross-linker concentration (group C) induced more repair tissue growth than other cross-linker concentrations. In contrast, 7% cross-linker concentration (group D) induced the least amount of repair tissue.

5. Scaffold pore occupation by repair tissue increased with increasing porosity of scaffolds as revealed in groups A, B and C. After a threshold in cross-linker concentration is reached (> 5%), stiffness of the biomaterial rises to a critical point where biomechanical properties are lost and therefore scaffold pore occupation by repair tissue diminished, as seen on group D.
6. The cross-linker concentration that induced the most repair cartilage and bone tissue growth inside the scaffolds was 5% (group C), with cartilage being the most abundant repair tissue in all scaffold areas.
7. 2% cross-linker concentration (group B) induced more undifferentiated tissue in all scaffold areas, when compared with other cross-linker concentrations.
8. A statistically significant inverse correlation exists between the amount of repair tissue and bone at injured joint surface, and the amount of cartilage inside the scaffolds.

6. Future research

Biotechnology is a broad field that continues to grow permanently. Cartilage tissue engineering has focused on a triad: cell source, scaffolds and signaling factors[239]; each branch with enormous contributions and yet huge potential to be explored.

Biomaterial components are in constant evolution, to provide the most suitable mechanical environments to host renewed tissue, as well as other purposes[240,241]. Nonstop improvement of scaffolding techniques, feasibly through nanotechnology, will continue to contribute in the future years. Furthermore, as stiffness of biomaterials actively affect their mechanical properties; additional research in this area could widely contribute in the establishment of stiffness thresholds for each biomaterial. This could be very useful, particularly in the manufacture of multilayered scaffolds, where different layers require certain mechanical properties that adapt to the specific demands of the tissue being sought. Supplementary in-depth investigation of biomaterial stiffness might also help clarify the behavioral patterns of scaffold establishment in deep or superficial positions and the host reaction towards the implant. While it is true that the type of biomaterial implanted is determinant for the outcome of regenerated articular cartilage, further knowledge of the impact of biomaterial stiffness will allow us to enhance tissue regeneration.

Alternatives and limitations to stem cell and pluripotent cells are being explored, while zonal organization of native articular cartilage, signaling pathways and mechanotransduction appear to play an essential role[242,243]. Bioactive molecules, gene therapy and mechanical loading strategies contribute to articular cartilage regeneration and are still under investigation[244].

On the quest for cartilage regeneration, small contributions make huge changes, still I believe, nature itself has all the answers.

7. References

1 Geneser F. Tejido esquelético. In: Histología. Ed: Panamericana, Buenos Aires: 2000; 263-97

2 Kaul G, Cucchiarini M, Remberger K*, et al.* Failed cartilage repair for early osteoarthritis defects: a biochemical, histological and immunohistochemical analysis of the repair tissue after treatment with marrow-stimulation techniques. *Knee Surg Sports Traumatol Arthrosc* 2012; **20**:2315-24

3 Smith GD, Knutsen G, Richardson JB. A clinical review of cartilage repair techniques. *J Bone Joint Surg Br* 2005; **87**:445-9

4 Filardo G, Kon E, Roffi A*, et al.* Scaffold-based repair for cartilage healing: a systematic review and technical note. *Arthroscopy* 2013; **29**:174-86

5 Khubutiya M, Kliukvin IY, Istranov LP*, et al.* Stimulation of regeneration of hyaline cartilage in experimental osteochondral injury. *Bull Exp Biol Med* 2008; **146**:658-61

6 Sabater i Serra R, Kyritsis A, Escobar Ivirico J*, et al.* Molecular mobility in biodegradable poly(ε-caprolactone)/poly(hydroxyethyl acrylate) networks. *Eur Phys J E Soft Matter* 2011; **34**:1-10

7 Perez Olmedilla M, Garcia-Giralt N, Pradas MM*, et al.* Response of human chondrocytes to a non-uniform distribution of hydrophilic domains on poly (ethyl acrylate-co-hydroxyethyl methacrylate) copolymers. *Biomaterials* 2006; **27**:1003-12

8 Campillo-Fernandez AJ, Pastor S, Abad-Collado M*, et al.* Future design of a new keratoprosthesis. Physical and biological analysis of polymeric substrates for epithelial cell growth. *Biomacromolecules* 2007; **8**:2429-36

9 Forriol F. Ingeniería tisular en el cartílago articular: Estudio *in vivo* del proceso de regeneración mediante scaffolds bioestables. Valencia, Spain: Universidad de Valencia, 2009

10 Zheng YH, Su K, Kuang SJ*, et al.* New bone and cartilage tissues formed from human bone marrow mesenchymal stem cells derived from human condyle in vivo. *Zhonghua Kou Qiang Yi Xue Za Zhi* 2012; **47**:10-3

11 Shi J, Zhang X, Zeng X*, et al.* One-step articular cartilage repair: combination of in situ bone marrow stem cells with cell-free poly(L-lactic-co-glycolic acid) scaffold in a rabbit model. *Orthopedics* 2012; **35**:e665-71

12 Veronesi F, Giavaresi G, Tschon M*, et al.* Clinical use of bone marrow, bone marrow concentrate, and expanded bone marrow mesenchymal stem cells in cartilage disease. *Stem Cells Dev* 2013; **22**:181-92

13 Eyre DR, Wu JJ, Fernandes RJ*, et al.* Recent developments in cartilage research: matrix biology of the collagen II/IX/XI heterofibril network. *Biochem Soc Trans* 2002; **30**:893-9

14 Vornehm SI, Dudhia J, Von der Mark K*, et al.* Expression of collagen types IX and XI and other major cartilage matrix components by human fetal chondrocytes in vivo. *Matrix Biol* 1996; **15**:91-8

15 Keene DR, Oxford JT, Morris NP. Ultrastructural localization of collagen types II, IX, and XI in the growth plate of human rib and fetal bovine epiphyseal cartilage: type XI collagen is restricted to thin fibrils. *J Histochem Cytochem* 1995; **43**:967-79

16 Macirowski T, Tepic S, Mann RW. Cartilage stresses in the human hip joint. *J Biomech Eng* 1994; **116**:10-8

17 Olsen S, Oloyede A. A finite element analysis methodology for representing the articular cartilage functional structure. *Comput Methods Biomech Biomed Engin* 2002; **5**:377-86

18 Mankin HJ. The reaction of articular cartilage to injury and osteoarthritis (first of two parts). *N Engl J Med* 1974; **291**:1285-92

19 Kempson GE, Muir H, Pollard C*, et al.* The tensile properties of the cartilage of human femoral condyles related to the content of collagen and glycosaminoglycans. *Biochim Biophys Acta* 1973; **297**:456-72

20 Kikukawa K, Suzuki K. Histochemical and immunohistochemical distribution of glycosaminoglycans, type II collagen, and fibronectin in developing fetal cartilage of congenital osteochondrodysplasia rat (ocd/ocd). *Teratology* 1992; **46**:509-23

21 van Weeren PR, Firth EC, Brommer H*, et al.* Early exercise advances the maturation of glycosaminoglycans and collagen in the extracellular matrix of articular cartilage in the horse. *Equine Vet J* 2008; **40**:128-35

22 Abedian R, Willbold E, Becher C*, et al.* In vitro electro-mechanical characterization of human knee articular cartilage of different degeneration levels: a comparison with ICRS and Mankin scores. *J Biomech* 2013; **46**:1328-34

23 Frank EH, Grodzinsky AJ. Cartilage electromechanics--I. Electrokinetic transduction and the effects of electrolyte pH and ionic strength. *J Biomech* 1987; **20**:615-27

24 Frank EH, Grodzinsky AJ. Cartilage electromechanics--II. A continuum model of cartilage electrokinetics and correlation with experiments. *J Biomech* 1987; **20**:629-39

25 Sun HB, Zhao L, Tanaka S*, et al.* Moderate joint loading reduces degenerative actions of matrix metalloproteinases in the articular cartilage of mouse ulnae. *Connect Tissue Res* 2012; **53**:180-6

26 Meszaros E, Malemud CJ. Prospects for treating osteoarthritis: enzyme-protein interactions regulating matrix metalloproteinase activity. *Ther Adv Chronic Dis* 2012; **3**:219-29

27 Groma G, Xin W, Grskovic I*, et al.* Abnormal bone quality in cartilage oligomeric matrix protein and matrilin 3 double-deficient mice caused by increased tissue inhibitor of metalloproteinases 3 deposition and delayed aggrecan degradation. *Arthritis Rheum* 2012; **64**:2644-54

28 Jay GD, Tantravahi U, Britt DE*, et al.* Homology of lubricin and superficial zone protein (SZP): products of megakaryocyte stimulating factor (MSF) gene expression by human synovial fibroblasts and articular chondrocytes localized to chromosome 1q25. *J Orthop Res* 2001; **19**:677-87

29 Swann DA, Hendren RB, Radin EL*, et al.* The lubricating activity of synovial fluid glycoproteins. *Arthritis Rheum* 1981; **24**:22-30

30 Hong E, Reddi AH. Dedifferentiation and redifferentiation of articular chondrocytes from surface and middle zones: changes in

microRNAs-221/-222, -140, and -143/145 expression. *Tissue Eng Part A* 2013; **19**:1015-22

31 Junqueira LC, Toledo OM, Montes GS. Correlation of specific sulfated glycosaminoglycans with collagen types I, II, and III. *Cell Tissue Res* 1981; **217**:171-5

32 Hoemann CD, Lafantaisie-Favreau CH, Lascau-Coman V*, et al.* The cartilage-bone interface. *J Knee Surg* 2012; **25**:85-97

33 Weiss C, Rosenberg L, Helfet AJ. An ultrastructural study of normal young adult human articular cartilage. *J Bone Joint Surg Am* 1968; **50**:663-74

34 Benninghoff A. Form und Bau der Gelenkknorpel in ihren Beziehungen zur Funktion. *Z Zellforsch* 1925; **2**:783

35 Hosseini SM, Wu Y, Ito K*, et al.* The importance of superficial collagen fibrils for the function of articular cartilage. *Biomech Model Mechanobiol* 2014; **13**:41-51

36 Matheney T, Sandell L, Foucher K*, et al.* Motion analysis, cartilage mechanics, and biology in femoroacetabular impingement: current understanding and areas of future research. *J Am Acad Orthop Surg* 2013; **21 (Suppl 1)**:S27-32

37 Singh M, Nagrath AR, Maini PS. Changes in trabecular pattern of the upper end of the femur as an index of osteoporosis. *J Bone Joint Surg Am* 1970; **52**:457-67

38 Aaron JE. Periosteal Sharpey's fibers: a novel bone matrix regulatory system? *Front Endocrinol (Lausanne)* 2012; Acc. Number: 22908007 Doi: 10.3389/fendo.2012.00098

39 Ducuing J, Marques P, Baux R*, et al.* [Physiology of bone circulation]. *J Radiol Electrol Arch Electr Medicale* 1951; **32**:189-96

40 Boskey AL. Mineral-matrix interactions in bone and cartilage. *Clin Orthop Relat Res* 1992:244-74

41 Wang X, Wang Y, Gou W*, et al.* Role of mesenchymal stem cells in bone regeneration and fracture repair: a review. *Int Orthop* 2013; **37**:2491-98

42 Pojda Z, Machaj E, Kurzyk A*, et al.* [Mesenchymal stem cells]. *Postepy Biochem* 2013; **59**:187-97

43 Almeida M. Aging mechanisms in bone. *Bonekey Rep* 2012; Acc. Number: 23705067 Doi: 10.1038/bonekey.2012.102

44 Jilka RL, Noble B, Weinstein RS. Osteocyte apoptosis. *Bone* 2013; **54**:264-71

45 Boyce BF. Advances in the regulation of osteoclasts and osteoclast functions. *J Dent Res* 2013; **92**:860-7

46 Chappard D. [Bone modeling and remodeling during osseointegration]. *Rev Stomatol Chir Maxillofac Chir Orale* 2013; **114**:159-65

47 Miao CG, Yang YY, He X*, et al.* Wnt signaling pathway in rheumatoid arthritis, with special emphasis on the different roles in synovial inflammation and bone remodeling. *Cell Signal* 2013; **25**:2069-78

48 Klein-Nulend J, Nijweide PJ, Burger EH. Osteocyte and bone structure. *Curr Osteoporos Rep* 2003; **1**:5-10

49 Parfitt AM. Osteonal and hemi-osteonal remodeling: the spatial and temporal framework for signal traffic in adult human bone. *J Cell Biochem* 1994; **55**:273-86

50 Teitelbaum SL, Tondravi MM, Ross FP. Osteoclasts, macrophages, and the molecular mechanisms of bone resorption. *J Leukoc Biol* 1997; **61**:381-8

51 Goldring SR. Bone and joint destruction in rheumatoid arthritis: what is really happening? *J Rheumatol Suppl* 2002; **65**:44-8

52 Portal-Nunez S, Lozano D, Esbrit P. Role of angiogenesis on bone formation. *Histol Histopathol* 2012; **27**:559-66

53 Ashwood N, Verma M, Hamlet M*, et al.* Transarticular shear fractures of the distal humerus. *J Shoulder Elbow Surg* 2010; **19**:46-52

54 Geissler WB, Adams JE, Bindra RR*, et al.* Scaphoid fractures: what's hot, what's not. *Instr Course Lect* 2012; **61**:71-84

55 Spahn G, Wittig R. [Biomechanical properties (compressive strength and compressive pressure at break) of hyaline cartilage under axial load]. *Zentralbl Chir* 2003; **128**:78-82

56 Tetsunaga T, Akazawa H. Intra-articular loose body caused by avascular necrosis of the femoral head in children. *J Pediatr Orthop B* 2014; **23**:44-48

57 Richie LB, Sytsma MJ. Matching osteochondritis dissecans lesions in identical twin brothers. *Orthopedics* 2013; **36**:e1213-6

58 Altman R, Alarcon G, Appelrouth D*, et al.* The American College of Rheumatology criteria for the classification and reporting of osteoarthritis of the hip. *Arthritis Rheum* 1991; **34**:505-14

59 Brandt KD, Fife RS. Ageing in relation to the pathogenesis of osteoarthritis. *Clin Rheum Dis* 1986; **12**:117-30

60 McDevitt C, Gilbertson E, Muir H. An experimental model of osteoarthritis; early morphological and biochemical changes. *J Bone Joint Surg Br* 1977; **59**:24-35

61 Arden N, Nevitt MC. Osteoarthritis: epidemiology. *Best Pract Res Clin Rheumatol* 2006; **20**:3-25

62 Mainil-Varlet P, Aigner T, Brittberg M*, et al.* Histological assessment of cartilage repair: a report by the Histology Endpoint Committee of the International Cartilage Repair Society (ICRS). *J Bone Joint Surg Am* 2003; **85-A (Suppl 2)**:45-57

63 Pritzker KP, Gay S, Jimenez SA*, et al.* Osteoarthritis cartilage histopathology: grading and staging. *Osteoarthritis Cartilage* 2006; **14**:13-29

64 Sayre EC, Jordan JM, Cibere J*, et al.* Quantifying the association of radiographic osteoarthritis in knee or hip joints with other knees or hips: the Johnston County Osteoarthritis Project. *J Rheumatol* 2010; **37**:1260-5

65 Griffith JF, Lau DT, Yeung DK*, et al.* High-resolution MR imaging of talar osteochondral lesions with new classification. *Skeletal Radiol* 2012; **41**:387-99

66 Cibere J, Zhang H, Thorne A*, et al.* Association of clinical findings with pre-radiographic and radiographic knee osteoarthritis in a population-based study. *Arthritis Care Res (Hoboken)* 2010; **62**:1691-8

67 Jackson DW, Lalor PA, Aberman HM*, et al.* Spontaneous repair of full-thickness defects of articular cartilage in a goat model. A preliminary study. *J Bone Joint Surg Am* 2001; **83-A**:53-64

68 Newman AP. Articular cartilage repair. *Am J Sports Med* 1998; **26**:309-24

69 Atala A. Engineering organs. *Curr Opin Biotechnol* 2009; **20**:575-92

70 Fitzgerald O, Hanly J, Callan A*, et al.* Effects of joint lavage on knee synovitis in rheumatoid arthritis. *Br J Rheumatol* 1985; **24**:6-10

71 Yetkinler DN, Greenleaf JE, Sherman OH. Histologic analysis of radiofrequency energy chondroplasty. *Clin Sports Med* 2002; **21**:649-61, viii

72 Horstman CL, McLaughlin RM. The use of radiofrequency energy during arthroscopic surgery and its effects on intraarticular tissues. *Vet Comp Orthop Traumatol* 2006; **19**:65-71

73 Reichenbach S, Rutjes AW, Nuesch E*, et al.* Joint lavage for osteoarthritis of the knee. *Cochrane Database Syst Rev* 2010; Acc. Number: 20464751 Doi: 10.1002/14651858.CD007320.pub2

74 Richmond J, Hunter D, Irrgang J*, et al.* Treatment of osteoarthritis of the knee (nonarthroplasty). *J Am Acad Orthop Surg* 2009; **17**:591-600

75 Ayral X. Arthroscopy and joint lavage. *Best Pract Res Clin Rheumatol* 2005; **19**:401-15

76 Pridie. A method of resurfacing osteoarthritic knee joints. *J Bone Joint Surg [Br]* 1959; **41**:618-19

77 Insall J. The Pridie debridement operation for osteoarthritis of the knee. *Clin Orthop Relat Res* 1974:61-7

78 Steadman JR, Rodkey WG, Briggs KK*, et al.* [The microfracture technic in the management of complete cartilage defects in the knee joint]. *Orthopade* 1999; **28**:26-32

79 Johnson LL. Arthroscopic abrasion arthroplasty historical and pathologic perspective: present status. *Arthroscopy* 1986; **2**:54-69

80 Rohde RS, Studer RK, Chu CR. Mini-pig fresh osteochondral allografts deteriorate after 1 week of cold storage. *Clin Orthop Relat Res* 2004; **427**:226-33

81 Kim HT, Teng MS, Dang AC. Chondrocyte apoptosis: implications for osteochondral allograft transplantation. *Clin Orthop Relat Res* 2008; **466**:1819-25

82 Hangody L, Kish G, Karpati Z*, et al.* Arthroscopic autogenous osteochondral mosaicplasty for the treatment of femoral condylar articular defects. A preliminary report. *Knee Surg Sports Traumatol Arthrosc* 1997; **5**:262-7

83 Hangody L, Kish G, Karpati Z*, et al.* Mosaicplasty for the treatment of articular cartilage defects: application in clinical practice. *Orthopedics* 1998; **21**:751-6

84 Bodo G, Hangody L, Szabo Z*, et al.* Arthroscopic autologous osteochondral mosaicplasty for the treatment of subchondral cystic lesion in the medial femoral condyle in a horse. *Acta Vet Hung* 2000; **48**:343-54

85 Morelli M, Nagamori J, Miniaci A. Management of chondral injuries of the knee by osteochondral autogenous transfer (mosaicplasty). *J Knee Surg* 2002; **15**:185-90

86 Szerb I, Hangody L, Duska Z*, et al.* Mosaicplasty: long-term follow-up. *Bull Hosp Jt Dis* 2005; **63**:54-62

87 Buckwalter JA, Mow VC, Ratcliffe A. Restoration of Injured or Degenerated Articular Cartilage. *J Am Acad Orthop Surg* 1994; **2**:192-201

88 Bruns J, Kersten P, Lierse W*, et al.* [Autologous transplantation of rib perichondrium in treatment of deep cartilage defects of the knee joint of sheep. Morphologic comparison of two resorbable fixation methods]. *Unfallchirurg* 1993; **96**:462-7

89 Bouwmeester P, Kuijer R, Terwindt-Rouwenhorst E*, et al.* Histological and biochemical evaluation of perichondrial transplants in human articular cartilage defects. *J Orthop Res* 1999; **17**:843-9

90 Engkvist O, Wilander E. Formation of cartilage from rib perichondrium grafted to an articular defect in the femur condyle of the rabbit. *Scand J Plast Reconstr Surg* 1979; **13**:371-76

91 Brittberg M, Lindahl A, Nilsson A*, et al.* Treatment of deep cartilage defects in the knee with autologous chondrocyte transplantation. *N Engl J Med* 1994; **331**:889-95

92 Gooding CR, Bartlett W, Bentley G*, et al.* A prospective, randomised study comparing two techniques of autologous chondrocyte implantation for osteochondral defects in the knee: Periosteum covered versus type I/III collagen covered. *Knee* 2006; **13**:203-10

93 Hettrich CM, Crawford D, Rodeo SA. Cartilage repair: third-generation cell-based technologies--basic science, surgical techniques, clinical outcomes. *Sports Med Arthrosc* 2008; **16**:230-5

94 Kerker JT, Leo AJ, Sgaglione NA. Cartilage repair: synthetics and scaffolds: basic science, surgical techniques, and clinical outcomes. *Sports Med Arthrosc* 2008; **16**:208-16

95 Afoke NY, Byers PD, Hutton WC. Contact pressures in the human hip joint. *J Bone Joint Surg Br* 1987; **69**:536-41

96 Hodge WA, Carlson KL, Fijan RS*, et al.* Contact pressures from an instrumented hip endoprosthesis. *J Bone Joint Surg Am* 1989; **71**:1378-86

97 Waters RL, Lunsford BR, Perry J*, et al.* Energy-speed relationship of walking: standard tables. *J Orthop Res* 1988; **6**:215-22

98 Elder BD, Athanasiou KA. Hydrostatic pressure in articular cartilage tissue engineering: from chondrocytes to tissue regeneration. *Tissue Eng Part B Rev* 2009; **15**:43-53

99 Franklin PD, Harrold L, Ayers DC. Incorporating patient-reported outcomes in total joint arthroplasty registries: challenges and opportunities. *Clin Orthop Relat Res* 2013; **471**:3482-88

100 Pruitt LA, Ansari F, Kury M, *et al.* Clinical trade-offs in cross-linked ultrahigh-molecular-weight polyethylene used in total joint arthroplasty. *J Biomed Mater Res B Appl Biomater* 2013; **101**:476-84

101 Hawker GA, Badley EM, Borkhoff CM, *et al.* Which patients are most likely to benefit from total joint arthroplasty? *Arthritis Rheum* 2013; **65**:1243-52

102 Williams GM, Chan EF, Temple-Wong MM, *et al.* Shape, loading, and motion in the bioengineering design, fabrication, and testing of personalized synovial joints. *J Biomech* 2010; **43**:156-65

103 Steadman JR, Rodkey WG, Rodrigo JJ. Microfracture: surgical technique and rehabilitation to treat chondral defects. *Clin Orthop Relat Res* 2001; **391 (Suppl)**:S362-69

104 Pang HN, Yeo SJ, Chong HC, *et al.* Joint line changes and outcomes in constrained versus unconstrained total knee arthroplasty for the type II valgus knee. *Knee Surg Sports Traumatol Arthrosc* 2013; **21**:2363-9

105 Blevins FT, Steadman JR, Rodrigo JJ, *et al.* Treatment of articular cartilage defects in athletes: an analysis of functional outcome and lesion appearance. *Orthopedics* 1998; **21**:761-68

106 Knapik DM, Harris JD, Pangrazzi G, *et al.* The Basic Science of Continuous Passive Motion in Promoting Knee Health: A Systematic Review of Studies in a Rabbit Model. *Arthroscopy* 2013; **29**:1722-31

107 Schenck RR. The dynamic traction method. Combining movement and traction for intra-articular fractures of the phalanges. *Hand Clin* 1994; **10**:187-98

108 Langer RS, Vacanti JP. Tissue engineering: the challenges ahead. *Sci Am* 1999; **280**:86-9

109 Andersson J, Stenhamre H, Backdahl H, *et al.* Behavior of human chondrocytes in engineered porous bacterial cellulose scaffolds. *J Biomed Mater Res A* 2010; **94**:1124-32

110 Nomoto Y, Okano W, Imaizumi M, *et al.* Bioengineered prosthesis with allogenic heterotopic fibroblasts for cricoid regeneration. *Laryngoscope* 2012; **122**:805-9

111 Diekman BO, Christoforou N, Willard VP*, et al.* Cartilage tissue engineering using differentiated and purified induced pluripotent stem cells. *Proc Natl Acad Sci U S A* 2012; **109**:19172-7

112 Yang X, Shang H, Katz A*, et al.* A modified aggregate culture for chondrogenesis of human adipose-derived stem cells genetically modified with growth and differentiation factor 5. *Biores Open Access* 2013; **2**:258-65

113 Benz K, Stippich C, Freudigmann C*, et al.* Maintenance of "stem cell" features of cartilage cell sub-populations during in vitro propagation. *J Transl Med* 2013; Acc. Number: 23363653 Doi: 10.1186/1479-5876-11-27

114 Gardner OF, Archer CW, Alini M*, et al.* Chondrogenesis of mesenchymal stem cells for cartilage tissue engineering. *Histol Histopathol* 2013; **28**:23-42

115 Chung C, Burdick JA. Engineering cartilage tissue. *Adv Drug Deliv Rev* 2008; **60**:243-62

116 Moroz A, Bittencourt RA, Almeida RP*, et al.* Platelet lysate 3D scaffold supports mesenchymal stem cell chondrogenesis: an improved approach in cartilage tissue engineering. *Platelets* 2013; **24**:219-25

117 Jeong CG, Hollister SJ. A comparison of the influence of material on in vitro cartilage tissue engineering with PCL, PGS, and POC 3D scaffold architecture seeded with chondrocytes. *Biomaterials* 2010; **31**:4304-12

118 Li WJ, Laurencin CT, Caterson EJ*, et al.* Electrospun nanofibrous structure: a novel scaffold for tissue engineering. *J Biomed Mater Res* 2002; **60**:613-21

119 Bray JC, Merrill EW. Poly(vinyl alcohol) hydrogels for synthetic articular cartilage material. *J Biomed Mater Res* 1973; **7**:431-43

120 Uematsu K, Hattori K, Ishimoto Y*, et al.* Cartilage regeneration using mesenchymal stem cells and a three-dimensional poly-lactic-glycolic acid (PLGA) scaffold. *Biomaterials* 2005; **26**:4273-9

121 Li WJ, Cooper JA, Jr., Mauck RL*, et al.* Fabrication and characterization of six electrospun poly(alpha-hydroxy ester)-based

fibrous scaffolds for tissue engineering applications. *Acta Biomater* 2006; **2**:377-85

122 Lee SY, Wee AS, Lim CK*, et al.* Supermacroporous poly(vinyl alcohol)-carboxylmethyl chitosan-poly(ethylene glycol) scaffold: an in vitro and in vivo pre-assessments for cartilage tissue engineering. *J Mater Sci Mater Med* 2013; **24**:1561-70

123 Liao E, Yaszemski M, Krebsbach P*, et al.* Tissue-engineered cartilage constructs using composite hyaluronic acid/collagen I hydrogels and designed poly(propylene fumarate) scaffolds. *Tissue Eng* 2007; **13**:537-50

124 Stenhamre H, Nannmark U, Lindahl A*, et al.* Influence of pore size on the redifferentiation potential of human articular chondrocytes in poly(urethane urea) scaffolds. *J Tissue Eng Regen Med* 2011; **5**:578-88

125 Miao X, Tan DM, Li J*, et al.* Mechanical and biological properties of hydroxyapatite/tricalcium phosphate scaffolds coated with poly(lactic-co-glycolic acid). *Acta Biomater* 2008; **4**:638-45

126 Sechriest VF, Miao YJ, Niyibizi C*, et al.* GAG-augmented polysaccharide hydrogel: a novel biocompatible and biodegradable material to support chondrogenesis. *J Biomed Mater Res* 1999; **49**:534-41

127 Smeds KA, Pfister-Serres A, Miki D*, et al.* Photocrosslinkable polysaccharides for in situ hydrogel formation. *J Biomed Mater Res* 2001; **54**:115-21

128 Zaborowska M, Bodin A, Backdahl H*, et al.* Microporous bacterial cellulose as a potential scaffold for bone regeneration. *Acta Biomater* 2010; **6**:2540-7

129 Muller FA, Muller L, Hofmann I*, et al.* Cellulose-based scaffold materials for cartilage tissue engineering. *Biomaterials* 2006; **27**:3955-63

130 Mintz BR, Cooper JA, Jr. Hybrid hyaluronic acid hydrogel/poly(varepsilon-caprolactone) scaffold provides mechanically favorable platform for cartilage tissue engineering studies. *J Biomed Mater Res A* 2013; Acc. Number: 24115629 Doi: 10.1002/jbm.a.34957

131 Rajangam T, An SS. Fibrinogen and fibrin based micro and nano scaffolds incorporated with drugs, proteins, cells and genes for therapeutic biomedical applications. *Int J Nanomedicine* 2013; **8**:3641-62

132 Zhu Y, Wan Y, Zhang J, *et al.* Manufacture of layered collagen/chitosan-polycaprolactone scaffolds with biomimetic microarchitecture. *Colloids Surf B Biointerfaces* 2013; **113C**:352-60

133 Zhao P, Deng C, Xu H, *et al.* Fabrication of Photo-crosslinked Chitosan- Gelatin Scaffold in Sodium Alginate Hydrogel for Chondrocyte Culture. *Biomed Mater Eng* 2013; **23**:S653-61

134 Tamaddon M, Walton RS, Brand DD, *et al.* Characterisation of freeze-dried type II collagen and chondroitin sulfate scaffolds. *J Mater Sci Mater Med* 2013; **24**:1153-65

135 Seyednejad H, Vermonden T, Fedorovich NE, *et al.* Synthesis and characterization of hydroxyl-functionalized caprolactone copolymers and their effect on adhesion, proliferation, and differentiation of human mesenchymal stem cells. *Biomacromolecules* 2009; **10**:3048-54

136 Cheung JW, Rose EE, Paul Santerre J. Perfused culture of gingival fibroblasts in a degradable/polar/hydrophobic/ionic polyurethane (D-PHI) scaffold leads to enhanced proliferation and metabolic activity. *Acta Biomater* 2013; **9**:6867-75

137 Campillo-Fernandez AJ, Unger RE, Peters K, *et al.* Analysis of the biological response of endothelial and fibroblast cells cultured on synthetic scaffolds with various hydrophilic/hydrophobic ratios: influence of fibronectin adsorption and conformation. *Tissue Eng Part A* 2009; **15**:1331-41

138 Soria JM, Martinez Ramos C, Bahamonde O, *et al.* Influence of the substrate's hydrophilicity on the in vitro Schwann cells viability. *J Biomed Mater Res A* 2007; **83**:463-70

139 Briz N, Antolinos-Turpin C, Alio J, *et al.* Fibronectin fixation on poly(ethyl acrylate)-based copolymers. *J Biomed Mater Res, Part B: Appl Biomater* 2013; **101B**:991-97

140 Schagemann JC, Kurz H, Casper ME, *et al.* The effect of scaffold composition on the early structural characteristics of chondrocytes

and expression of adhesion molecules. *Biomaterials* 2010; **31**:2798-805

141 García Cruz D, Sardinha V, Escobar Ivirico J*, et al.* Gelatin microparticles aggregates as three-dimensional scaffolding system in cartilage engineering. *J Mater Sci Mater Med* 2013; **24**:503-13

142 Garcia Cruz D, Salmeron-Sanchez M, Gomez Ribelles J. Stirred flow bioreactor modulates chondrocyte growth and extracellular matrix biosynthesis in chitosan scaffolds. *J Biomed Mater Res A* 2012; **100A**:2330-41

143 Gamboa-Martinez T, Rodenas-Rochina J, Tortosa P*, et al.* Chondrocytes cultured in adhesive macroporous scaffold subjected to stirred flow bioreactor behave like in static culture. *J Biomater Tissue Eng* 2013; **3**:312-19

144 Oh SH, Lee JH. Hydrophilization of synthetic biodegradable polymer scaffolds for improved cell/tissue compatibility. *Biomed Mater* 2013; **8**:014101

145 Sancho-Tello M, García-Gómez R, Monleón-Pradas M*, et al.* Articular cartilage regeneration by using synthetic biodegradable scaffolds. *Histol Histopathol* 2009; **24 (Suppl 1)**:S95

146 Sancho-Tello M, Forriol F, Novella E*, et al.* Tissue engineering of articular cartilage: use of bioresorbible scaffolds preseeded with chondrocytes. *Histol Histopathol* 2009; **24 (Suppl 1)**:S93

147 Sancho-Tello M, Martín de Llano JJ, Ruiz Saurí A*, et al.* Time course of joint cartilage regeneration using Poly-ethyl-acrilate scaffolds in rabbits. *Histol Histopathol* 2011; **26 (Suppl 1)**:84

148 Oh SH, Kim TH, Im GI*, et al.* Investigation of pore size effect on chondrogenic differentiation of adipose stem cells using a pore size gradient scaffold. *Biomacromolecules* 2010; **11**:1948-55

149 Kwon SH, Lee TJ, Park J*, et al.* Modulation of BMP-2-induced chondrogenic versus osteogenic differentiation of human mesenchymal stem cells by cell-specific extracellular matrices. *Tissue Eng Part A* 2013; **19**:49-58

150 Lu CH, Yeh TS, Yeh CL*, et al.* Regenerating Cartilages by Engineered ASCs: Prolonged TGF-beta3/BMP-6 Expression Improved

Articular Cartilage Formation and Restored Zonal Structure. *Mol Ther* 2013; Acc. Number: 23851345 Doi: 10.1038/mt.2013.165

151 Craft AM, Ahmed N, Rockel JS*, et al.* Specification of chondrocytes and cartilage tissues from embryonic stem cells. *Development* 2013; **140**:2597-610

152 Hicks DL, Sage AB, Shelton E*, et al.* Effect of bone morphogenetic proteins 2 and 7 on septal chondrocytes in alginate. *Otolaryngol Head Neck Surg* 2007; **136**:373-9

153 Giatsidis G, Dalla Venezia E, Bassetto F. The role of gene therapy in regenerative surgery: updated insights. *Plast Reconstr Surg* 2013; **131**:1425-35

154 Thorpe SD, Buckley CT, Steward AJ*, et al.* European Society of Biomechanics S.M. Perren Award 2012: the external mechanical environment can override the influence of local substrate in determining stem cell fate. *J Biomech* 2012; **45**:2483-92

155 Mesallati T, Buckley CT, Nagel T*, et al.* Scaffold architecture determines chondrocyte response to externally applied dynamic compression. *Biomech Model Mechanobiol* 2013; **12**:889-99

156 Schubert T, Xhema D, Veriter S*, et al.* The enhanced performance of bone allografts using osteogenic-differentiated adipose-derived mesenchymal stem cells. *Biomaterials* 2011; **32**:8880-91

157 Kagami H, Agata H, Tojo A. Bone marrow stromal cells (bone marrow-derived multipotent mesenchymal stromal cells) for bone tissue engineering: basic science to clinical translation. *Int J Biochem Cell Biol* 2011; **43**:286-9

158 Rezwan K, Chen QZ, Blaker JJ*, et al.* Biodegradable and bioactive porous polymer/inorganic composite scaffolds for bone tissue engineering. *Biomaterials* 2006; **27**:3413-31

159 Duan P, Pan Z, Cao L*, et al.* The effects of pore size in bilayered poly(lactide-co-glycolide) scaffolds on restoring osteochondral defects in rabbits. *J Biomed Mater Res A* 2013; Acc. Number: 23637068 Doi: 10.1002/jbm.a.34683

160 Guda T, Walker JA, Singleton B*, et al.* Hydroxyapatite scaffold pore architecture effects in large bone defects in vivo. *J Biomater Appl* 2013; Acc. Number: 23771772 Doi: 10.1177/0885328213491790

161 Holmes B, Castro NJ, Zhang LG*, et al.* Electrospun fibrous scaffolds for bone and cartilage tissue generation: recent progress and future developments. *Tissue Eng Part B Rev* 2012; **18**:478-86

162 Castro NJ, Hacking SA, Zhang LG. Recent progress in interfacial tissue engineering approaches for osteochondral defects. *Ann Biomed Eng* 2012; **40**:1628-40

163 Chu CR, Coutts RD, Yoshioka M*, et al.* Articular cartilage repair using allogeneic perichondrocyte-seeded biodegradable porous polylactic acid (PLA): a tissue-engineering study. *J Biomed Mater Res* 1995; **29**:1147-54

164 Cao T, Ho KH, Teoh SH. Scaffold design and in vitro study of osteochondral coculture in a three-dimensional porous polycaprolactone scaffold fabricated by fused deposition modeling. *Tissue Eng* 2003; **9 Suppl 1**:S103-12

165 Brun P, Abatangelo G, Radice M*, et al.* Chondrocyte aggregation and reorganization into three-dimensional scaffolds. *J Biomed Mater Res* 1999; **46**:337-46

166 Chen J, Chen H, Li P*, et al.* Simultaneous regeneration of articular cartilage and subchondral bone in vivo using MSCs induced by a spatially controlled gene delivery system in bilayered integrated scaffolds. *Biomaterials* 2011; **32**:4793-805

167 Kon E, Delcogliano M, Filardo G*, et al.* Novel nano-composite multilayered biomaterial for osteochondral regeneration: a pilot clinical trial. *Am J Sports Med* 2011; **39**:1180-90

168 Chen K, Shi P, Teh TK*, et al.* In vitro generation of a multilayered osteochondral construct with an osteochondral interface using rabbit bone marrow stromal cells and a silk peptide-based scaffold. *J Tissue Eng Regen Med* 2013; Acc. Number: 23413023 Doi: 10.1002/term.1708

169 Qu D, Li J, Li Y*, et al.* Ectopic osteochondral formation of biomimetic porous PVA-n-HA/PA6 bilayered scaffold and BMSCs

construct in rabbit. *J Biomed Mater Res B Appl Biomater* 2011; **96**:9-15

170 Oliveira JM, Rodrigues MT, Silva SS*, et al.* Novel hydroxyapatite/chitosan bilayered scaffold for osteochondral tissue-engineering applications: Scaffold design and its performance when seeded with goat bone marrow stromal cells. *Biomaterials* 2006; **27**:6123-37

171 Reyes R, Delgado A, Solis R*, et al.* Cartilage repair by local delivery of transforming growth factor-beta1 or bone morphogenetic protein-2 from a novel, segmented polyurethane/polylactic-co-glycolic bilayered scaffold. *J Biomed Mater Res A* 2013; Acc. Number: 23766296 Doi: 10.1002/jbma.34769

172 Liu M, Yu X, Huang F*, et al.* Tissue engineering stratified scaffolds for articular cartilage and subchondral bone defects repair. *Orthopedics* 2013; **36**:868-73

173 Mouthuy PA, El-Sherbini Y, Cui Z*, et al.* Layering PLGA-based electrospun membranes and cell sheets for engineering cartilage-bone transition. *J Tissue Eng Regen Med* 2013; 10.1002/term.1765

174 Hindle P, Hendry JL, Keating JF*, et al.* Autologous osteochondral mosaicplasty or TruFit plugs for cartilage repair. *Knee Surg Sports Traumatol Arthrosc* 2013; 10.1007/s00167-013-2493-0

175 Vundelinckx B, De Mulder K, De Schepper J. Osteochondral defect in femoral head: Trufit implantation under fluoroscopic and arthroscopic control. *Acta Orthop Belg* 2012; **78**:796-9

176 Dhollander AA, Liekens K, Almqvist KF*, et al.* A pilot study of the use of an osteochondral scaffold plug for cartilage repair in the knee and how to deal with early clinical failures. *Arthroscopy* 2012; **28**:225-33

177 Marchevsky AM, Gil J. Applications of computerized interactive morphometry in pathology. II. A model for computer generated diagnosis. *Lab Invest* 1986; **54**:708-16

178 Hall TL, Fu YS. Applications of quantitative microscopy in tumor pathology. *Lab Invest* 1985; **53**:5-21

179 Baak JP. The principles and advances of quantitative pathology. *Anal Quant Cytol Histol* 1987; **9**:89-95

180 True LD. Morphometric applications in anatomic pathology. *Hum Pathol* 1996; **27**:450-67

181 Collan Y, Montironi R, Mariuzzi GM*, et al.* Observer variation in interactive computerized morphometry. *Appl Pathol* 1986; **4**:9-14

182 Weger AR, Lindholm J, Glaser K*, et al.* Morphometry and prognosis in cancer of the pancreatic head. *Pathol Res Pract* 1992; **188**:764-9

183 van Diest PJ, Baak JP, Matze-Cok P*, et al.* Prediction of response to adjuvant chemotherapy in premenopausal lymph node positive breast cancer patients with morphometry, DNA flow cytometry and HER-2/neu oncoprotein expression. Preliminary results. *Pathol Res Pract* 1992; **188**:344-9

184 Mohler JL, Metts JC, Zhang XZ*, et al.* Nuclear morphometry in automatic biopsy and radical prostatectomy specimens of prostatic carcinoma. A comparison. *Anal Quant Cytol Histol* 1994; **16**:415-20

185 Mohanty SK, Dey P, Rana P. Manual and automated AgNOR count in differentiating reactive mesothelial from metastatic malignant cells in serous effusions. *Anal Quant Cytol Histol* 2003; **25**:273-6

186 Rubin AS, Roberts ED. Morphometric quantitation of histopathologic changes in articular cartilage in an immunologically-induced rabbit model of rheumatoid arthritis. *Lab Invest* 1987; **57**:342-6

187 Goyal N, Gupta M. Computerized morphometric analysis of human femoral articular cartilage. *ISRN Rheumatol* 2012; **2012**:360201

188 Ruiz Saurí A, Sancho-Tello M, Forriol F*, et al.* Regeneración del complejo articular en un modelo animal: Estudio morfométrico de la diferenciación condral y ósea. INVESCOT. Valencia, 2010

189 Stenkvist B, Strande G. Entropy as an algorithm for the statistical description of DNA cytometric data obtained by image analysis microscopy. *Anal Cell Pathol* 1990; **2**:159-65

190 Pertusa Grau JF. In: Técnicas de Análisis de Imagen: Aplicaciones en Biología. Ed: Universitat de Valencia, Valencia, Spain: 2003; 31-100

191 Lin-Gibson S, Cooper JA, Landis FA*, et al.* Systematic investigation of porogen size and content on scaffold morphometric parameters and properties. *Biomacromolecules* 2007; **8**:1511-8

192 Hehne HJ, Oelze C, Riede UN. [Morphometric analysis of the proximal tibial cartilage tissue (author's transl)]. *Z Orthop Ihre Grenzgeb* 1981; **119**:449-54

193 Dam EB, Folkesson J, Pettersen PC*, et al.* Automatic morphometric cartilage quantification in the medial tibial plateau from MRI for osteoarthritis grading. *Osteoarthritis Cartilage* 2007; **15**:808-18

194 Ranz FB, Aceitero J, Gaytan F. Morphometric study of cartilage dynamics in the chick embryo tibia. II. Dexamethasone-treated embryos. *J Anat* 1987; **154**:73-9

195 Brígido Diego R, Pérez Olmedilla M, Serrano Aroca A*, et al.* Acrylic scaffolds with interconnected spherical pores and controled hydrophilicity for tissue engineering. *J Mat Sci Mat Medicine* 2005; **16**:693-98

196 Martinez-Diaz S, Garcia-Giralt N, Lebourg M*, et al.* In vivo evaluation of 3-dimensional polycaprolactone scaffolds for cartilage repair in rabbits. *Am J Sports Med* 2010; **38**:509-19

197 Davies DV, Barnett CH, Cochrane W*, et al.* Electron microscopy of articular cartilage in the young adult rabbit. *Ann Rheum Dis* 1962; **21**:11-22

198 Hoch DH, Grodzinsky AJ, Koob TJ*, et al.* Early changes in material properties of rabbit articular cartilage after meniscectomy. *J Orthop Res* 1983; **1**:4-12

199 Hulth A, Lindberg L, Telhag H. Experimental osteoarthritis in rabbits. Preliminary report. *Acta Orthop Scand* 1970; **41**:522-30

200 Junqueira LC, Bignolas G, Brentani RR. Picrosirius staining plus polarization microscopy, a specific method for collagen detection in tissue sections. *Histochem J* 1979; **11**:447-55

201 Montes GS, Junqueira LC. The use of the Picrosirius-polarization method for the study of the biopathology of collagen. *Mem Inst Oswaldo Cruz* 1991; **86 (Suppl 3)**:1-11

202 Zambrano NZ, Montes GS, Shigihara KM*, et al.* Collagen arrangement in cartilages. *Acta Anat (Basel)* 1982; **113**:26-38

203 Masuoka K, Asazuma T, Ishihara M*, et al.* Tissue engineering of articular cartilage using an allograft of cultured chondrocytes in a membrane-sealed atelocollagen honeycomb-shaped scaffold (ACHMS scaffold). *J Biomed Mater Res B Appl Biomater* 2005; **75**:177-84

204 Hu Z, Peel SA, Ho SK*, et al.* The expression of bone matrix proteins induced by different bioimplants in a rabbit sinus lift model. *J Biomed Mater Res A* 2010; **95**:1048-54

205 Solchaga LA, Yoo JU, Lundberg M*, et al.* Hyaluronan-based polymers in the treatment of osteochondral defects. *J Orthop Res* 2000; **18**:773-80

206 Lebourg M, Martinez-Diaz S, Garcia-Giralt N*, et al.* Cell-free cartilage engineering approach using hyaluronic acid-polycaprolactone scaffolds: A study in vivo. *J Biomater Appl* 2013; Acc. Number: 24108064 Doi: 10.1177/0885328213507298

207 He X, Fu W, Feng B*, et al.* Electrospun collagen-poly(L-lactic acid-co-epsilon-caprolactone) membranes for cartilage tissue engineering. *Regen Med* 2013; **8**:425-36

208 Bozzini S, Petrini P, Altomare L*, et al.* Fabrication of chemically cross-linked porous gelatin matrices. *J Appl Biomater Biomech* 2009; **7**:194-9

209 Vickers SM, Squitieri LS, Spector M. Effects of cross-linking type II collagen-GAG scaffolds on chondrogenesis in vitro: dynamic pore reduction promotes cartilage formation. *Tissue Eng* 2006; **12**:1345-55

210 Tayton E, Purcell M, Aarvold A*, et al.* A comparision of polymer and polymer-hydroxyapatite composite tissue engineered scaffolds for use in bone regeneration. An in vitro and in vivo study. *J Biomed Mater Res A* 2013; Acc. Number: 24038868 Doi: 10.1002/jbm.a.34926

211 Aulin C, Jensen-Waern M, Ekman S*, et al.* Cartilage repair of experimentally 11 induced osteochondral defects in New Zealand White rabbits. *Lab Anim* 2013; **47**:58-65

212 Gigante A, Calcagno S, Cecconi S*, et al.* Use of collagen scaffold and autologous bone marrow concentrate as a one-step cartilage repair in the knee: histological results of second-look biopsies at 1 year follow-up. *Int J Immunopathol Pharmacol* 2011; **24**:69-72

213 Lane Smith R, Trindade MC, Ikenoue T*, et al.* Effects of shear stress on articular chondrocyte metabolism. *Biorheology* 2000; **37**:95-107

214 Waldman SD, Couto DC, Grynpas MD*, et al.* Multi-axial mechanical stimulation of tissue engineered cartilage: review. *Eur Cell Mater* 2007; **13**:66-74

215 Thampi P, Nair D, R L*, et al.* Pathological effects of processed bovine pericardial scaffolds--a comparative in vivo evaluation. *Artif Organs* 2013; **37**:600-5

216 Yoon SJ, Kim SH, Ha HJ*, et al.* Reduction of inflammatory reaction of poly(d,l-lactic-co-glycolic Acid) using demineralized bone particles. *Tissue Eng Part A* 2008; **14**:539-47

217 Chang NJ, Lam CF, Lin CC*, et al.* Transplantation of autologous endothelial progenitor cells in porous PLGA scaffolds create a microenvironment for the regeneration of hyaline cartilage in rabbits. *Osteoarthritis Cartilage* 2013; **21**:1613-22

218 Kreuz PC, Steinwachs MR, Erggelet C*, et al.* Results after microfracture of full-thickness chondral defects in different compartments in the knee. *Osteoarthritis Cartilage* 2006; **14**:1119-25

219 Redman SN, Oldfield SF, Archer CW. Current strategies for articular cartilage repair. *Eur Cell Mater* 2005; **9**:23-32

220 Bentley G, Biant LC, Carrington RW*, et al.* A prospective, randomised comparison of autologous chondrocyte implantation versus mosaicplasty for osteochondral defects in the knee. *J Bone Joint Surg Br* 2003; **85**:223-30

221 Hunziker EB. Articular cartilage repair: basic science and clinical progress. A review of the current status and prospects. *Osteoarthritis Cartilage* 2002; **10**:432-63

222 Spiller KL, Maher SA, Lowman AM. Hydrogels for the repair of articular cartilage defects. *Tissue Eng Part B Rev* 2011; **17**:281-99

223 Smith RL, Rusk SF, Ellison BE*, et al.* In vitro stimulation of articular chondrocyte mRNA and extracellular matrix synthesis by hydrostatic pressure. *J Orthop Res* 1996; **14**:53-60

224 Suh JK, Baek GH, Aroen A*, et al.* Intermittent sub-ambient interstitial hydrostatic pressure as a potential mechanical stimulator for chondrocyte metabolism. *Osteoarthritis Cartilage* 1999; **7**:71-80

225 Garcia Cruz DM, Salmeron-Sanchez M, Gomez-Ribelles JL. Stirred flow bioreactor modulates chondrocyte growth and extracellular matrix biosynthesis in chitosan scaffolds. *J Biomed Mater Res A* 2012; **100**:2330-41

226 Solchaga LA, Temenoff JS, Gao J*, et al.* Repair of osteochondral defects with hyaluronan- and polyester-based scaffolds. *Osteoarthritis Cartilage* 2005; **13**:297-309

227 Rodrigues MT, Lee SJ, Gomes ME*, et al.* Bilayered constructs aimed at osteochondral strategies: the influence of medium supplements in the osteogenic and chondrogenic differentiation of amniotic fluid-derived stem cells. *Acta Biomater* 2012; **8**:2795-806

228 Munirah S, Kim SH, Ruszymah BH*, et al.* The use of fibrin and poly(lactic-co-glycolic acid) hybrid scaffold for articular cartilage tissue engineering: an in vivo analysis. *Eur Cell Mater* 2008; **15**:41-52

229 Iwamoto M, Ohta Y, Larmour C*, et al.* Toward regeneration of articular cartilage. *Birth Defects Res C Embryo Today* 2013; **99**:192-202

230 Nuernberger S, Cyran N, Albrecht C*, et al.* The influence of scaffold architecture on chondrocyte distribution and behavior in matrix-associated chondrocyte transplantation grafts. *Biomaterials* 2011; **32**:1032-40

231 Genes NG, Rowley JA, Mooney DJ*, et al.* Effect of substrate mechanics on chondrocyte adhesion to modified alginate surfaces. *Arch Biochem Biophys* 2004; **422**:161-7

232 Ng KW, Wang CC, Mauck RL*, et al.* A layered agarose approach to fabricate depth-dependent inhomogeneity in chondrocyte-seeded constructs. *J Orthop Res* 2005; **23**:134-41

233 Qiu J, Li J, Wang G*, et al.* In vitro investigation on the biodegradability and biocompatibility of genipin cross-linked porcine acellular dermal matrix with intrinsic fluorescence. *ACS Appl Mater Interfaces* 2013; **5**:344-50

234 Petersen W, Zelle S, Zantop T. Arthroscopic implantation of a three dimensional scaffold for autologous chondrocyte transplantation. *Arch Orthop Trauma Surg* 2008; **128**:505-8

235 Zelle S, Zantop T, Schanz S*, et al.* Arthroscopic techniques for the fixation of a three-dimensional scaffold for autologous chondrocyte transplantation: structural properties in an in vitro model. *Arthroscopy* 2007; **23**:1073-8

236 Knecht S, Erggelet C, Endres M*, et al.* Mechanical testing of fixation techniques for scaffold-based tissue-engineered grafts. *J Biomed Mater Res B Appl Biomater* 2007; **83**:50-7

237 Drobnic M, Radosavljevic D, Ravnik D*, et al.* Comparison of four techniques for the fixation of a collagen scaffold in the human cadaveric knee. *Osteoarthritis Cartilage* 2006; **14**:337-44

238 Kock L, van Donkelaar CC, Ito K. Tissue engineering of functional articular cartilage: the current status. *Cell Tissue Res* 2012; **347**:613-27

239 Caplan AI. New era of cell-based orthopedic therapies. *Tissue Eng Part B Rev* 2009; **15**:195-200

240 Pedraza W. Membranas de quitosano reticulado para la liberación controlada de fármacos. Valencia, Spain: Universidad Politécnica de Valencia, 2012

241 Madihally SV, Matthew HW. Porous chitosan scaffolds for tissue engineering. *Biomaterials* 1999; **20**:1133-42

242 Schulz RM, Bader A. Cartilage tissue engineering and bioreactor systems for the cultivation and stimulation of chondrocytes. *Eur Biophys J* 2007; **36**:539-68

243 Grad S, Eglin D, Alini M*, et al.* Physical stimulation of chondrogenic cells in vitro: a review. *Clin Orthop Relat Res* 2011; **469**:2764-72

244 Gigante A, Bevilacqua C, Zara C*, et al.* Autologous chondrocyte implantation: cells phenotype and proliferation analysis. *Knee Surg Sports Traumatol Arthrosc* 2001; **9**:254-8